POLITECNICO
MILANO 1863

SCUOLA DI INGEGNERIA INDUSTRIALE
E DELL'INFORMAZIONE

Thermodynamic Modelling and Component Sizing of Wastewater Source Heat Pump for District Line Including On - Off Design Analysis and CO_2 Reduction Assessment

Tesi di Laurea Magistrale in
Energy Engineering - Ingegneria Energetica

Author: **Angelica Cortinovis**

Student ID: 248821
Advisor: Professor Paolo Chiesa
Academic Year: 2024-25

Ringraziamenti

Desidero esprimere la mia più sincera gratitudine al professor Chiesa per la disponibilità e il costante supporto forniti durante lo sviluppo di questo lavoro di tesi. La sua esperienza e i suoi preziosi suggerimenti hanno rappresentato un punto di riferimento fondamentale.

Un ringraziamento speciale va ai miei genitori, per il sostegno incondizionato, la fiducia e la pazienza con cui mi hanno accompagnata in ogni fase del mio percorso di studi. Il loro esempio, la loro dedizione e il loro incoraggiamento costante sono stati per me una fonte di forza e motivazione nei momenti di maggiore impegno e difficoltà.

Desidero inoltre ringraziare tutte le persone che mi sono state accanto lungo questo cammino, condividendo con me soddisfazioni, sfide e traguardi. Il loro supporto, la loro comprensione e la loro presenza hanno contribuito in modo significativo al raggiungimento di questo importante obiettivo personale e professionale.

Un pensiero particolare va a Matteo, per esserci stato con costanza, per la pazienza e per il sostegno silenzioso ma fondamentale nei momenti più intensi di questo percorso.

Infine, desidero dedicare un ringraziamento anche a me stessa e alla ragazza di cinque anni fa che sognava di intraprendere questo percorso universitario: per aver creduto in quel sogno e per aver avuto la determinazione di trasformarlo in realtà.

Abstract

The decarbonisation of urban heating systems represents one of the most critical challenges of the energy transition, particularly in dense metropolitan areas where concentrated thermal demand coincides with an extensive and continuously available wastewater network. In this context, the exploitation of urban wastewater as a low grade thermal resource offers a structurally integrated solution to enhance the performance and the decarbonisation of district heating networks.

The objective of this thesis is to develop a thermodynamic model of a wastewater source heat pump supplying a district heating network, including on design sizing and off design operation, and to employ this framework to identify the district heating load configuration that maximises CO_2 emission reductions compared to a natural gas based heating scenario.

First, a detailed thermodynamic model of a double vapour compression heat pump cycle is formulated, including full characterisation of all state points and component level sizing of compressors and heat exchangers. This stage defines the reference operating conditions and geometric parameters of the system. Second, an off design model is developed to describe adaptive cycle operation under variable wastewater temperature, mass flow rate, and district heating demand.

Finally, the off design model is embedded within an annual simulation framework based on hourly time series datasets to reproduce realistic source and sink dynamics. The system operates as a hybrid configuration in which the wastewater source heat pump is operated up to its technical limits, while the remaining demand is covered by an auxiliary electric boiler. For fixed wastewater availability conditions, the model is used to determine the district heating load sizing that maximises CO_2 emission reductions relative to a conventional natural gas based scenario. The resulting framework constitutes a quantitative decision support tool for the optimal integration of wastewater-source heat pumps into urban district heating networks.

Keywords: Heat pump, Wastewater, On - Off design Modelling, District heating network, CO_2 emission.

Abstract in lingua italiana

La decarbonizzazione dei sistemi di riscaldamento urbano rappresenta una delle principali sfide della transizione energetica, soprattutto nelle aree metropolitane dense, dove una domanda termica concentrata coincide con una rete fognaria estesa e continuamente disponibile. In questo contesto, lo sfruttamento delle acque reflue urbane come risorsa termica a bassa temperatura, costituisce una soluzione integrata per migliorare le prestazioni e favorire la decarbonizzazione delle reti di teleriscaldamento.

L'obiettivo della tesi è sviluppare un modello termodinamico di una pompa di calore alimentata da acque reflue a servizio di una rete di teleriscaldamento, facendone l'analisi in condizioni di progetto (on design), la quale include anche il dimensionamento dei componenti e l'analisi fuori progetto (off design), al fine di individuare la configurazione di carico lato teleriscaldamento che massimizza la riduzione delle emissioni di CO_2 rispetto a uno scenario basato su gas naturale.

Viene quindi formulato il modello di un ciclo a doppia compressione di vapore, che caratterizza tutti i punti del ciclo e dimensiona i principali componenti, quali compressori e scambiatori di calore, al fine di definire le condizioni operative di riferimento. Successivamente, il modello di off-design descrive il funzionamento adattivo del ciclo al variare della temperatura, della portata dei reflui e della domanda termica della rete.

Il modello di off-design è integrato in una simulazione annuale con risoluzione oraria per riprodurre dinamiche realistiche della sorgente e del pozzo termico. Il sistema opera in configurazione ibrida: la pompa di calore è esercita fino ai propri limiti tecnici, mentre il carico residuo è coperto da una caldaia elettrica ausiliaria. A parità di disponibilità dei reflui, il modello consente di determinare il dimensionamento lato teleriscaldamento che massimizza la riduzione delle emissioni di CO_2 rispetto a uno scenario convenzionale a gas naturale. Il framework sviluppato costituisce uno strumento quantitativo di supporto decisionale per l'integrazione ottimale di pompe di calore alimentate da acque reflue nelle reti urbane di teleriscaldamento.

Parole chiave: Pompa di calore, Acque Reflue, Modellazione On-Off design, Rete di teleriscaldamento, Emissioni di CO_2.

Contents

1 | Energy Context And Heat Pump Fundamentals

1.1. Heating Sector in the Energy And Enviromental Context

Heating is the largest energy end use worldwide and represents a fundamental component of the global energy system. According to recent assessments by the International Energy Agency, heat demand accounts for approximately 50% of global final energy consumption, exceeding the energy use associated with electricity and transport combined, as shown in Figure 1.1 [1]. Despite growing attention to efficiency improvements and renewable energy deployment, a substantial share of global heat demand is still satisfied through the direct combustion of fossil fuels, primarily natural gas, oil and coal, making the heating sector one of the major contributors to global energy related CO_2 emissions [2].

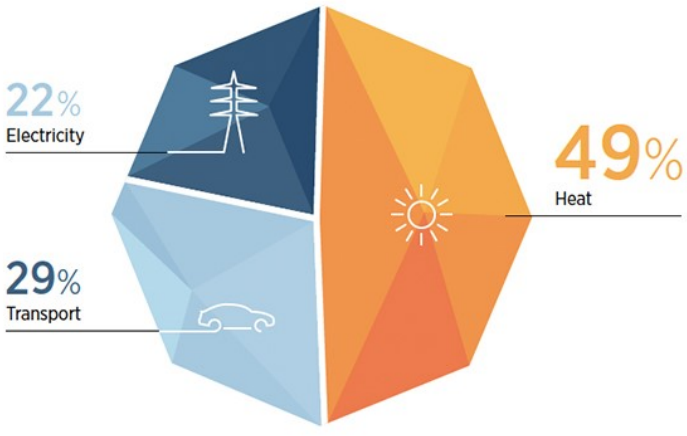

Figure 1.1: Global final energy consumption by end use [1].

The relevance of heating demand is particularly pronounced within the built environment.

According to the International Energy Agency (IEA), space heating and domestic hot water production, account for approximately 45-50% of the total final energy consumption in buildings worldwide, across both residential and tertiary sectors [2].

Consistent estimates are reported in the literature and illustrated in Figure 1.2. Ürge-Vorsatz et al. show that heating services constitute the dominant energy end use in both residential and commercial buildings. In the residential sector, space heating accounts for approximately 32% of final energy use, with water heating contributing an additional 24%. In commercial buildings, the corresponding shares are approximately 33% for space heating and around 12% for water heating.

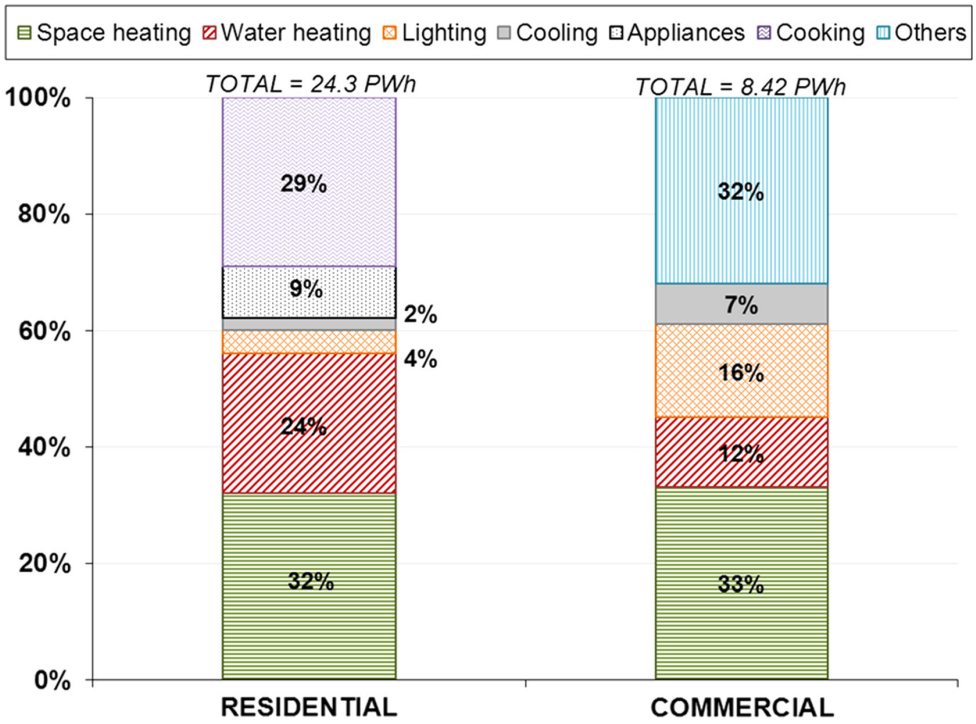

Figure 1.2: Final building energy consumption in the world by end use [3].

Despite substantial advancements in building envelope performance, insulation standards, and heating system efficiencies, a considerable share of existing buildings worldwide continues to depend on conventional fossil fuel based heating technologies. The low turnover rate of the existing building stock, together with the long operational lifetime of heating systems, significantly complicates the decarbonisation of the building sector and underscores its strategic role in energy transition pathways [3].

From a climate perspective, the building sector is a major contributor to global greenhouse gas emissions, as illustrated in Figure 1.3. According to the Sixth Assessment Report of the Intergovernmental Panel on Climate Change, emissions from buildings reached

approximately 12 $GtCO_2$-equivalent in 2019, accounting for about 21% of total global GHG emissions. These include both direct emissions from on site fuel combustion for space heating and domestic hot water, and indirect emissions associated with electricity and district heat supply. Given the dominant role of heating in building energy use, the decarbonisation of heating technologies is widely recognised as a key mitigation strategy within the sector [4].

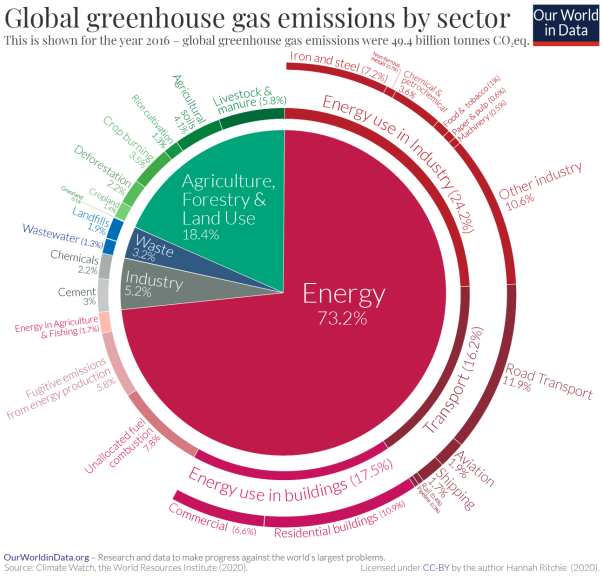

Figure 1.3: Greenhouse gas emissions by sector [5].

More recent assessments confirm that the building sector remains a key driver of global energy use and emissions. According to the Global Status Report for Buildings and Construction 2024/25, in 2023 the buildings and construction sector accounted for approximately 34% of global CO_2 emissions and 32% of total global energy demand, when emissions associated with both building operation and construction activities are considered [6].

Residential and commercial heating based on fuel combustion represents a major source of nitrogen oxides, NO_x, and fine particulate matter, $PM_{2.5}$, in urban areas. In particular, residential combustion has been identified as a dominant contributor to ambient $PM_{2.5}$ concentrations in Europe, especially during the heating season, with significant implications for public health [7]. Emissions from decentralised heating systems have been shown to substantially contribute to urban air pollution during the heating season, increasing population exposure due to the proximity of emission sources to end users [8]. The concentration of heating demand in densely populated cities further amplifies these effects, making the heating sector a critical interface between energy systems, air quality, and public health.

Given the magnitude of heating demand and its associated environmental and health impacts, the heating sector is therefore widely recognised as a priority area for the energy transition. Achieving sustained reductions in CO_2 emissions requires a structural shift away from fossil fuel based heating technologies toward more efficient and low-carbon solutions, particularly within the building sector [9].

1.2. Heats Pump And Energy Transition

The decarbonisation of the heating sector is a key component of the energy transition. It is primarily driven by the electrification of thermal energy services, coupled with the gradual decarbonisation of electricity supply.

In this context, heat pumps are recognised as a key technology for the decarbonisation of thermal energy services. They allow thermal energy services to be provided with significantly lower primary energy consumption and greenhouse gas emissions compared to conventional fossil fuel based heating systems. By replacing direct fuel combustion with electrically driven systems, capable of exploiting renewable and low temperature heat sources, heat pumps constitute a crucial pathway for reducing emissions in the building sector while supporting the large scale integration of renewable electricity [10].

Heat pumps transfer thermal energy from a low temperature source to a higher temperature sink through the input of external work, typically electricity. Unlike conventional boilers, which generate heat through fuel combustion and are inherently limited by combustion efficiency and chemical energy content of the fuel, heat pumps exploit existing low grade thermal energy available in the environment, such as ambient air, ground, or water [11].

A heat pump operates by transferring energy between two thermal reservoirs, as illustrated in Figure 1.4.

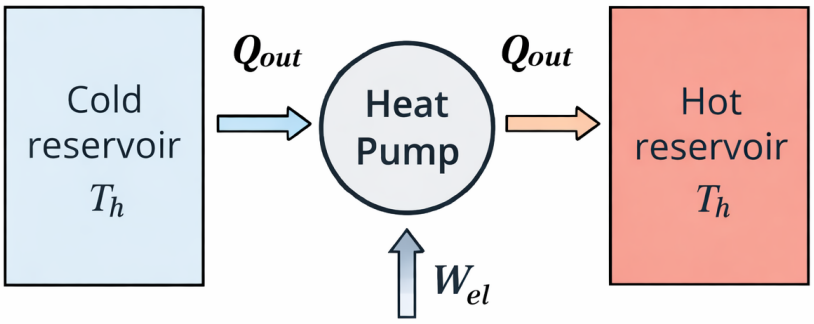

Figure 1.4: Representation of a heat pump operating between a cold thermal reservoir at temperature T_c and a hot thermal reservoir at temperature T_h.

In this representation:

- $\dot{Q}_{\text{in}}$ is the heat absorbed from the low temperature reservoir;
- $\dot{Q}_{\text{out}}$ is the heat delivered to the high temperature reservoir;
- $\dot{W}_{\text{el}}$ is the electrical work input driving the process.

From a thermodynamic standpoint, most heat pumps used for space heating and domestic hot water, are based on the vapour compression refrigeration cycle. At a conceptual level, the cycle involves the evaporation of a working fluid at low pressure through heat absorption from the source, followed by compression to a higher pressure, condensation with heat rejection to the heating system, and finally expansion to complete the cycle.

This configuration enables the transfer of thermal energy from a lower to a higher temperature level in accordance with the second law of thermodynamics, through the input of mechanical or electrical work.

The performance of a heat pump is commonly quantified through the coefficient of performance COP, defined as the ratio between the useful thermal power delivered to the user and the work input required to operate the system:

$$\text{COP} = \frac{\dot{Q}_{\text{out}}}{\dot{W}_{\text{el}}}, \tag{1.1}$$

where:

- $\dot{Q}_{\text{out}}$ denotes the heat released at the condenser;
- $\dot{W}_{\text{el}}$ represents the electrical power consumption of the compressor and, where applicable, auxiliary components.

The COP is introduced here as a global performance indicator, providing a synthetic measure of heat pump efficiency. To be evaluated rigorously, it requires a detailed thermodynamic description of the cycle and its value is strongly dependent on the operating temperature levels of the heat source and heat sink. In general, larger temperature differences between the heat source and the heat sink result in lower COP values.

When compared to conventional fossil fuel based boilers, heat pumps can achieve significantly higher effective efficiencies, as the useful heat output is not constrained by the chemical energy content of a fuel. While modern condensing boilers typically reach thermal efficiencies close to unity with respect to the lower heating value of the fuel, heat pumps are capable of delivering several units of heat per unit of electrical energy consumed, provided that suitable operating conditions are ensured [11]. This fundamental

difference explains the strong potential of heat pumps to reduce both final energy consumption and CO_2 emissions in the heating sector.

Beyond their thermodynamic advantages, heat pumps play a strategic role in the energy transition by enabling the decarbonisation of heating in parallel with the decarbonisation of the electricity sector. The shift away from on site fuel combustion also leads to the elimination of local emissions of nitrogen oxides and particulate matter, resulting in important air quality and public health co-benefits, particularly in urban environments [9]. For these reasons, heat pumps are consistently identified as a foundation technology in long term decarbonisation pathways for the building sector [10].

The detailed thermodynamic modelling of the heat pump system considered in this work is presented in Chapter 2.

1.3. Heat Recovery from Urban Wastewater

Urban sewer systems consist of extensive underground networks designed to collect and convey wastewater generated by human activities together with surface runoff from urban areas. Beyond their primary function of mass transport, wastewater streams also carry a significant amount of thermal energy originating from domestic hot water use and other anthropogenic processes.

In residential buildings, a substantial share of supplied water is heated for domestic purposes such as showers, dishwashers, and washing machines and subsequently discharged into the sewer network. As a result, a non negligible fraction of the thermal energy delivered to buildings, is dissipated through wastewater flows and released into the environment without recovery.

The recovery of this waste heat, therefore represents a promising strategy to improve overall energy efficiency and reduce greenhouse gas emissions in the heating sector, particularly when wastewater is employed as the low temperature heat source of a heat pump system [12, 13].

A conceptual layout of a wastewater heat recovery system integrated into an urban heating infrastructure is shown in Figure 1.5.

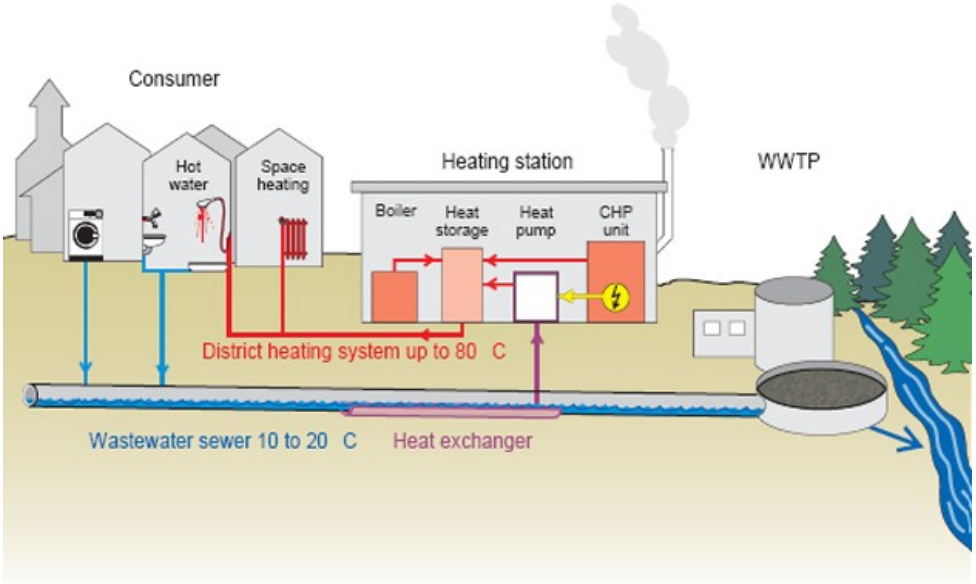

Figure 1.5: Conceptual layout of an urban wastewater heat recovery system [14].

Technical studies indicate that heat losses through wastewater may represent approximately 10–15% of the total thermal energy supplied to buildings, with values increasing up to 30% in highly insulated or low energy buildings, where domestic hot water becomes the dominant load [14, 15].

From an energy systems perspective, wastewater offers favourable conditions for heat recovery due to the combination of relatively stable temperatures, continuous flow rates, and spatial proximity to urban heat demand. When coupled with heat pump technology, these characteristics enable efficient heat extraction within existing sewer infrastructure, as demonstrated in several urban scale applications [13].

Although still limited in large scale deployment, pilot projects and feasibility studies have confirmed the technical feasibility and energy saving potential of wastewater heat recovery systems [15]. By exploiting existing public infrastructure, these solutions minimise additional land use and reduce the environmental footprint associated with new energy installations, making them a promising option for sustainable heating in dense metropolitan areas.

The objective of this thesis is therefore to analyse and model a heat pump system that exploits urban wastewater as a low grade thermal source within a dense metropolitan context.

1.3.1. Urban Wastewater as a Source of Low-Grade Thermal Energy

Urban wastewater can be regarded as a reliable source of low grade thermal energy due to its characteristic temperature levels, flow rates, and temporal availability, without compromising the primary hydraulic function of the sewer system [13]. Monitoring campaigns conducted in urban sewer networks have shown that wastewater retains a significant amount of thermal energy originating from domestic hot water use and other human related activities.

In sewer systems serving residential and mixed use urban areas, wastewater temperatures, during the heating season, are often higher than ambient air temperatures due to domestic hot water usage and other indoor activities [12]. Moreover, unlike air source systems, wastewater exhibits relatively limited short term temperature fluctuations and reduced sensitivity to outdoor weather conditions. Monitoring studies have shown that its temperature remains within a comparatively narrow range even under cold ambient conditions, resulting in more stable and predictable operating conditions for heat pump systems. The combination of comparatively higher winter temperature levels and enhanced thermal stability makes urban wastewater a particularly favourable low temperature heat source for heat pump applications in cold and temperate climates.

In addition to temperature, the thermal potential of wastewater is strongly influenced by the flow rates conveyed through the sewer network. In dense urban environments, wastewater flows are typically continuous and closely correlated with population density and daily water consumption patterns [13].

These features are particularly relevant in dense urban contexts, where reliability and continuity of heating supply are critical requirements [14, 16].

An example of the simultaneous variability of wastewater temperature, outdoor air temperature and flow rate is shown in Figure 1.6, which reports monitoring data collected in the sewer network of Bologna during an experimental study [13]. The figure highlights the reduced thermal variability of wastewater compared to ambient air, as well as the characteristic daily oscillations of flow rate driven by user behaviour. It should be emphasised that the dataset presented in the figure is reported here for illustrative purposes only, in order to qualitatively demonstrate the typical variability of the source. The specific boundary conditions adopted for the thermodynamic modelling developed in this work are based on different datasets, which are introduced and discussed in detail in the following sections.

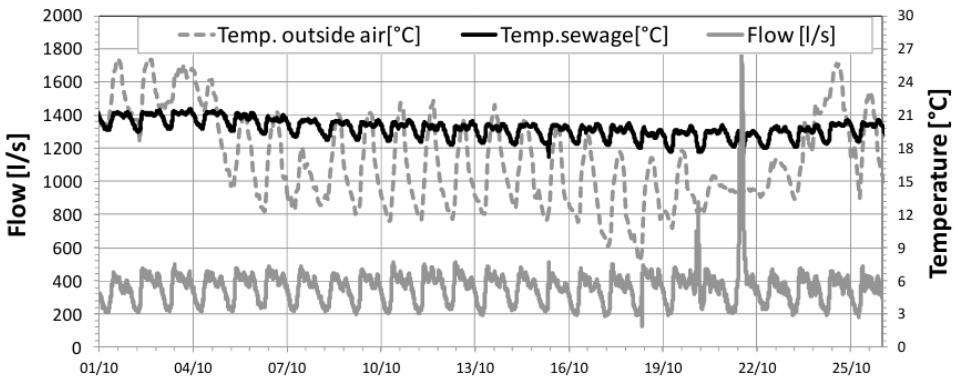

Figure 1.6: Monitoring data of wastewater temperature and flow rate in the Bologna sewer network [13].

1.3.2. Comparative advantages and limitations

Beyond technological aspects, wastewater heat recovery presents both advantages and limitations when compared to other low-temperature heat sources commonly exploited by heat pumps.

Main advantages:

- Wastewater exhibits relatively limited short term temperature fluctuations and reduced exposure to extreme winter conditions compared to air source systems, resulting in more favourable and stable heat pump performance [13].
- Compared to ground source systems, sewer based solutions avoid borehole drilling and the associated spatial, economic, and regulatory constraints, which are particularly limiting in dense urban areas [13].
- Urban sewer networks enable a distributed approach to heat recovery, exploiting existing underground infrastructure without the need for dedicated insulated heat distribution pipelines, thereby reducing land use, construction impacts, and social disruption [15].
- The combination of stable temperature levels and sustained flow rates makes wastewater particularly suitable for medium and large scale heat recovery applications.

Main limitations and constraints:

- The recoverable thermal power depends on the allowable temperature reduction of the effluent, which is limited by hygiene requirements, sedimentation risks, and downstream biological treatment constraints [15].

- Heat extraction systems must not interfere with the primary hydraulic function of the sewer network, requiring careful design and regulatory compliance [15].

In the Italian context, feasibility studies conducted on existing sewer networks have confirmed the relevance of wastewater as a low grade heat source in metropolitan areas such as Milan, where high thermal demand and extensive sewer infrastructure coexist [15]. This technological approach forms the basis of the system investigated in the present work.

1.3.3. Technologies of Wastewater Heat Recovery

From a technological perspective, wastewater heat recovery in sewer networks can be implemented through different configurations, which mainly differ in the way thermal energy is extracted from the wastewater stream.

- The most commonly adopted solution in dense urban contexts consists in the installation of heat exchangers directly integrated into the sewer conduits. In this configuration, thermal energy is transferred from the wastewater flow to an intermediate heat transfer fluid without extracting the wastewater from the network. The heat exchanger is incorporated into the sewer structure itself, ensuring hydraulic continuity and avoiding disturbances to the primary function of the sewer system [15]. A schematic representation of this technological solution is shown in Figure 1.7. This configuration represents the reference technology considered in the present work, in accordance with the feasibility studies conducted on the sewer network of the city of Milan.

Figure 1.7: Example of an in sewer integrated heat exchanger installed directly within an urban sewer conduit [14].

In the system analysed in this thesis, the in sewer heat exchanger is hydraulically

coupled to the heat pump through a closed intermediate water loop. This circuit transfers heat from the wastewater to the evaporator while ensuring hydraulic decoupling, operational flexibility, and protection of heat pump components from fouling and contamination. Although the wastewater flow remains within the sewer network, the intermediate loop introduces design and control features partially analogous to those of external heat exchanger configurations.

- An alternative technological option involves the temporary extraction of wastewater from the sewer network through dedicated interception structures. In this case, the wastewater is conveyed to an external heat exchanger after undergoing preliminary filtration to remove coarse solids and sediments. Following heat extraction, the cooled wastewater is subsequently returned downstream to the sewer network. While this configuration offers greater flexibility in terms of heat exchanger sizing and maintenance, it generally entails higher auxiliary energy consumption associated with pumping and filtration systems, as well as increased system complexity [13, 14].

Each configuration presents specific advantages and operational constraints that must be evaluated according to the urban context and the scale of application.

In sewer heat exchangers are generally characterised by lower auxiliary energy consumption, compact integration within existing infrastructure, and minimal impact on the hydraulic regime of the sewer network. These features make them particularly suitable for dense urban environments, where spatial and logistical constraints limit the feasibility of additional installations.

Conversely, external heat exchanger configurations provide greater accessibility for maintenance and more flexible control of the heat transfer process, but typically require additional pumping and filtration systems. As a result, they involve higher operational complexity, increased auxiliary energy demand, and a more significant impact on overall system layout [15].

1.3.4. Urban Infrastructure and Applicability in Dense Cities

The feasibility and effectiveness of wastewater based heat recovery systems are strongly dependent on the characteristics of the urban environment in which they are deployed. Dense cities are characterised by high and continuous thermal demand, primarily driven by space heating and domestic hot water consumption in residential and tertiary buildings, while at the same time being served by extensive sewer networks that continuously collect wastewater generated by human activities. The coexistence of concentrated heat demand and significant wastewater flows creates favourable boundary conditions for the

implementation of wastewater heat recovery technologies [13, 16].

This relationship is illustrated in Figures 1.8 and 1.9. Figure 1.8 shows the spatial distribution of the hourly heat demand in the city of Milan, highlighting the concentration of thermal loads within the dense urban areas. Figure 1.9 presents the spatial distribution of the wastewater heat recovery potential along the main sewer collectors.

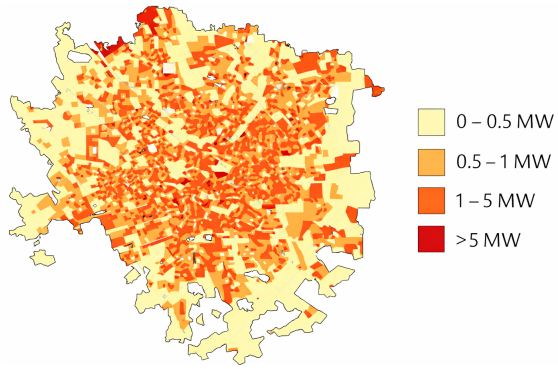

Figure 1.8: GIS map of the heat demand distribution in Milan [17].

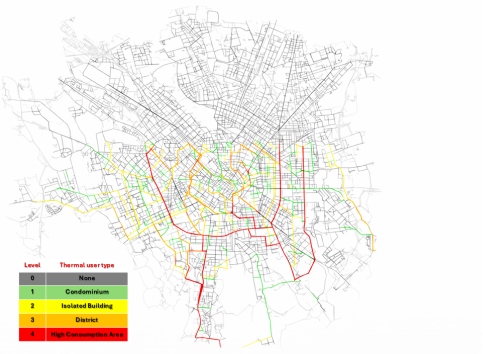

Figure 1.9: GIS map of the wastewater heat recovery potential in Milan [18].

A clear spatial correspondence emerges between zones characterised by high heat demand and sections of the sewer network with higher thermal potential. Areas with significant heating requirements are typically associated with intensive domestic hot water use and daily activities that increase wastewater flow rates and temperatures. As a consequence, the availability of recoverable thermal energy in the sewer system naturally increases where the demand for heating is higher, leading to a favourable demand supply matching for wastewater based heat pump applications.

From an infrastructural perspective, sewer networks constitute an extensive underground system that permeates the entire urban fabric. This spatial distribution enables potential heat recovery points to be located close to thermal users, thereby reducing distribution losses and facilitating the integration of heat pump systems at building or district scale. Compared to conventional district heating systems, which require the installation of dedicated insulated pipelines, wastewater based heat recovery solutions exploit existing infrastructure, limiting additional land use and construction works in highly urbanised areas [15].

From an economic and social standpoint, the integration of heat recovery systems within sewer infrastructure offers additional advantages. By avoiding extensive excavation works and the construction of new energy distribution networks, this approach reduces capital costs and limits disruptions to urban activities, traffic, and residents. Such aspects are

especially important in historical city centres and densely built districts, where technical, regulatory, and social constraints often limit the adoption of conventional renewable heating solutions [13, 15].

All these considerations are particularly relevant for large metropolitan areas such as the city of Milan, which represents a well documented case study for the application of wastewater based heat recovery in dense urban environments.

In this framework, the integration of wastewater heat recovery within existing district heating infrastructures represents a coherent and technically viable strategy for large urban systems. In the present work, the wastewater source heat pump is conceived as a generation unit supplying thermal energy to an existing district heating network in the city of Milan.

The specific characteristics of the urban context and sewer infrastructure considered in this work are analysed in detail in the subsequent case study section, providing the real world framework for the system modelling and performance assessment.

1.4. Cases Study: from MM Feasibility Studies to the Development of the Wastewater Source Heat Pump Model for District Heating Integration

1.4.1. MM Feasibility Study on CHP–Heat Pump Integration for District Heating

MM S.p.A. carried out an executive feasibility study concerning the implementation of a pilot cogeneration plant integrated with a large scale heat pump in the city of Milan [19], [20],[21].

The project, entitled “Progetto sperimentale per un impianto pilota di cogenerazione asservito alla centrale AP Salemi”, was conceived as an energy efficiency intervention aimed at improving the overall performance of the MM aqueduct service centre while simultaneously supplying thermal energy to the existing district heating network operated by A2A Calore & Servizi.

The installation site is located within the premises of the MM aqueduct facility in the northern area of Milan, in close proximity to the district heating plant. The spatial relationship between the two infrastructures is shown in Figure 1.10, which highlights the aqueduct service centre, the district heating plant, and the designated installation area.

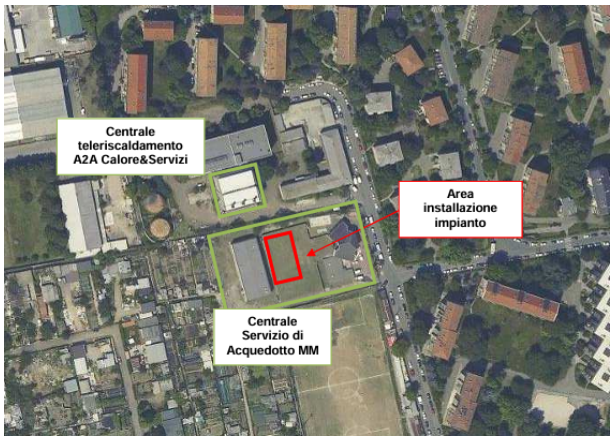

Figure 1.10: Installation site and adjacent district heating plant [19].

The executive design includes two natural gas fired combined heat and power units and a 3 MW_{th} water-water heat pump. In the proposed configuration, the heat pump extracts low grade thermal energy from groundwater upstream of the drinking water treatment process, while the cogeneration units generate both electricity and recoverable heat. The thermal output of the integrated system is delivered to the district heating network, contributing to its overall heat production.

A central objective of the study is the evaluation of the plant under high efficiency cogeneration criteria, including the assessment of primary energy savings and energy production balances. The electricity generated by the cogeneration units partially supplies the heat pump compressor and auxiliary systems, creating a coupled electricity and heat generation scheme aimed at maximising overall system efficiency.

It is important to emphasise that the MM study focuses primarily on the design, optimisation, and regulatory qualification of the generation plant. Although the district heating network constitutes the thermal sink of the system, the detailed characterisation of the urban heat demand and its temporal variability is not addressed in the original analysis, which remains focused on the performance of the cogeneration and groundwater heat pump configuration.

1.4.2. MM Feasibility Study on Wastewater Heat Recovery for District Heating

MM s.p.a studied also the feasibility of a wastewater heat pump recovery system implemented within the urban sewer network of the city of Milan and derives from the feasibility study provided by the local water utility. The analysed configuration refers to a specific sewer conduit located along a defined street within the city and connected to a residential

social housing building comprising 156 apartments, which represents the reference thermal user considered in the original technical documentation. The spatial location of the sewer conduit and the associated residential building within the urban fabric of Milan is illustrated in Figure 1.11.

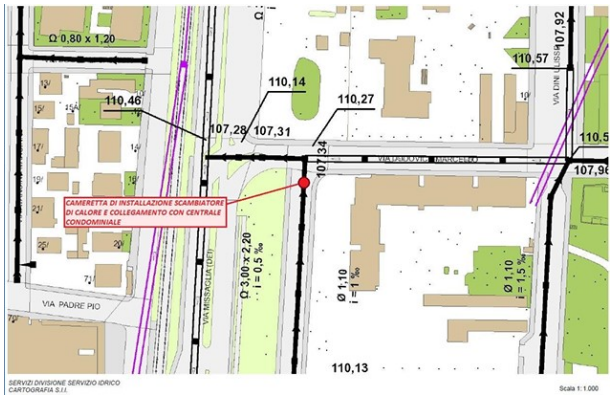

Figure 1.11: Urban location of the sewer conduit and the residential building considered in the case study [15].

The wastewater side of the system, which acts as the low temperature heat source for the heat pump analysed, is described in the technical documentation provided by the local water utility and referred to a specific sewer conduit where conveys wastewater generated primarily by residential users, with a heat exchanger integrated directly into the sewer infrastructure as showed in Figure 1.12 [15]. Although the sewer section is associated with a specific location, it is considered representative of typical operating conditions encountered within the Milan urban sewer network. It provides a realistic generalisable framework for investigating the applicability of wastewater based heating solutions in dense urban environments.

Figure 1.12: Example of an existing urban sewer conduit equipped with an integrated heat exchanger for wastewater heat recovery, as considered for the case study [15].

1.4.3. Model-Based Extension of the MM Wastewater Heat Recovery System

Building upon this real infrastructure configuration, the present work focuses on the design and performance analysis of a heat pump system using urban wastewater as the low temperature heat source and supplying thermal energy to a district heating network, which represents the thermal demand to be satisfied by the residential users. The heat pump is dimensioned to operate as the primary heat generation unit for the considered thermal users, while auxiliary systems are assumed to supply the residual load when the heat pump operates at its maximum feasible thermal output. A schematic representation of the overall system layout, highlighting the wastewater side, the heat pump unit, and the district heating network, is shown in Figure 1.13.

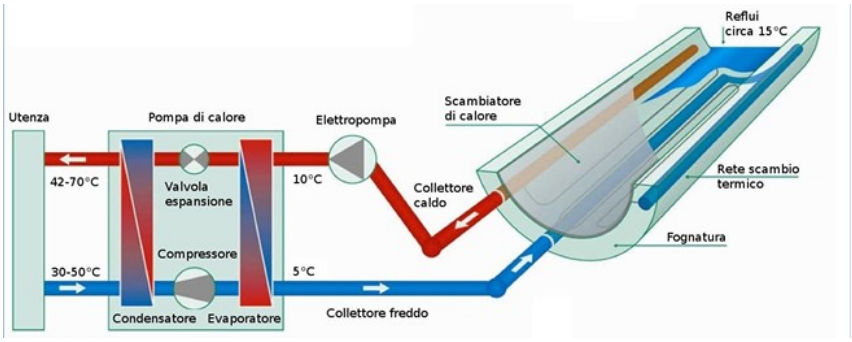

Figure 1.13: Schematic representation of the wastewater source heat pump system integrated into the urban sewer network [15].

The scope and modelling approach of the present work are outlined in Section 1.5, with particular emphasis on the development of on design and of -design models to account for the variability of both the heat source and the heat sink, together with the assessment of the corresponding CO_2 emissions.

1.5. Scope of the Work and Methodological Approach

The objective of this thesis is to develop and apply a comprehensive modelling framework for the analysis of a wastewater source heat pump system coupled with an electric boiler supplying an urban heating network under realistic, time varying operating conditions. The work focuses first on the detailed thermodynamic modelling of a heat pump based on a double vapour compression cycle, through the development of both on design and off design models when coupled with urban wastewater as a low grade heat source and district heating as the thermal sink. Building upon the heat pump model, the overall

hybrid system including the electric boiler is then analysed. For assigned wastewater mass flow rate and temperature levels, the study investigates the appropriate sizing of the district heating load that maximises CO_2 emission savings compared to a fully natural gas based heating scenario.

As a first step, a detailed on design thermodynamic model of the heat pump cycle is developed. The vapour compression cycle is fully characterised by calculating all the thermodynamic state points and ensuring convergence on the condenser operating temperature. Energy and mass balances are systematically verified, and the main system components are dimensioned, including the two compressors and the evaporator, condenser and subcooler heat exchangers, by means of appropriate heat transfer equations. This on design analysis defines the reference operating conditions of the system and provides the geometric and performance parameters required for subsequent analyses.

Building upon the on design formulation, an off design modelling approach is then developed in order to describe the heat pump behaviour under variable operating conditions. The off design model accounts for variations in both the heat source and the heat sink, allowing the system performance to be evaluated as a function of changing wastewater temperatures and flow rates, as well as time dependent thermal demand imposed by the district heating network.

In parallel, a dedicated data processing procedure is implemented to organise the available input data on an annual basis with hourly resolution. For each hour of the reference year, both the thermal demand of the district heating network and the corresponding availability of wastewater are defined. The dataset is further classified according to ambient temperature ranges, allowing operating conditions to be grouped into representative thermal regimes. This approach enables a structured and consistent analysis of system behaviour under different climatic and demand conditions.

Finally, the developed off design model is integrated into a numerical simulation framework operating on an hourly basis over the annual time. Both the wastewater source and the district heating demand are described through time resolved datasets covering an entire year, allowing the system to be analysed under realistic and dynamically varying operating conditions. The organised time series data are used to reproduce realistic operating conditions, and the heat pump system is simulated in combination with an auxiliary heat generation unit to ensure full coverage of the thermal load.

The analysed configuration therefore operates as a hybrid heat generation system, in which the wastewater-source heat pump supplies the base thermal load while an auxiliary electric boiler covers residual loads under constrained operating conditions.

For assigned wastewater mass flow rate and temperature levels, treated as fixed source constraints over the analysed period, the study investigates the appropriate sizing of the district heating side served by the heat pump. Starting from a reference district heating demand profile, the share of thermal load supplied by the heat pump and the electric boiler is varied, changing the heating demand profile considered. For each configuration, annual simulations are performed to evaluate system performance and associated CO_2 emissions.

This approach enables the identification of the district heating integration level that maximises greenhouse gas emission reductions compared to a reference scenario in which the entire thermal demand is supplied by conventional natural gas boilers. The results therefore demonstrate that, for a given wastewater availability, an optimal an optimal integration level and system sizing exists, corresponding to the maximum achievable CO_2 mitigation potential of the proposed configuration.

2 | Heat Pump Cycle Description

This chapter focuses on the wastewater source heat pump cycle adopted for both the on design and off design analyses, which constitutes the core component of the overall hybrid energy system analysed in this work. The system considered consists of a heat pump integrated with an urban wastewater heat source and coupled to a district heating network, forming a complete and coherent framework for the recovery and upgrading of low temperature thermal energy.

From a system perspective, the configuration showed in Figure 2.1, includes the heat pump and an auxiliary electric boiler which supplies the residual thermal demand whenever the heat pump reaches its maximum available capacity or, more generally, in hybrid sizing scenarios. In the present work, however, the reference on design condition is defined and sized to cover the full nominal district heating load, while the auxiliary unit is only activated under off design operating conditions.

Figure 2.1: Hybrid Configuration of the system.

The heat pump represents the core of the system and is based on a double stage vapour compression cycle. Its thermodynamic layout, the selected working fluid and all the main components are described in detail, including the evaporator, the condenser, the intermediate heat exchangers, the two compressors, the expansion devices and the auxiliary hydraulic circuits, in order to provide a clear and physically consistent representation of the cycle operation.

2.1. System layout and cycle configuration

The heat pump system analysed in this work is based on a double stage vapour compression cycle, selected to accommodate the large temperature lift required between the low

temperature wastewater heat source and the district heating network. In accordance with established design practices for high temperature lift applications [11], the total pressure rise between the evaporation and condensation levels is distributed across two compression stages, leading to a reduction of the compression ratio associated with each compressor.

Compared to a conventional single stage vapour compression cycle, this configuration results in lower compressor discharge temperatures and reduced thermodynamic irreversibilities, which is particularly relevant for the present application. Moreover, due to vapour separation in the flash chamber, the first compressor handles a reduced refrigerant mass flow rate, leading to lower compression power for a given enthalpy rise. The combination of a low temperature heat source and a high temperature district heating network would otherwise impose severe operating conditions on a single stage compressor, potentially leading to reduced efficiency and critical discharge temperatures.

As a consequence, the adoption of a double stage vapour compression cycle enables higher coefficients of performance and improved operational reliability under the boundary conditions imposed by the wastewater source and the district heating network.

A schematic representation of the system configuration is shown in Figure 2.2.

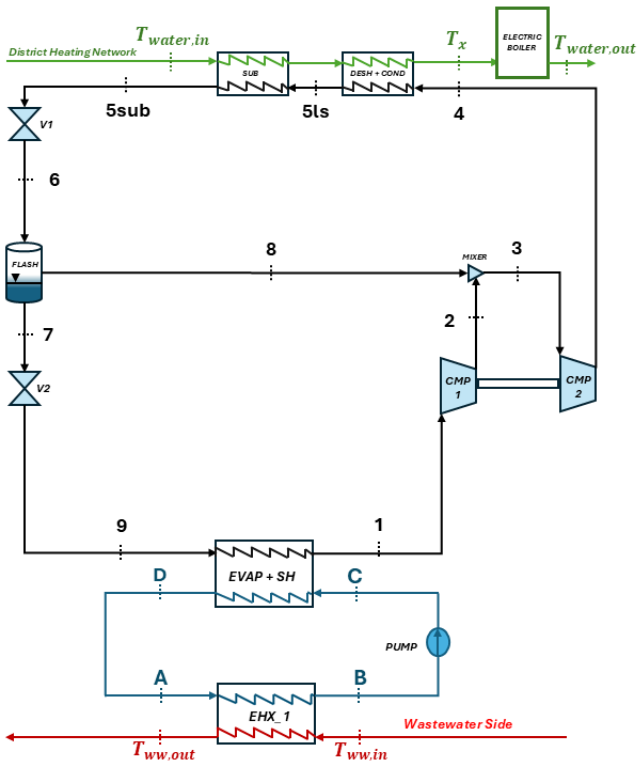

Figure 2.2: Layout of the system.

The corresponding thermodynamic cycle is represented in the T–s diagram shown in

Figure 2.3.

The overall system is structured into three main sections: the wastewater side, which acts as the low temperature heat source coupled with the intermediate water loop, the heat pump unit, responsible for upgrading the recovered thermal energy; and the district heating network, which represents the thermal sink and defines the heat delivery requirements. On the source side, thermal energy is extracted from the urban wastewater flowing in the sewer network. In order to ensure hydraulic separation, mitigate fouling related issues, and guarantee operational flexibility, the wastewater stream does not interact directly with the refrigerant. Instead, heat is transferred to an intermediate water circuit through a dedicated heat exchanger integrated into the sewer conduit. The intermediate loop operates with water as heat transfer fluid.

The intermediate water loop conveys the recovered thermal energy to the evaporator of the heat pump, where heat is transferred to the refrigerant of the low temperature stage of the double vapour compression cycle. The refrigerant selected for the heat pump is R1234ze, which circulates within the vapour compression cycle. After evaporation and slight superheating at low pressure, the refrigerant enters the first compression stage, where it is compressed up to an intermediate pressure level.

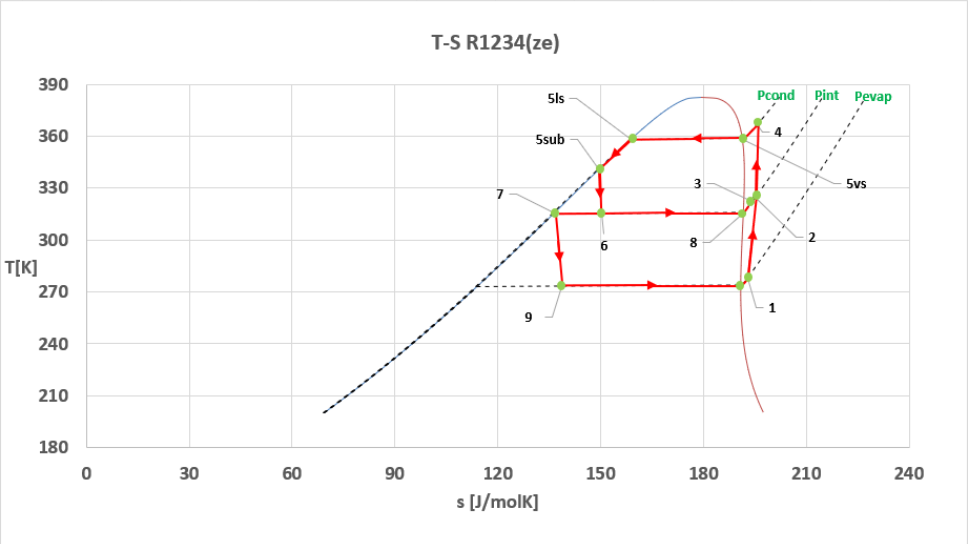

Figure 2.3: T–s diagram of the thermodynamic cycle.

Upstream of the evaporator, the cycle includes a flash chamber operating at an intermediate pressure, where partial phase separation of the refrigerant occurs. The separated liquid fraction is expanded to the evaporation pressure and sent to the evaporator, where it contributes to heat absorption from the intermediate water loop. Downstream of the first compression stage, the vapour at evaporator pressure mixes with the vapour frac-

tion originating from the flash chamber, and the combined stream is then directed to the second compression stage.

The refrigerant vapour is subsequently compressed to the high pressure level by the second compressor and releases thermal energy on the sink side of the system. Heat rejection occurs at condenser pressure and supplies thermal energy to the district heating network, covering space heating and domestic hot water demand for residential users. After heat rejection, the refrigerant completes the cycle through the expansion processes before returning to the low-pressure side.

Overall, this configuration allows the heat pump to operate efficiently under the temperature constraints imposed by both the wastewater heat source and the district heating network. The combined adoption of a double vapour compression cycle and an intermediate water loop provides a flexible and robust system layout, which is particularly suitable for integration within existing urban sewer infrastructure and district heating systems. In the Subsection 2.1.2, the individual components of the heat pump cycle are introduced from a functional perspective only, while their detailed thermodynamic modelling and geometric sizing under on design conditions are addressed in Chapter 3 and 4.

2.1.1. Acronyms

For clarity and reference purposes, Table 2.1 reports the acronyms adopted in this work for the main components of the heat pump cycle.

Acronym	Component
EVAP	Evaporator
COND	Condenser
SUB	Subcooler
FC	Flash Chamber
CMP_LP	Low-Pressure Compressor
CMP_HP	High-Pressure Compressor
V1	Expansion Valve 1
V2	Expansion Valve 2
EHX_1	Heat Exchanger between wastewater side and intermediate cycle

Table 2.1: Acronyms adopted for the main components of the heat pump cycle.

2.1.2. Heat Pump Cycle Components

Evaporator

The evaporator is the component in which thermal energy recovered from the intermediate water loop is transferred to the refrigerant of the heat pump cycle. Its primary function is to promote the phase change of the refrigerant at low pressure, enabling indirect heat recovery from the wastewater source through the intermediate circuit.

As shown schematically in Figure 2.4, the refrigerant enters the evaporator at state point **9** in two phase conditions, at the evaporation pressure P_{evap} of the cycle, at which the evaporator operates, as will be discussed in more detail in Chapter 3 and 4. Within the evaporator, the refrigerant undergoes complete evaporation and is subsequently slightly superheated within the same component, reaching state point **1** at the evaporator outlet. The combined evaporation and superheating processes ensure that only vapour enters the first compression stage, thereby preventing liquid ingestion by the compressor and contributing to stable system operation.

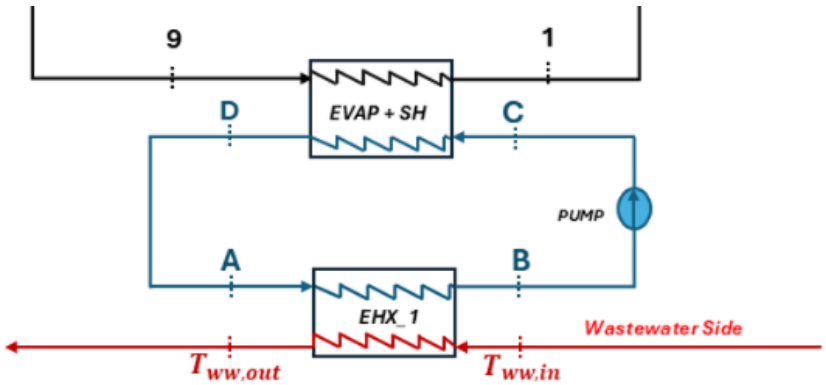

Figure 2.4: Evaporator and EHX_1 in the layout of the system.

The thermal energy required for the evaporation and superheating of the refrigerant is supplied by the intermediate water loop. Water flows through the evaporator on the secondary side and is cooled from an inlet temperature T_c to an outlet temperature T_d as heat is transferred to the refrigerant. In this way, the intermediate circuit provides the thermal link between the wastewater heat exchanger and the refrigerant cycle while maintaining hydraulic separation between the two systems.

Condenser

The condenser is the component in which thermal energy is released from the refrigerant to the district heating network. It operates at the condensation pressure of the cycle and

represents the interface between the heat pump and the thermal sink.

As shown schematically in Figure 2.5, the refrigerant enters the condenser at state point **4** as superheated vapour. Within the condenser, the refrigerant is first desuperheated until saturated vapour conditions at condensation pressure P_{cond} at state point **5sv**. Subsequently, condensation occurs at approximately constant pressure, leading the refrigerant to the saturated liquid state at point **5ls**. During these processes, thermal energy is transferred from the refrigerant to the district heating water. The heat rejected by the refrigerant is used to supply the district heating network, thereby covering space heating and domestic hot water demand.

On the secondary side, water flows through the condenser and is heated from an inlet temperature denoted as T_x to the outlet temperature $T_{\text{water,out}}$. The inlet temperature T_x is calculated as part of the thermodynamic analysis of the system and therefore assumes a well defined value under on design conditions, while it is allowed to vary during off-design operation. The outlet temperature $T_{\text{water,out}}$ is fixed according to the district heating requirements and is set to 80 °C.

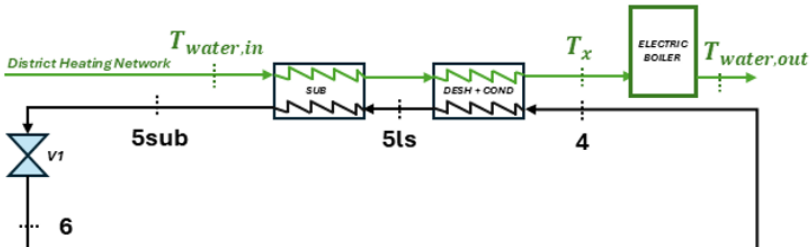

Figure 2.5: Condenser and Subcooler in the layout of the system.

Subcooler

The subcooler is a heat exchanger located downstream of the condenser and is used to further cool the refrigerant after the condensation process. Its primary function is to subcool the refrigerant at high pressure, thereby increasing the overall thermodynamic efficiency and stability of the heat pump cycle.

As shown schematically in Figure 2.5, the refrigerant enters the subcooler at state point **5ls** as saturated liquid at the condensation pressure P_{cond}. Within the subcooler, the refrigerant is cooled below the saturation temperature at approximately constant pressure, reaching the subcooled liquid state at point **5sub**. This additional cooling reduces the vapour quality at the inlet of the subsequent expansion process and contributes to a more stable and efficient operation of the evaporator. The thermal energy released during the subcooling process is transferred to the district heating water.

On the secondary side, water flows through the subcooler and is heated from the inlet temperature $T_{\text{water,in}}$ to the intermediate temperature T_x. As will be discussed, the inlet temperature $T_{\text{water,in}}$ is fixed under design conditions and set equal to 60 °C, while the temperature T_x is calculated as discussed in the condenser description.

Expansion valves

The expansion valves including are two. They operates at different pressure levels, which are used to reduce the refrigerant pressure between the condensation pressure P_{cond}, the intermediate pressure P_{int} and the evaporation pressure P_{evap}. The value of the intermediate pressure P_{int} is determined as part of the thermodynamic analysis of the cycle, as discussed in Chapter 4. Both expansion devices are modelled as throttling valves, in which the pressure reduction occurs through an isenthalpic process.

As shown schematically in Figure 2.6, the first expansion valve is located downstream of the subcooler and expands the refrigerant from the condensation pressure P_{cond} to the intermediate pressure P_{int}. The refrigerant enters at state point **5sub** and exits at state point **6**. This pressure reduction allows the refrigerant to reach the intermediate pressure level required for the subsequent flash separation process.

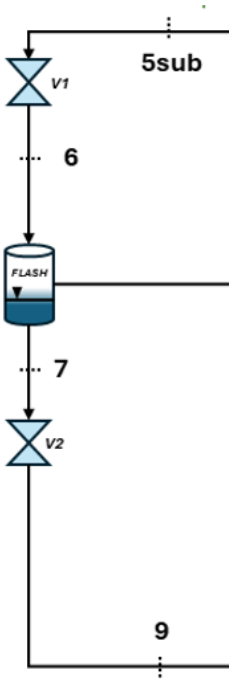

Figure 2.6: Expansion valves in the layout of the system.

Downstream of the flash chamber, the second expansion valve further reduces the refrigerant pressure from the intermediate pressure P_{int} to the evaporation pressure P_{evap}. The

liquid fraction separated in the flash chamber at state point **7** is expanded through this second expansion valve and reaches the evaporator in two phase conditions at state point **9**.

The use of two expansion valves is intrinsic into the double stage vapour compression cycle, as it allows the overall pressure drop to be split into two throttling processes, defining an intermediate pressure level for vapour liquid separation in the flash chamber and reducing thermodynamic irreversibilities compared to a single stage cycle [11].

Flash chamber

The flash chamber is an intermediate separation device integrated within the double vapour compression cycle and operates at the intermediate pressure P_{int}. Its primary function is to separate the refrigerant stream into vapour and liquid phases following the first expansion process. It performes vapour liquid phase separation, directing the vapour fraction to the second compression stage and the liquid fraction to the evaporator, thereby improving thermodynamic performance and cycle stability.

As shown schematically in Figure 2.7, the refrigerant enters the flash chamber at state point **6** in two phase conditions after undergoing an isenthalpic expansion from the condensation pressure P_{cond} to the intermediate pressure P_{int} through the first expansion valve. Inside the flash chamber, the refrigerant is separated into a vapour fraction and a liquid fraction at the same pressure level. The liquid phase exits the flash chamber at state point **7**, while the vapour phase is extracted at state point **8**. The liquid fraction separated at state point **7** is subsequently expanded through the second expansion valve from the intermediate pressure P_{int} to the evaporation pressure P_{evap}, reaching the evaporator inlet at state point **9**. In parallel, the vapour fraction extracted at state point **8** is sent to the high pressure side of the cycle and mixed with the vapour stream compressed by the low pressure compressor. This mixing process results in a homogeneous vapour stream at state point **3**, which is then compressed by the second compressor.

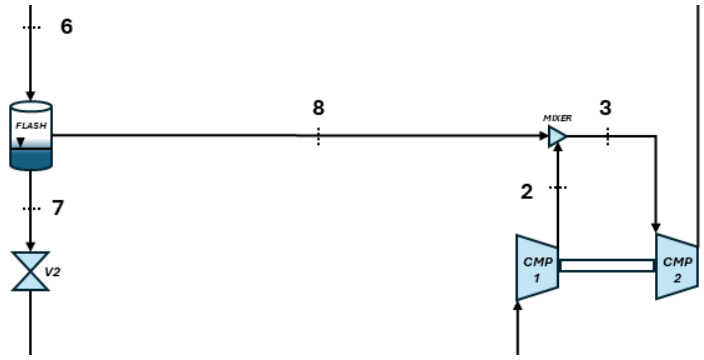

Figure 2.7: Flash chamber in the layout of the system.

Compressors

The compressors are two and operating at different pressure levels, which allow the overall pressure rise between the evaporation pressure P_{evap} and the condensation pressure P_{cond} to be distributed across two compression stages. This configuration is adopted to improve the thermodynamic performance of the cycle and to reduce the compression ratio and discharge temperature associated with each individual compressor. In this way a more favourable distribution of the total compression work is possibile, reducing thermodynamic irreversibilities and improving efficiency and reliability [11].

As shown schematically in Figure 2.8, the first compressor operates at low pressure and compresses the refrigerant between the evaporation pressure P_{evap} and an intermediate pressure P_{int}, processing the refrigerant stream from point **1** to **2**. The refrigerant mass flow rate handled by this compressor corresponds to the vapour flow rate leaving the evaporator. The liquid fraction separated in the flash chamber at state point **7**, is expanded through the second expansion valve down to state point **9** and therefore does not pass through the low pressure compression stage. Downstream of the first compressor, the compressed vapour stream at state point **2** is mixed with the vapour fraction separated in the flash chamber at state point **8**. This mixing process occurs in a dedicated mixer located upstream of the second compression stage and results in a homogeneous vapour stream at state point **3**.

The second compressor operates between the intermediate pressure P_{int} and the condensation pressure P_{cond} and processes the entire refrigerant mass flow rate circulating in the cycle. The refrigerant is compressed from state point **3** to state point **4** before entering the condenser. Unlike the first compression stage, the high pressure compressor therefore handles the full mass flow rate, but over a smaller pressure ratio.

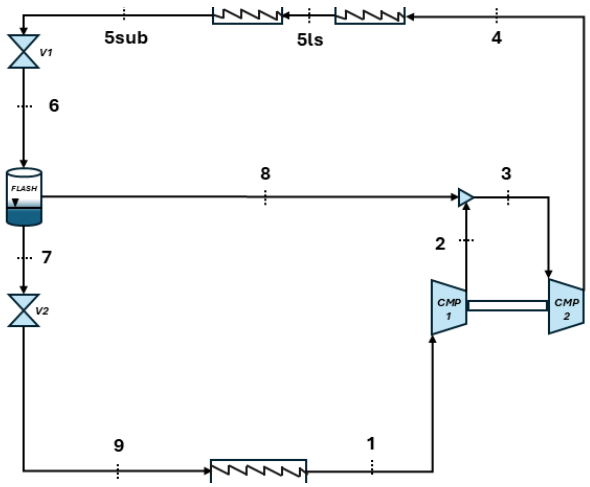

Figure 2.8: Compressors in the layout of the system.

2.2. Working fluids selection and characterisation

The analysed heat pump system is characterised by the use of different working fluids in the vapour compression cycle, the intermediate heat transfer loop and the wastewater source side, according to the specific requirements of each subsystem. The selection of the working fluids is a key design aspect, as it affects the thermodynamic performance, environmental impact, operational reliability, and modelling assumptions adopted for the system.

2.2.1. Refrigerant in the heat pump cycle

The selection of R1234ze as working refrigerant in the present heat pump system is supported by the study of Ben Jemaa et al. [22], who investigated the use of R1234ze as a replacement for R134a in a vapour compression chiller through a detailed energy and exergy analysis. Although the reference system analysed in the paper is a chiller, the reported results are directly applicable to heat pump applications, as both technologies are based on the same vapour compression cycle and the thermodynamic properties of the refrigerant remain unchanged.

From an environmental perspective, the primary motivation for replacing R134a with R1234ze is the significant reduction in global warming potential. As reported by Ben Jemaa et al. [22] and summarised in Figure 2.9, R1234ze is characterised by a GWP of only a few units, whereas R134a exhibits a GWP which exceeding 1400. This marked difference highlights the substantial environmental advantage of R1234ze and explains its progressive adoption as a substitute for R134a, which had been widely used as a standard refrigerant in vapour compression systems until recent years but is increasingly restricted by regulations on fluorinated greenhouse gases.

Table 1 – Safety and environment refrigerant properties.

	R134a	R1234ze
ODP	0	0
GWP	1430	4
ASHRAE safety group	A2L	A1
ASHRAE flammability	No	Yes (low)
ASHRAE toxity	No	No

Figure 2.9: Comparison of the GWP values of R1234ze and R134a [22].

In addition to environmental benefits, the thermodynamic suitability of R1234ze is demonstrated by the performance analysis reported in the same study. The authors evaluated the coefficient of performance and the exergy behaviour of the system as a function of the

evaporating temperature. As shown in Figure 2.10, for a fixed evaporating temperature, the vapour compression system operating with R1234ze achieves coefficients of performance equal to or slightly higher than those obtained with R134a. This indicates that, at comparable heat source temperature levels, the adoption of R1234ze(E) does not penalise the energy efficiency of the cycle.

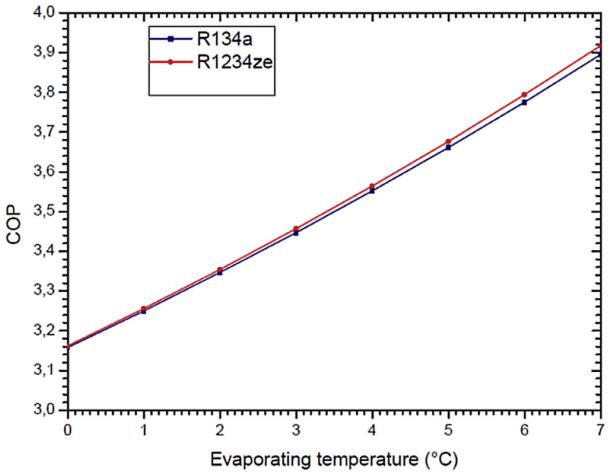

Figure 2.10: COP as a function of T_{evap} for R1234ze and R134a [22].

At the same time, the exergy analysis reveals a systematic reduction in thermodynamic irreversibilities when R1234ze is used as working fluid. For a given evaporating temperature, the total exergy destruction of the cycle is lower than that obtained with R134a, as illustrated in Figure 2.11. This behaviour reflects reduced irreversibilities in the main components of the system, with the compressor representing the dominant source of exergy destruction. Lower exergy losses indicate a more favourable thermodynamic operation and contribute to improved efficiency and operational stability.

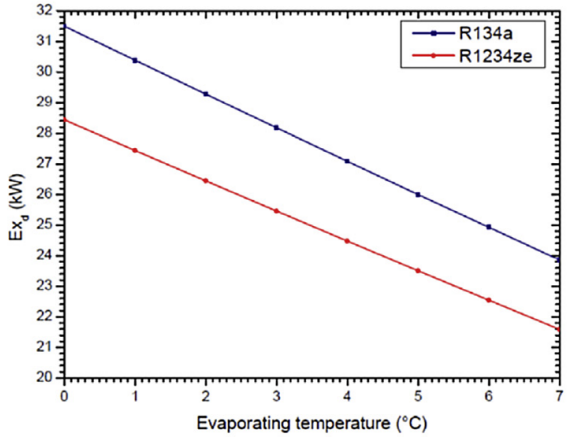

Figure 2.11: Exergy destruction as a function of T_{evap} for R1234ze and R134a [22].

Overall, the combined environmental and thermodynamic analysis confirms that R1234ze represents a suitable replacement for R134a, offering a substantial reduction in climate impact while maintaining, and in some cases improving, the energetic and exergetic performance of vapour compression systems. These considerations justify the adoption of R1234ze as the working refrigerant for the heat pump cycle analysed in this work.

2.2.2. Intermediate heat transfer loop fluid

Heat recovery from the wastewater stream is achieved through an intermediate heat transfer loop operating with water as working fluid. The intermediate circuit provides hydraulic separation between the wastewater and the refrigerant cycle, therefor reducing the risk of fouling and corrosion associated with direct heat exchange with sewer flows [23].

As showed in Figure 2.4, within the wastewater heat exchanger (EHX_1), the intermediate water absorbs thermal energy from the wastewater stream and is heated from state **a** to state **b**. The heated water is then circulated by a dedicated pump, which increases its pressure and conveys the flow from state **b** to state **c**. Downstream of the pump, the intermediate water enters the evaporator of the heat pump, where it transfers the recovered thermal energy to the refrigerant R1234ze.

As heat is released to the refrigerant, the intermediate water is cooled within the evaporator from state **c** to state **d**, thereby providing the thermal input required for the evaporation process. The mass flow rate of the intermediate water loop is not imposed a priori, but is determined as part of the thermodynamic analysis through an energy balance on EHX_1. Since the wastewater side operating conditions are known, the intermediate water mass flow rate can be consistently calculated to satisfy the required heat transfer.

2.2.3. Wastewater heat source

Urban wastewater represents the low temperature heat source for the heat pump system analysed in this work. Thermal energy is extracted from the wastewater stream through the wastewater heat exchanger (EHX_1) and transferred to the intermediate water loop, which supplies the evaporator of the heat pump.

For the purposes of thermodynamic modelling, the wastewater stream is treated as liquid water when evaluating its thermophysical properties. This assumption is adopted in order to simplify the analysis and is justified by the limited influence of dissolved and suspended solids on the bulk thermodynamic behaviour of the fluid within the operating conditions considered in this study.

2.3. Refprop

The thermodynamic modelling of the heat pump cycle requires the accurate evaluation of thermophysical properties of the working fluids at each state point of the cycle. In this work, the thermodynamic properties are evaluated using *REFPROP* (Reference Fluid Thermodynamic and Transport Properties Database), which is an high accuracy property database developed and maintained by the National Institute of Standards and Technology (*NIST*).

REFPROP is based on state of the art equations of state and provides reliable thermodynamic and transport properties for pure fluids and mixtures over wide ranges of temperature and pressure. The database is applicable to subcooled, two phase, and superheated regions, ensuring thermodynamic consistency across all operating conditions encountered in heat pump applications.

For a given working fluid and a selected pair of independent variables, *REFPROP* provides all the thermodynamic and transport properties considered in this work in a consistent manner. These include temperature, pressure, specific enthalpy, specific entropy, vapour quality, density, dynamic viscosity, thermal conductivity, and specific heat capacity at constant pressure. For clarity and compactness, the properties evaluated using *REFPROP* are expressed throughout this thesis using a functional notation, in which each property is represented as a function of the selected pair of independent variables. In the present work, the database is used with the *MOLAR SI* unit system selected, so that thermodynamic properties are returned on a molar basis. This choice ensures internal consistency in the evaluation of thermodynamic properties across the different state points of the cycle and simplifies the direct interfacing with the property routines. The adopted notation, together with the corresponding units returned by *REFPROP* in the *MOLAR SI* unit system, is summarised in Table 2.2.

However, for the purposes of energy balance calculations, mass flow rate determination, and component sizing, several thermodynamic properties must be expressed in mass-specific *SI* units. Consequently, the main molar based properties obtained from *REFPROP* are systematically converted into mass-based quantities using conversion relations to the International System of Units summarised in Table 2.3.

In addition to these quantities, all energy related variables arising from the thermodynamic analysis, such as heat duties and compressor power, are consistently converted from a molar to a mass basis by accounting for the molar mass of the working fluid. In particular, thermal and mechanical energies initially expressed in J/mol are divided by the

molar mass M_{mol} of R1234ze(E), yielding mass-specific values in J/kg and, consequently, power quantities expressed in W.

Property	Function	Description	MOLAR SI
Temperature	$T = f(P, x)$	From pressure and vapour quality	K
Pressure	$P = f(T, x)$	From temperature and vapour quality	Pa
Density	$\rho = f(T, P)$	Molar density	mol/m^3
Enthalpy	$h = f(T, P)$	Molar specific enthalpy	J/mol
Entropy	$s = f(P, h)$	Molar specific entropy	J/(mol K)
Vapour quality	$x = f(P, h)$	Vapour mass fraction	–
Dynamic viscosity	$\mu = f(T, P)$	Dynamic viscosity	$\mu\text{Pa s}$
Thermal conductivity	$k = f(T, P)$	Thermal conductivity	mW/(m K)
Specific heat capacity	$c_p = f(T, P)$	Molar heat capacity at constant pressure	J/(mol K)
Surface tension	$\lambda = f(T, x)$	Surface tension	N/m

Table 2.2: Properties returned by *REFPROP* in the *MOLAR SI* unit system.

Property	MOLAR SI	SI	Conversion relation
T	K	K	–
P	Pa	Pa	–
ρ	mol/m^3	kg/m^3	$\rho = \rho_{\text{mol}}\, M_{\text{mol}}$
h	J/mol	J/kg	$h = h_{\text{mol}}/M_{\text{mol}}$
s	J/(mol K)	J/(kg K)	$s = s_{\text{mol}}/M_{\text{mol}}$
μ	$\mu\text{Pa s}$	Pa s	$\mu = \mu_{\text{mol}} \times 10^{-6}$
k	mW/(m K)	W/(m K)	$k = k_{\text{mol}} \times 10^{-3}$
c_p	J/(mol K)	J/(kg K)	$c_p = c_{p,\text{mol}}/M_{\text{mol}}$
λ	N/m	N/m	–

Table 2.3: Conversion of property units from the *MOLAR SI* unit system to the corresponding mass based *SI* units.

3 | On Design Thermodynamic Model and Component Sizing

This chapter addresses the design phase of the thermodynamic model of the heat pump considered in this work and introduced in Chapter 2. Starting from a set of known boundary conditions and reference operating data, the thermodynamic cycle is dimensioned under on-design conditions in order to determine the nominal pressures, temperatures, mass flow rates, and thermodynamic state points. During this process, the mass and energy balances of the overall cycle and of its main components are systematically verified to ensure the physical consistency of the on-design solution.

The model defines the relationships between the operating variables and the thermodynamic state points under on-design conditions and provides the basis for the on-design performance calculation and component sizing procedure. At this stage of the analysis, the isentropic efficiencies of the compressors are assumed and fixed to a reference value of 0.8. This assumption allows the thermodynamic behaviour of the cycle to be analysed independently of specific machine characteristics and provides a consistent basis for the initial sizing of the system. Subsequently, the isentropic compressor maps are integrated into the model.

The numerical implementation, which computes all cycle state points through an iterative solution procedure and evaluates the energy balance, system performance, and component sizing, is described in Chapter 4.

It should be noted that the T–Q diagrams of heat exchangers presented in Chapter 3 are intended solely for illustrative purposes, while the diagrams including the numerical values of the on design results are reported in Section 4.5. Additionally, it should be clarified that in all T–Q diagrams presented in this work, Q represents the heat duty exchanged under steady state conditions and is expressed in kW, whereas in the analytical formulation the heat transfer rate is explicitly denoted by $\dot{Q}$.

3.1. Model Assumptions and Boundary Conditions

In order to define a consistent reference configuration for the design phase, the heat pump system is analysed under a set of general modelling assumptions. The on design analysis corresponds explicitly to the project phase of the heat pump system and aims at defining a physically consistent reference operating point.

The main modelling assumptions adopted in this work are summarised as follows:

- the analysis is carried out under steady state conditions for all components, with no accumulation of mass or energy;
- all components of the system are assumed to be adiabatic and heat losses to the ambient environment are neglected;
- thermodynamic properties of the working fluid are evaluated assuming local thermodynamic equilibrium;
- pressure losses in the refrigerant circuit are accounted for through equivalent concentrated pressure drops applied at the evaporator and condenser inlets. The adopted values, taken from literature data and reported in Table 3.1, correspond to the lower bound of the ranges reported for refrigerant side pressure drops in heat pump heat exchangers [24], allowing the main effects on operating pressures and compression work to be captured without increasing model complexity;
- pressure drops in the intermediate water loop are modelled through equivalent concentrated losses. A circulation pump is included, and the corresponding pressure losses, taken from literature [25] and reported in Table 3.2, account for both the evaporator side and the EHX_1 side contributions; the resulting pumping power is therefore included in the system model;
- the intermediate water loop is modelled as a single phase incompressible flow, characterised by inlet and outlet temperatures and by the mass flow rate. Under on design conditions, these quantities are uniquely determined from the imposed wastewater boundary conditions and from the prescribed temperature difference across the wastewater to water heat exchanger;
- fouling effects on heat exchanger surfaces are accounted for through fixed fouling thermal resistances derived from literature data [26]. In particular, external fouling is neglected, while internal fouling is retained; this allows their impact on heat transfer performance to be included within the on design modelling framework without resorting to time dependent fouling models,

- the overall electromechanical efficiencies of the two centrifugal compressors and of the circulation pump are assumed constant; the adopted values, accounting for both electric motor and inverter (VFD) efficiencies, are taken from literature data [27, 28] and reported in Table 3.3,
- the hydraulic efficiency of the circulation pump is assumed constant from literature [28] and value is reported in Table 3.3.

REFRIGERANT	
Symbol	**Value**
$\Delta P_{\text{evap,r}}$	2% P_{evap}
$\Delta P_{\text{cond,r}}$	1.5% P_{cond}

Table 3.1: ΔP_{loss} in the heat pump circuit.

INTERMEDIATE CIRCUIT	
Symbol	**Value**
ΔP_{evap}	20 kPa
ΔP_{EHX1}	30 kPa

Table 3.2: ΔP_{loss} in the intermediate flow.

Under these assumptions, the thermodynamic cycle can be fully defined and dimensioned in a physically consistent manner. The resulting on design solution represents the reference configuration of the heat pump system and provides the basis for the off design modelling developed in the following chapter.

Symbol	**Value**
$\eta_{\text{el-mecc,c1}}$	0.95
$\eta_{\text{el-mecc,c2}}$	0.95
$\eta_{\text{el-mecc,pump}}$	0.95
$\eta_{\text{hyd,pump}}$	0.70

Table 3.3: $\eta_{\text{el-mecc}}$ for the two compressors and the circulation pump and hydraulic efficiency $\eta_{\text{hyd,pump}}$ in the on design analysis.

In addition to the general modelling assumptions, the on design analysis is carried out starting from a set of known thermal boundary conditions, derived from the wastewater source, the hydraulic configuration of the system and the requirements imposed by the district heating network.

In particular:

- on the wastewater side, inlet and outlet temperatures ($T_{\text{ww,in}}$, $T_{\text{ww,out}}$) and the wastewater mass flow rate ($\dot{m}_{\text{ww}}$) are treated as known and fixed quantities under design conditions. These parameters define the thermal availability of the heat source and constitute boundary conditions for the on design analysis. The values are reported in Table 3.4.

Quantity	Symbol	Value	Unit
Wastewater inlet temperature	$T_{\mathrm{ww,in}}$	14	°C
Wastewater outlet temperature	$T_{\mathrm{ww,out}}$	10	°C
Wastewater mass flow rate	$\dot{m}_{\mathrm{ww}}$	100	l/s

Table 3.4: Boundary conditions of the wastewater heat source adopted for the on design analysis.

- On the district heating side, the supply and return temperature levels ($T_{\mathrm{water,in}}$, $T_{\mathrm{water,out}}$) are known and fixed, both under on design and off design operating conditions. Values are reported in Table 3.5. Variations in the thermal demand are represented through changes in the required thermal power, which are accommodated by corresponding adjustments of the mass flow rate in the district heating network. Under design conditions, the thermal power exchanged at the condenser is determined consistently within the thermodynamic cycle as a function of the imposed temperature levels and of the thermal availability of the wastewater heat source.

Quantity	Symbol	Value	Unit
District heating supply temperature	$T_{\mathrm{water,in}}$	60	°C
District heating return temperature	$T_{\mathrm{water,out}}$	80	°C

Table 3.5: Boundary conditions of the district heating network adopted for the on design analysis.

- Additionally some temperature differences are imposed across selected heat exchangers within the refrigerant cycle, in order to ensure realistic heat transfer conditions and feasible component sizing. These include the pinch point temperature differences at the wastewater intermediate heat exchanger ($\Delta T_{\mathrm{pp,EHX\_1}}$) and at the evaporator ($\Delta T_{\mathrm{pp,eva}}$), as well as the refrigerant superheating temperature differences (ΔT_{sh}). A minimum approach temperature difference is imposed at the condenser between the condensation temperature and the outlet temperature of the district heating water ($\Delta T_{\mathrm{ap,cond}}$), which is used within the iterative procedure to determine

the condensation temperature T_{cond}. In addiction, an approach temperature difference is imposed at the subcooler between the temperature water inlet of the discrict line and the refrigerant outlet of the subccoler ($\Delta T_{\text{ap,sub}}$). The adopted values of all temperature differences are reported in Table 3.6.

Quantity	Symbol	Value	Unit
EHX_1 pinch point temperature difference	$\Delta T_{\text{pp,EHX\_1}}$	5	K
Evaporator pinch point temperature difference	$\Delta T_{\text{pp,evap}}$	5	K
Refrigerant superheating temperature difference	ΔT_{sh}	5	K
Subcooler approach temperature difference	$\Delta T_{\text{ap,sub}}$	8	K
Condenser approach temperature difference	$\Delta T_{\text{ap,cond}}$	5	K

Table 3.6: Assumed temperature differences adopted for the on design thermodynamic analysis.

3.2. Preliminary Calculation

The first step of the preliminary calculations concerns the thermal analysis of the heat exchange process between the wastewater stream and the intermediate water loop in the wastewater intermediate heat exchanger (EHX_1), showed in Figure 2.4. Under on design conditions, the wastewater mass flow rate and its inlet and outlet temperatures are treated as known quantities. As a result, the thermal power available from the wastewater stream can be directly evaluated as:

$$\dot{Q}_{\text{ww}} = \dot{m}_{\text{ww}}\, c_{p,\text{ww}}\, \left(T_{\text{ww,in}} - T_{\text{ww,out}}\right). \tag{3.1}$$

In accordance with the modelling assumptions introduced in the previous section, the heat exchangers are assumed to operate under adiabatic conditions and heat losses to the surroundings are neglected. As a result, the heat extracted from the wastewater stream is equal to the heat transferred to the intermediate water loop

$$\dot{Q}_{\text{ww}} = \dot{Q}_{\text{EHX\_1}}. \tag{3.2}$$

The intermediate water mass flow rate is therefore determined from the energy balance on EHX_1 as:

$$\dot{m}_{\text{int}} = \frac{\dot{Q}_{\text{EHX\_1}}}{c_{p,\text{int}}\,(T_b - T_a)}, \tag{3.3}$$

where T_a and T_b denote the inlet and outlet temperatures of the intermediate water stream within the heat exchanger.

The temperatures T_a and T_b are determined from the wastewater inlet and outlet temperatures by imposing a minimum pinch point temperature difference $\Delta T_{\text{pp,EHX\_1}}$ at both ends of the heat exchanger. Specifically,

$$T_a = T_{\text{ww,out}} - \Delta T_{\text{pp,EHX\_1}}, \qquad T_b = T_{\text{ww,in}} - \Delta T_{\text{pp,EHX\_1}}. \tag{3.4}$$

The temperatures T_a and T_b can be determined in this manner because the wastewater stream and the intermediate water loop are characterised by equal heat capacity rates, defined as $\dot{m}c_p$. such that $\dot{m}_{\text{ww}}c_{p,\text{ww}} = \dot{m}_{\text{int}}c_{p,\text{int}}$. Under this condition, the temperature profiles of the two fluids within the heat exchanger, represented in a temperature-heat duty (T–Q) diagram, are parallel, as can be observed in Figure 3.1.

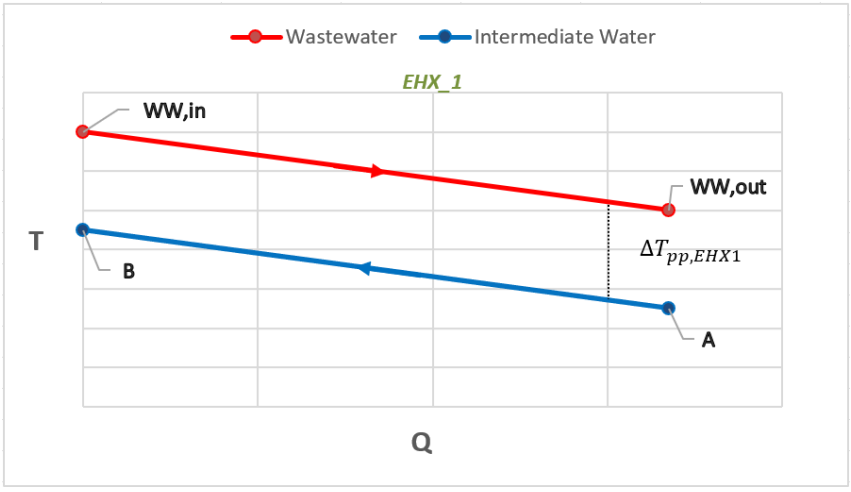

Figure 3.1: T–Q diagram of the EHX1 heat exchanger.

As a consequence, the temperature difference between the wastewater and the intermediate water remains approximately constant along the entire length of the heat exchanger. This allows the imposed pinch point temperature difference $\Delta T_{\text{pp,EHX\_1}}$ to be maintained over the full heat exchange process and enables the direct evaluation of the intermediate water inlet and outlet temperatures, T_a and T_b, from the wastewater inlet and outlet temperatures.

Once the intermediate loop mass flow rate $\dot{m}_{\text{int}}$ is determined, the corresponding volumetric flow rate can be evaluated as:

$$\dot{V}_{\text{int}} = \frac{\dot{m}_{\text{int}}}{\rho_{\text{int}}}, \tag{3.5}$$

where ρ_{int} is computed using *REFPROP* at the known operating pressure and temperature of the intermediate water stream. Although the intermediate loop operates at ambient pressure, a circulation pump is required to compensate the pressure losses occurring across the two heat exchangers on the water side, both EHX_1 and the evaporator. The total pressure drop and the pump mechanical power is then estimated as:

$$\Delta p_{\text{tot}} = \Delta p_{\text{EVA}} + \Delta p_{\text{EHX\_1}} \tag{3.6}$$

$$\dot{W}_{\text{pump}} = \frac{\dot{V}_{\text{int}}\, \Delta p_{\text{tot}}}{\eta_{\text{hyd,pump}}}. \tag{3.7}$$

Values of $\eta_{\text{hyd,pump}}$, Δp_{EVA}, and $\Delta p_{\text{EHX\_1}}$ considered in the present analysis are reported in Table 3.2 and 3.3.

On the intermediate water side of the evaporator, the outlet temperature is assumed to coincide with the inlet temperature of EHX_1

$$T_d = T_a. \tag{3.8}$$

The heat rate available at the evaporator is given by the sum of the thermal power extracted from the wastewater stream and the mechanical power supplied by the circulation pump

$$\dot{Q}_{\text{evap}} = \dot{Q}_{\text{ww}} + \dot{W}_{\text{pump}}. \tag{3.9}$$

Accordingly, the evaporator inlet temperature T_c is obtained from the energy balance on the evaporator as:

$$T_c = T_d + \frac{\dot{Q}_{\text{evap}}}{\dot{m}_{\text{int}}\, c_{p,\text{int}}}. \tag{3.10}$$

The refrigerant evaporation temperature, as shown in Figure 3.2, is then determined by imposing a minimum pinch point temperature difference at the cold end of the evaporator

$$T_{\text{evap}} = T_d - \Delta T_{\text{pp,evap}}. \tag{3.11}$$

Finally, the refrigerant temperature at the evaporator outlet ,T_1, is set by the pre-

scribed superheating degreeΔT_{sh} as:

$$T_1 = T_{\mathrm{evap}} + \Delta T_{\mathrm{sh}}. \tag{3.12}$$

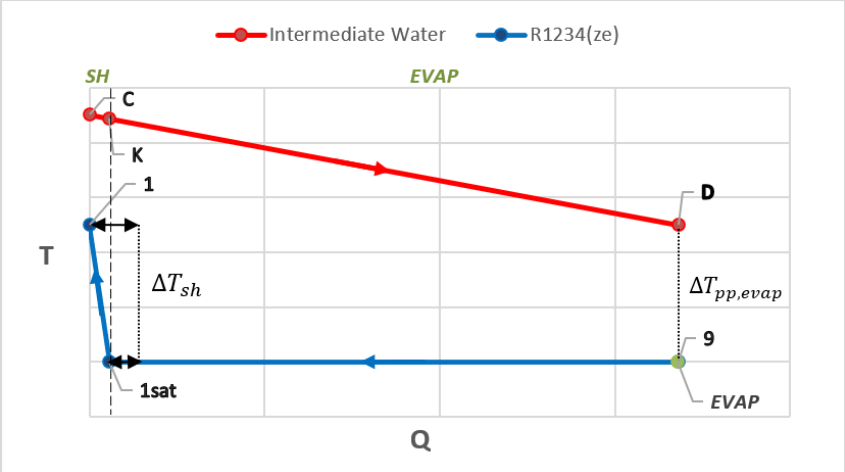

Figure 3.2: T–Q diagram of the evaporator heat exchanger.

Starting from state **1**, the thermodynamic state of the refrigerant at the remaining points of the cycle is determined by enforcing mass and energy balances across each component, as described in the thermodynamic cycle model presented in this chapter.

The numerical solution strategy adopted to solve the cycle and to determine the condensation temperature through an iterative convergence procedure is described in detail in Chapter 4.

3.3. Thermodynamic formulation of the double-stage vapour compression cycle

This section describes the thermodynamic formulation adopted to characterise the on design operating point of the double stage vapour compression cycle. Reference is made to the T–s diagram shown in Figure 2.3. Thermophysical properties are evaluated using the *REFPROP* database within a numerical environment to ensure thermodynamic consistency across all components.

The analysis starts from the evaporator outlet condition, defined by the evaporation temperature and the prescribed superheating degree. From this reference state, the remaining cycle states are obtained by enforcing mass and energy balances across the

two compression stages, the flash chamber, the condenser and the expansion devices. At this stage, the compressors are modelled using fixed isentropic efficiencies, treated as input parameters; a more detailed representation based on performance maps is introduced in a subsequent step of the modelling framework.

Once the thermodynamic states are determined, the refrigerant mass flow rate is calculated from the evaporator energy balance, where the absorbed thermal power is prescribed. The condenser heat duty and compressor power consumptions are then evaluated from the corresponding enthalpy differences, allowing the calculation of the main performance indicators, including the cycle COP and the overall system COP, which account for the interaction with the auxiliary heating system on the condenser side and the intermediate circuit pump.

The numerical strategy adopted to solve the resulting system of equations, including the iterative determination of the condensation temperature and the integration of component sizing and compressor performance maps, is described in detail in Chapter 4.

3.3.1. Thermodynamic definition of the cycle state points

Given the evaporation temperature T_{evap}, the condensation temperature T_{cond}, and the isentropic efficiencies of the first and second compressors η_1 and η_2, the thermodynamic state of the refrigerant at all points of the double stage vapour compression cycle can be uniquely determined.

Based on these inputs, all the cycle state points represented in the T–s diagram of Figure 2.3 are calculated.

First, the evaporating and condensing pressures are determined from the known evaporation temperature T_{evap} and from the trial condensation temperature $T_{\text{cond}}^{(n)}$. Both pressures are obtained from saturation conditions of the working fluid as:

$$P_{\text{evap}} = P(T_{\text{evap}},\, x = 1)\,, \tag{3.13}$$

$$P_{\text{cond}} = P\Big(T_{\text{cond}}^{(n)},\, x = 1\Big)\,. \tag{3.14}$$

A key aspect of the cycle formulation is the definition of the intermediate pressure level between the two compression stages. In the present model, two alternative

methods are implemented:

- the first method determines the intermediate pressure as the geometric mean of the evaporating and condensing pressures;
- the second method defines the intermediate saturation temperature as the arithmetic mean of the corresponding saturation temperatures at the evaporator and condenser, with the associated intermediate pressure obtained from saturation conditions.

Both approaches are implemented within the calculation routine and can be selected by the user at run time. In the present work, the option based on the arithmetic mean of the saturation temperatures is adopted; accordingly, the intermediate saturation temperature is first evaluated and the corresponding intermediate pressure is subsequently obtained as:

$$T_{\text{int}} = \frac{T_{\text{sat}}(P_{\text{evap}}) + T_{\text{sat}}(P_{\text{cond}})}{2}, \tag{3.15}$$

$$P_{\text{int}} = P(T_{\text{int}},\, x = 1)\,. \tag{3.16}$$

Once the pressure levels are defined, the remaining cycle states are obtained starting from the evaporator outlet condition (Point **1**). The remaining point are obtained by applying:

- isentropic relations for the ideal compression stages;
- compressor isentropic efficiencies for the actual outlet states;
- isenthalpic expansion across the throttling devices;
- phase equilibrium conditions at the evaporator, condenser and flash chamber;
- mass and energy balances at the mixing section.

All the thermodynamic properties at each state point are evaluated using functions reported in Table 2.2 and their consistency is verified by checking the mass and energy balances across the individual components of the cycle.

3.3.2. Cycle energy balances and performance indicators

Once the thermodynamic state of the refrigerant at all points of the cycle has been defined, the corresponding mass flow rates, heat duties, and power consumptions

can be evaluated by enforcing the energy balances on the main components of the system.

The energy balance equations reported in this section define the thermodynamic consistency of the heat pump cycle and represent the reference relations used to evaluate heat duties, power consumptions, and performance indicators under on-design conditions. These balances are not enforced only once, but are continuously verified within the iterative numerical procedure described in Chapter 4, in order to ensure convergence toward a thermodynamically consistent operating point.

In particular, the refrigerant molar flow rate is not prescribed a priori. Within the iterative solution procedure, the molar flow rate $\dot{n}_{\text{ref}}$ is determined from the energy balance at the evaporator, where the thermal power $\dot{Q}_{\text{evap}}$ is treated as a known input. Once the refrigerant molar flow rate is obtained, the corresponding mass flow rate $\dot{m}_{\text{ref}}$ is directly evaluated through the molar mass of the working fluid as:

$$\dot{m}_{\text{ref}} = \dot{n}_{\text{ref}}\, M_{\text{mol}}. \tag{3.17}$$

While the numerical determination of the refrigerant flow rates and the iterative enforcement of the energy balances are addressed in detail in Chapter 4, the formulations presented here provide the underlying thermodynamic relations that govern the behaviour of the cycle.

The thermal power absorbed at the evaporator is evaluated from the enthalpy increase experienced by the refrigerant across the evaporator. Owing to the adopted flash configuration, only the fraction $(1 - x_6)$ of the total refrigerant flow rate flows through the evaporator. Accordingly, the evaporator heat duty is expressed as:

$$\dot{Q}_{\text{evap}} = \dot{n}_{\text{ref}}\,(1 - x_6)\,(h_1 - h_9)\,, \tag{3.18}$$

while the heat duty at the evaporator is expressed as:

$$\dot{Q}_{\text{sh}} = \dot{n}_{\text{ref}}\,(1 - x_6)\,(h_1 - h_1 sat)\,. \tag{3.19}$$

Once $\dot{n}_{\text{ref}}$ is obtained from the evaporator balance, the power required by the two compression stages can be evaluated from the corresponding enthalpy rises. The

mechanical power absorbed by the first compressor is

$$\dot{W}_{\mathrm{cmp},1} = \dot{n}_{\mathrm{ref}} \left(1 - x_6\right) \left(h_2 - h_1\right), \tag{3.20}$$

while the mechanical power absorbed by the second compressor, acting on the mixed stream at the intermediate pressure level is

$$\dot{W}_{\mathrm{cmp},2} = \dot{n}_{\mathrm{ref}} \left(h_4 - h_3\right). \tag{3.21}$$

The total mechanical power absorbed by the compression process is therefore

$$\dot{W}_{\mathrm{cmp,mech}} = \dot{W}_{\mathrm{cmp},1} + \dot{W}_{\mathrm{cmp},2}. \tag{3.22}$$

On the hot side, the heat rejected at the condenser is evaluated from the enthalpy decrease of the refrigerant across condensation and subcooling as:

$$\dot{Q}_{\mathrm{cond,tot}} = \dot{n}_{\mathrm{ref}} \left(h_4 - h_{5,\mathrm{sub}}\right), \tag{3.23}$$

where we can consider the single contributions of desuperheater, condenser and subcooling as follows:

$$\dot{Q}_{\mathrm{desh}} = \dot{n}_{\mathrm{ref}} \left(h_4 - h_{5,\mathrm{vs}}\right), \tag{3.24}$$

$$\dot{Q}_{\mathrm{cond}} = \dot{n}_{\mathrm{ref}} \left(h_{5,\mathrm{vs}} - h_{5,\mathrm{ls}}\right), \tag{3.25}$$

$$\dot{Q}_{\mathrm{sub}} = \dot{n}_{\mathrm{ref}} \left(h_{5,\mathrm{ls}} - h_{5,\mathrm{sub}}\right). \tag{3.26}$$

The heat pump cycle must satisfy the overall energy balance

$$\dot{Q}_{\mathrm{evap}} + \dot{W}_{\mathrm{cmp},1} + \dot{W}_{\mathrm{cmp},2} = \dot{Q}_{\mathrm{cond}}. \tag{3.27}$$

In addition, by extending the balance to the entire system starting from the wastewater heat source, the condenser heat duty corresponds to the thermal power extracted

from the wastewater plus all auxiliary power inputs, namely

$$\dot{Q}_{\text{reflui}} + \dot{W}_{\text{pump}} + \dot{W}_{\text{cmp,1}} + \dot{W}_{\text{cmp,2}} = \dot{Q}_{\text{cond}}. \tag{3.28}$$

To account for electromechanical losses in the motor and drive system, the electrical power consumption of the compressors is obtained through the overall electromechanical efficiency of the compressors

$$\dot{W}_{\text{cmp,elec}} = \frac{\dot{W}_{\text{cmp,mech}}}{\eta_{\text{el-mecc,cmp}}}. \tag{3.29}$$

Similarly, the electromechanical power consumption of the pump in the intermediate circuit is evaluated from the corresponding mechanical power, calculate as equation 3.7, by accounting for the electromechanical efficiency of the pump motor drive system

$$\dot{W}_{\text{pump,elec}} = \frac{\dot{W}_{\text{pump,mech}}}{\eta_{\text{el-mecc,pump}}}. \tag{3.30}$$

Both value of electromechanical efficiencies are reported inTable 3.3.

Finally, the coefficient of performance of the heat pump cycle is defined as:

$$\text{COP}_{\text{cycle}} = \frac{\dot{Q}_{\text{cond}}}{\dot{W}_{\text{cmp,elec}} + \dot{W}_{\text{pump,elec}}}. \tag{3.31}$$

The coefficient of performance of the cycle, $\text{COP}_{\text{cycle}}$, represents the intrinsic energetic efficiency of the heat pump operating under on-design conditions. It quantifies the ratio between the useful thermal power delivered at the condenser and the electrical power absorbed by the compressors plus the electrical power taken by the pump in the intermediate circuit. It therefore provides a direct measure of the effectiveness of the vapour compression cycle in upgrading low temperature heat to a higher temperature level.

In the present formulation, $\text{COP}_{\text{cycle}}$ characterises the thermodynamic performance of the heat pump alone, independently of any auxiliary heating devices or system-level integration effects, which are introduced and discussed in the subsequent sections.

3.3.3. Role of the condensation temperature in the on-design model

The condensation temperature T_{cond} plays a central role in the thermodynamic behaviour of the heat pump and represents one of the key coupling variables between the refrigerant cycle and the heating water circuit. From a physical perspective, T_{cond} directly determines the pressure level of the high pressure side of the cycle, thus affecting the compression ratios, the compressor power consumption, and the overall efficiency of the system.

In the present on design formulation, the condensation temperature is not assigned arbitrarily, but is constrained by the heat transfer process occurring on the condenser side. In particular, T_{cond} is linked to the outlet temperature of the water stream heated by the heat pump through a prescribed minimum temperature difference, commonly referred to as the condenser approach temperature. This condition can be expressed as:

$$T_{\text{cond}} = T_x + \Delta T_{\text{ap,cond}}, \tag{3.32}$$

where T_x denotes the water temperature at the outlet of the desuperheater section of the condenser and $\Delta T_{\text{ap,cond}}$ is the imposed approach temperature difference, as showed in Figure 3.3.

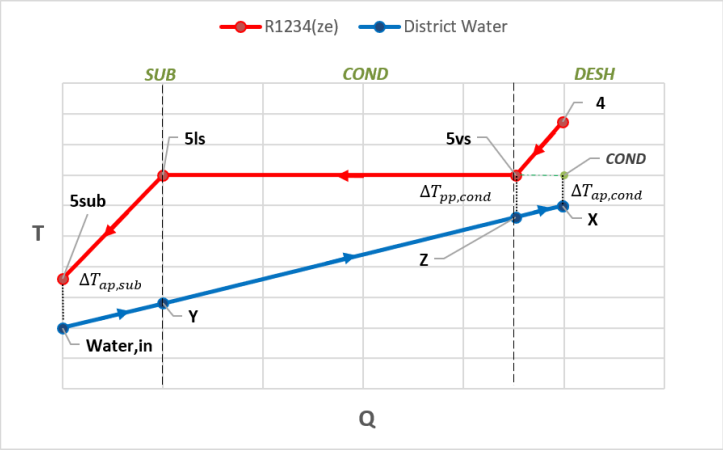

Figure 3.3: T–Q diagram of the condenser heat exchanger.

In the system configuration considered in this work, the temperature T_x corresponds to the outlet temperature of the heating water stream delivered by the heat pump, i.e. $T_x = T_{\text{water,out}}$ under full load operating conditions. As a result, the condensation temperature is ultimately dictated by the required supply temperature of the heating network and by the selected thermal approach at the condenser.

From a thermodynamic standpoint, an increase in T_{cond} leads to a higher condensing pressure, larger compression ratios and increased compressor power consumption. Conversely, a reduction in T_{cond} results in more favourable operating conditions for the compressors and an improvement in the cycle efficiency. For this reason, the condensation temperature represents a critical design variable that reflects the trade off between thermal requirements on the user side and achievable performance of the heat pump cycle.

Although the physical relation linking T_{cond} to the water side boundary conditions is defined at the modelling level, the numerical determination of the condensation temperature is carried out within the iterative solution procedure described in Chapter 4. The present section therefore focuses on the physical role of T_{cond} within the thermodynamic model, while the details of its numerical evaluation are addressed separately.

3.3.4. Extension of the thermodynamic model through the heat pump load factor

In order to generalise the thermodynamic framework and introduce greater flexibility at the system design level, a heat pump load factor f_{hp} is defined to represent the fraction of the total thermal demand that is intentionally assigned to the heat pump at nominal conditions. The load factor is defined as: The load factor is defined as:

$$f_{\text{hp}} = \frac{\dot{Q}_{\text{hp}}}{\dot{Q}_{\text{max}}}, \tag{3.33}$$

where $\dot{Q}_{\text{hp}}$ denotes the thermal power delivered by the heat pump and $\dot{Q}_{\text{max}}$ is the maximum thermal power required to heat the water stream from its inlet temperature $T_{\text{water,in}}$ to the target supply temperature $T_{\text{water,out}}$.

From a physical standpoint, the heat pump load factor does not describe a partial-load operating condition of the machine. Instead, it reflects a design choice imposed a priori, whereby the nominal capacity of the heat pump is intentionally sized to cover only a given fraction of the total district heating demand, with the remaining share supplied by an auxiliary electric boiler, as showed in the overall configuration reported in Figure 2.1. For a given value of f_{hp}, the heat pump is therefore evaluated at its corresponding on-design operating point and operates at its maximum available thermal output.

The total thermal power required by the heating system is given by:

$$\dot{Q}_{\text{tot}} = \dot{m}_{\text{water}}\, c_{p,\text{w}}\, (T_{\text{water,out}} - T_{\text{water,in}})\,. \tag{3.34}$$

When $f_{\text{hp}} < 1$, the nominal capacity of the heat pump is intentionally sized to supply only a fraction of the total thermal demand, while the remaining share is covered by the auxiliary heating device. The corresponding residual thermal power is

$$\dot{Q}_{\text{res}} = \dot{m}_{\text{water}}\, c_{p,\text{w}}\, (T_{\text{water,out}} - T_x)\,. \tag{3.35}$$

In this condistion, two different performance indicators must be distinguished. The coefficient of performance of the heat pump cycle, $\text{COP}_{\text{cycle}}$, defined previously in Equation 3.31, quantifies the intrinsic thermodynamic efficiency of the heat pump alone. In order to account for the overall performance of the heating system, including the auxiliary heating device, an overall system coefficient of performance is introduced and defined as:

$$\text{COP}_{\text{system}} = \frac{\dot{Q}_{\text{max}}}{\dot{W}_{\text{cmp,elec}} + \dot{W}_{\text{pump,elec}} + \dot{Q}_{\text{res}}}. \tag{3.36}$$

The physical implications of the heat pump load factor, as well as the relation between $\text{COP}_{\text{cycle}}$ and $\text{COP}_{\text{system}}$, can be clearly understood by distinguishing the following two operating conditions:

– **Heat pump full coverage operation ($f_{\text{hp}} = 1$).** The heat pump supplies the entire thermal demand of the heating system. The whole temperature lift of the water stream is provided within the condenser and the outlet temperature of the water from the heat pump coincides with the target supply temperature, i.e. $T_x = T_{\text{water,out}}$. Under this condition, the condenser heat duty is equal to the maximum required thermal power

$$\dot{Q}_{\text{cond}} = \dot{Q}_{\text{tot}}. \tag{3.37}$$

The auxiliary thermal contribution goes to zero ($\dot{Q}_{\text{res}} = 0$) and the two performance indicators coincide

$$\text{COP}_{\text{cycle}} = \text{COP}_{\text{system}}. \tag{3.38}$$

The condensation temperature assumes its maximum value consistent with the imposed condenser approach condition.

– **Hybrid load-sharing condition ($f_{\text{hp}} < 1$).** The heat pump supplies only a fraction of the total thermal demand, while the remaining fraction is provided by the auxiliary heating device. The water stream exits the condenser at an intermediate temperature $T_x < T_{\text{water,out}}$, while the remaining temperature increase is provided by the auxiliary electric heater, as showed in Figure 2.1. The thermal power supplied by the heat pump corresponds to

$$\dot{Q}_{\text{cond}} = \dot{m}_{\text{water}}\, c_{p,\text{w}}\, (T_x - T_{\text{water,in}})\,, \tag{3.39}$$

whereas the residual thermal power supplied by the auxiliary device is expressed by Equation 3.35.

In this case, the two performance indicators differ, since $\text{COP}_{\text{cycle}}$ characterises the heat pump alone, while $\text{COP}_{\text{system}}$ accounts for the combined contribution of the heat pump and the auxiliary heater.

The reduction in the outlet temperature T_x leads to a lower condensation temperature, resulting in reduced compression ratios, lower compressor power consumption and more favourable thermodynamic operating conditions for the heat pump cycle.

In the present work, the thermodynamic analysis and the on design results refer exclusively to the full coverage condition ($f_{\text{hp}} = 1$). The introduction of the heat pump load factor therefore extends the modelling framework at the system level, enabling parametric investigations on alternative sizing strategies without altering the intrinsic thermodynamic behaviour of the machine. For completeness, this extension is also implemented in the algorithm described in Chapter 4.

3.4. Component Modelling: Design and Correlations

This section presents the modelling approach adopted for the main components of the heat pump system analysed in this work and presented in Chapeter 2. In particular, the type of components considered and the physical models used to describe their behaviour are discussed, with specific focus on the correlations employed for the evaluation of the heat transfer processes occurring within the heat exchangers

and on the performance maps adopted for the compressors.

For the heat exchangers, the modelling strategy follows a component oriented approach, in which each device is treated as a steady state control volume and analysed through mass and energy conservation equations coupled with appropriate heat transfer correlations. The evaporator, condenser, subcooler and wastewater heat exchanger are modelled by distinguishing the different thermodynamic processes taking place within each component (i.e. phase change, superheating, desuperheating and subcooling), allowing a more accurate description of the local heat transfer mechanisms.

The design and sizing of the heat exchangers were carried out in accordance with the TEMA (Tubular Exchanger Manufacturers Association) standards [26]. These standards were adopted because they provide a systematic nomenclature for the identification of the main constructive elements of shell and tube heat exchangers, such as the front head, the rear head, the tube bundle configuration and the shell geometry. Each exchanger layout is defined through a letter based classification, which allows the different component types to be univocally identified. The TEMA nomenclature adopted in the present work is summarised in Figure 3.4 reported below. The heat transfer correlations adopted for the different heat exchange processes are presented in this section.

The explicit calculation of the heat transfer coefficients is not performed here, since it is embedded within a dedicated numerical routine described in the Chapter 4. The routine employs the correlations introduced below to evaluate the heat transfer coefficients consistently within the iterative calculation procedure. The selected correlations vary depending on the thermodynamic state of the working fluid, i.e. single phase or two phase conditions, as well as on whether the fluid flows inside the tubes or on the shell side of the heat exchanger, where the heat transfer process takes place.

The tube side water flow model is explicitly presented only for the evaporator, since the same formulation is applied to the condenser and the subcooler, where water always flows inside the tubes under single phase liquid conditions.

The modelling of the heat exchangers is not limited to the evaluation of the heat transfer coefficients, but also provides the basis for their geometrical sizing. The determination of the heat transfer area, number of tubes, tube length and shell volume is therefore performed within the numerical routine described in Chapter 4, where the on design calculation procedure is introduced.

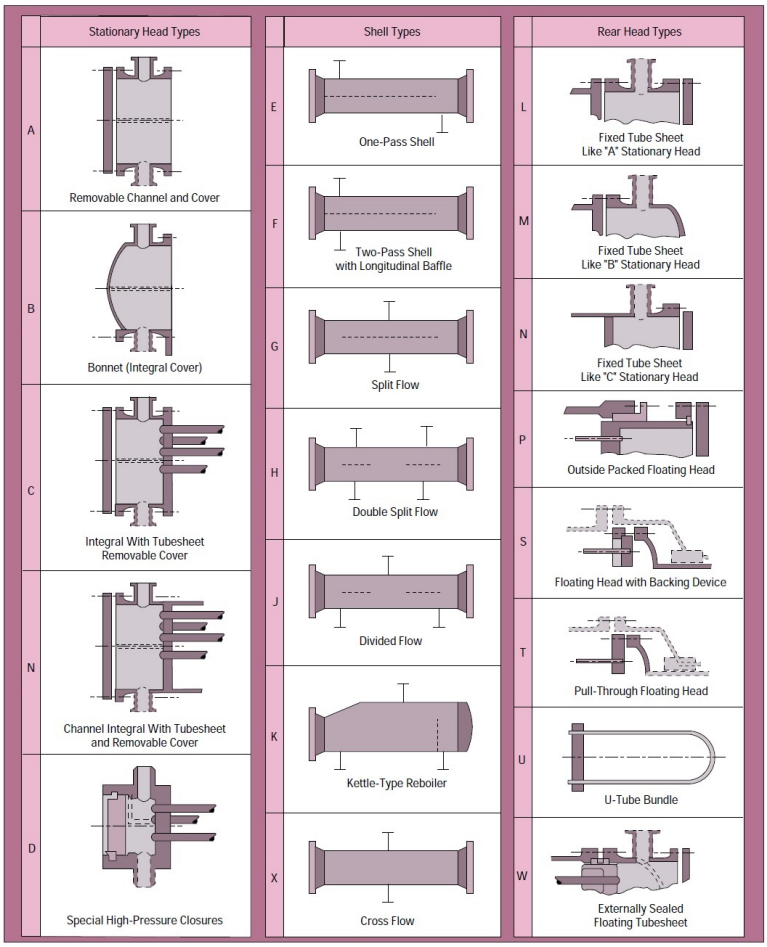

Figure 3.4: TEMA nomenclature for shell and tube heat exchangers [26].

Addictionaly is carried out a compressor modelling based on performance maps supplied by the manufacturer, which allow the evaluation of the electrical power consumption and isentropic efficiency as a function of the operating conditions. These maps are integrated within the overall component modelling framework and are used to characterise the compressor behaviour both at the nominal operating point and under off design conditions.

Finally other cycle components such as the throttling valves and the flash chamber are also analysed, with their behaviour described through appropriate thermodynamic assumptions and conservation equations.

3.4.1. Input data and tube bundle definition

In order to ensure consistency within the component modelling framework, the same tube bundle geometrical parameters are assumed for all the heat exchangers considered in this work: the evaporator, the condenser and the subcooler. These

parameters are introduced as fixed input data and provide the geometrical basis for the evaluation of the all heat transfer coefficients. The wastewater heat exchanger is treated separately, as it represents a dedicated and application specific device integrated into the sewer conduit. Its modelling assumptions and geometrical characterisation are therefore addressed in a subsequent section.

The assumed tube bundle geometry is characterised by the tube external diameter D_{o}, the tube thickness t and the internal diameter D_{i}, which define the cross sectional area available for tube side and shell side flow. These represent the characteristic lengths employed in the heat transfer correlations. The internal diameter is evaluated from the external diameter and the tube thickness as:

$$D_{\mathrm{i}} = D_{\mathrm{o}} - 2t. \tag{3.40}$$

The shell diameter D_s represents the characteristic dimension of the shell side flow domain, while Cs denotes the bundle to shell clearance, defined as the distance between the outermost tubes of the bundle and the inner shell wall. This clearance accounts for manufacturing tolerances and assembly constraints. The baffle spacing B determines the distance between consecutive baffles and directly affects the shell side flow pattern and the resulting heat transfer performance.

A schematic representation of the tube bundle geometry and the main geometrical parameters is shown in Figure 3.5.

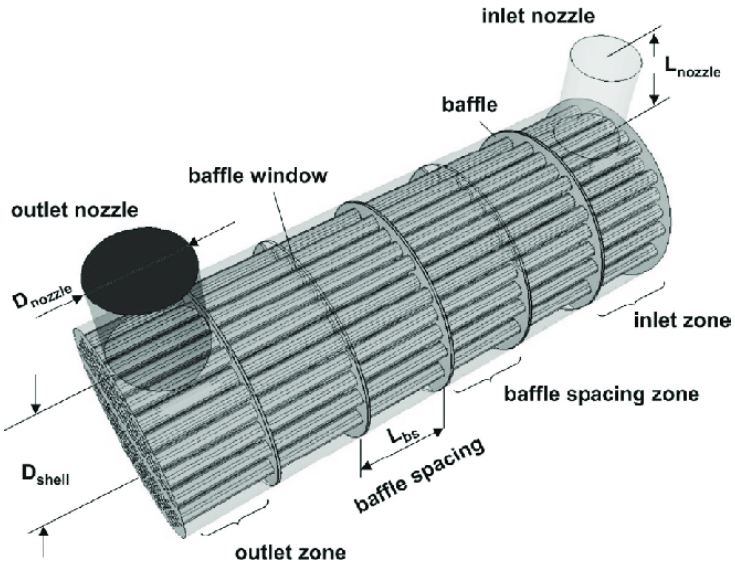

Figure 3.5: Schematic representation of the main geometrical parameters of a shell and tube heat exchanger [29].

The numerical values adopted for the tube bundle dimensions are summarised in Table 3.7 and are kept constant for all the heat exchangers analysed in the present work.

Parameter	Value
Tube external diameter (D_o)	19.05 mm
Tube thickness (t)	1.24 mm
Tube internal diameter (D_i)	16.57 mm
Diameter ratio (D_o/D_i)	1.15
Shell diameter (D_s)	1417 mm
Bundle-to-shell clearance (C_s)	4.76 mm
Baffle spacing (B)	708.5 mm

Table 3.7: Tube bundle geometrical parameters assumed for all the heat exchangers considered in this work.

The tube bundle arrangement plays a fundamental role in the evaluation of the shell side heat transfer coefficients, as it directly affects the characteristic flow passages, the equivalent diameter and the effective crossflow area. In the present work, the evaporator, the condenser and the subcooler are all designed adopting a triangular tube layout with a 30° pattern, corresponding to a staggered configuration, rappresented in Figure 3.6. This layout is widely employed in shell and tube heat exchangers to enhance shell side heat transfer performance.

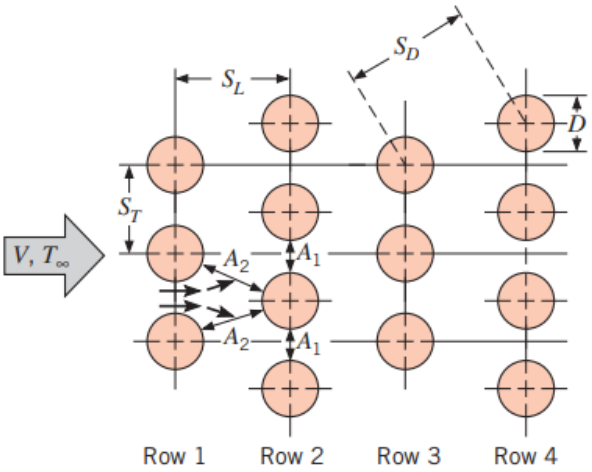

Figure 3.6: Staggered configuration [30].

Compared to in line tube banks, staggered tube arrangements generally promote enhanced shell side heat transfer due to the more tortuous flow path and the increased

mixing of the cross flowing fluid, which results in higher turbulence levels. As a consequence, staggered configurations are associated with higher Nusselt numbers at comparable Reynolds numbers, while they also lead to larger shell side pressure drops. On this basis, triangular 30° staggered tube arrangements are adopted in the present work, and in line configurations are not considered [30]. The flow conditions characterising staggered tube arrangements, in terms of flow path tortuosity and wake development, is schematically illustrated in Figure 3.7.

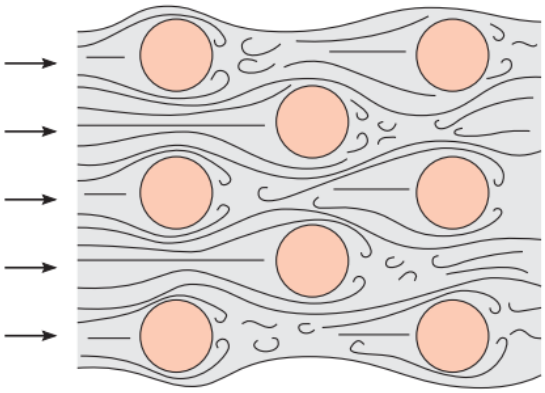

Figure 3.7: Flow condition of staggered tubes [30].

The adopted tube layout is schematically illustrated in Figure 3.8, where the tube pitch P_t and the tube external diameter D_o are highlighted. The tube pitch is defined as the centre to centre distance between adjacent tubes within the bundle, while the tube to tube clearance C_t is evaluated as:

$$C_t = P_t - D_o \tag{3.41}$$

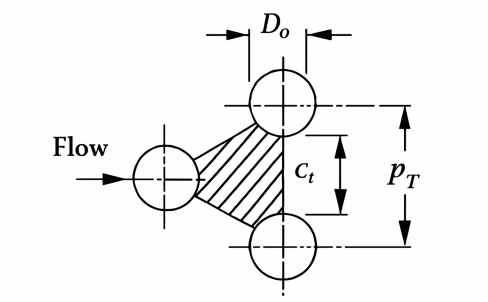

Figure 3.8: Triangular 30° staggered tube layout illustrating the tube pitch P_t and the tube external diameter D_o.

The selected tube layout directly affects the definition of the equivalent diameter

D_e, which is employed in the evaluation of the shell side Reynolds number. For a triangular 30° staggered tube arrangement, the equivalent diameter is defined according to standard shell side flow modelling as:

$$D_e = \frac{4\left(\frac{\sqrt{3}}{4}P_t^2 - \frac{\pi}{4}D_o^2\right)}{\pi D_o}. \tag{3.42}$$

The shell side flow velocity is governed by the effective bundle crossflow area, which depends on the shell diameter D_s, the tube to tube clearance C_t, the tube pitch P_t and the baffle spacing B. Since no unique free flow area can be identified on the shell side, the crossflow area at the centre of the shell is commonly adopted and is defined as:

$$A_s = \frac{D_s\, C_t\, B}{P_t}. \tag{3.43}$$

Based on this definition, the shell side mass velocity G_s is introduced as a fictitious quantity and is evaluated as:

$$G_s = \frac{\dot{m}_{\text{ref}}}{A_s}. \tag{3.44}$$

Finally, the shell side Reynolds number is computed using the equivalent diameter D_e, the shell side mass velocity G_s and the dynamic viscosity μ of the working fluid:

$$\text{Re} = \frac{G_s D_e}{\mu}. \tag{3.45}$$

These geometrical definitions and derived flow quantities provide the basis for the evaluation of the shell side heat transfer coefficients through the correlations adopted in the following sections.

3.4.2. Evaporator

Design

The evaporator is modelled as a kettle reboiler, corresponding to the K-type shell according to the TEMA classification. According to the TEMA standards, the kettle reboiler represents a specific variant of the conventional shell and tube heat exchanger. Unlike standard shell and tube configurations, where the shell side flow is mainly transversal and guided by baffles, the kettle reboiler is characterised by a large shell volume acting as a drum, which allows the liquid and vapor phases to

coexist during the boiling process, as showed in Figure 3.9.

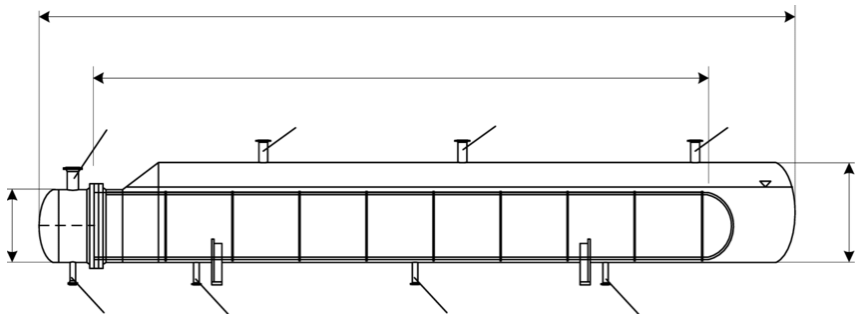

Figure 3.9: TEMA K-type kettle reboiler heat exchanger [31].

In this configuration, approximately 60% of the shell volume is occupied by the liquid phase, which fully immerses the tube bundle, while the remaining upper portion of the shell is filled with vapor. The working fluid enters the shell through a nozzle located in the lower part of the heat exchanger, flows around the tube bundle and progressively evaporates as heat is transferred from the fluid flowing inside the tubes. A dedicated outlet nozzle placed at the bottom of the shell is used to control the liquid level and maintain it at the desired height, ensuring stable boiling conditions [26],[31].

Within the modelling framework adopted in this work, the evaporator is treated as a single heat exchanger in which both evaporation and superheating processes take place. The main geometrical parameters of the kettle reboiler, including the number of tubes, the total heat transfer area, the tube length and the shell volume, are determined through the numerical routine described in the Chapter 4. This approach allows the evaporator to be consistently dimensioned as a single component covering both the evaporation and the superheating regions.

Correlation

The evaporator involves heat transfer between two different working fluids. On the shell side, the refrigerant R1234ze flows outside the tubes and undergoes a phase change process. In particular, the refrigerant evaporates and is subsequently superheated within the same heat exchanger. As a consequence, two different heat transfer regimes are identified on the shell side and different methods are adopted to evaluate the external heat transfer coefficient in the evaporation and superheating sections.

Inside the tubes, water from the district heating circuit flows in single phase liquid conditions and is progressively cooled along the evaporator. Since the thermody-

namic state of the water does not change throughout the component, the same heat transfer correlation is applied for the tube side flow in both the evaporation and superheating sections.

This modelling approach allows the evaporator to be treated as a single component while accounting for the different heat transfer mechanisms occurring on the shell side, and ensures a consistent evaluation of the heat transfer coefficients for both fluids.

Superheating Section: it is where the refrigerant, completely evaporated, enters the superheating unit of the evaporator. In this region, the refrigerant R1234ze flows in vapor phase on the shell side and is involved in a forced convection heat transfer process, driven by the action of the low pressure compressor, which increases the fluid pressure from the evaporation pressure to the intermediate pressure.

The tube bundle is arranged in a staggered configuration, leading to different flow conditions across successive tube rows. In particular, after the first rows, the flow enters a fully turbulent regime, resulting in enhanced heat transfer. In order to obtain an average heat transfer coefficient representative of the entire tube bundle, the external convective heat transfer coefficient in the superheating region is evaluated using the Zukauskas correlation for cross flow over tube banks [30].

The thermophysical properties of the refrigerant, including dynamic viscosity μ, specific heat capacity c_p and thermal conductivity k, are evaluated using the *REFPROP* database at the average superheating temperature. The Reynolds number is computed as described in the Subsections 3.4.1, consistently with the adopted tube bundle arrangement

$$\mathrm{Re}_D = \frac{G_s D_e}{\mu}, \tag{3.46}$$

while the Prandtl number is defined as:

$$\mathrm{Pr} = \frac{\mu c_p}{k}. \tag{3.47}$$

The Nusselt number is evaluated according to the Zukauskas correlation as:

$$\mathrm{Nu}_D = C\,\mathrm{Re}_D^m\,\mathrm{Pr}^{0.36}\left(\frac{\mathrm{Pr}}{\mathrm{Pr}_s}\right)^{0.25}, \tag{3.48}$$

which is applied within the following validity ranges:

$$0.7 \leq \mathrm{Pr} \leq 500, \tag{3.49}$$

$$10^3 \leq \mathrm{Re}_D \leq 2 \times 10^6. \tag{3.50}$$

The coefficients C and m are selected as a function of the Reynolds number, according to the values reported in Figure 3.10. Finally, the external convective heat transfer coefficient is obtained as:

$$h_{\mathrm{ext}} = \frac{\mathrm{Nu}_D\, k}{D_e}. \tag{3.51}$$

Configuration	$Re_{D,\max}$	C_1	m
Aligned	10–10^2	0.80	0.40
Staggered	10–10^2	0.90	0.40
Aligned	10^2–10^3	Approximate as a single (isolated) cylinder	
Staggered	10^2–10^3		
Aligned $(S_T/S_L > 0.7)^a$	10^3–2×10^5	0.27	0.63
Staggered $(S_T/S_L < 2)$	10^3–2×10^5	$0.35(S_T/S_L)^{1/5}$	0.60
Staggered $(S_T/S_L > 2)$	10^3–2×10^5	0.40	0.60
Aligned	2×10^5–2×10^6	0.021	0.84
Staggered	2×10^5–2×10^6	0.022	0.84

[a]For $S_T/S_L < 0.7$, heat transfer is inefficient and aligned tubes should not be used.

Figure 3.10: C and m coefficients using in Zukauskas correlation for the tube bank in cross flow [30].

This formulation is implemented within the numerical routine described in the following chapter, which employs the same tube bundle configuration and thermophysical properties definitions introduced in the present section.

Evaporating Section: the first heat transfer process occurring in the evaporator is the evaporation of the refrigerant on the shell side. At the inlet, the refrigerant enters in two phase conditions with a vapour quality typically lower than unity. Owing to the adopted kettle reboiler configuration, the liquid and vapour phases are effectively separated and the evaporation process takes place around the tube

bundle immersed in the liquid phase. Under these conditions, the boiling process can be modelled as pool boiling.

The Nukiyama boiling curve, rappresented in Figure 3.11, which expresses the wall heat flux q_s'' as a function of the wall superheat ΔT_e, identifies different heat transfer regimes. At low wall superheats, heat transfer is dominated by natural convection, where no bubble formation is observed and heat is removed primarily by buoyancy-driven liquid motion. As the wall superheat increases, the onset of nucleate boiling occurs, characterised by the formation and detachment of vapour bubbles from discrete nucleation sites on the heated surface[30].

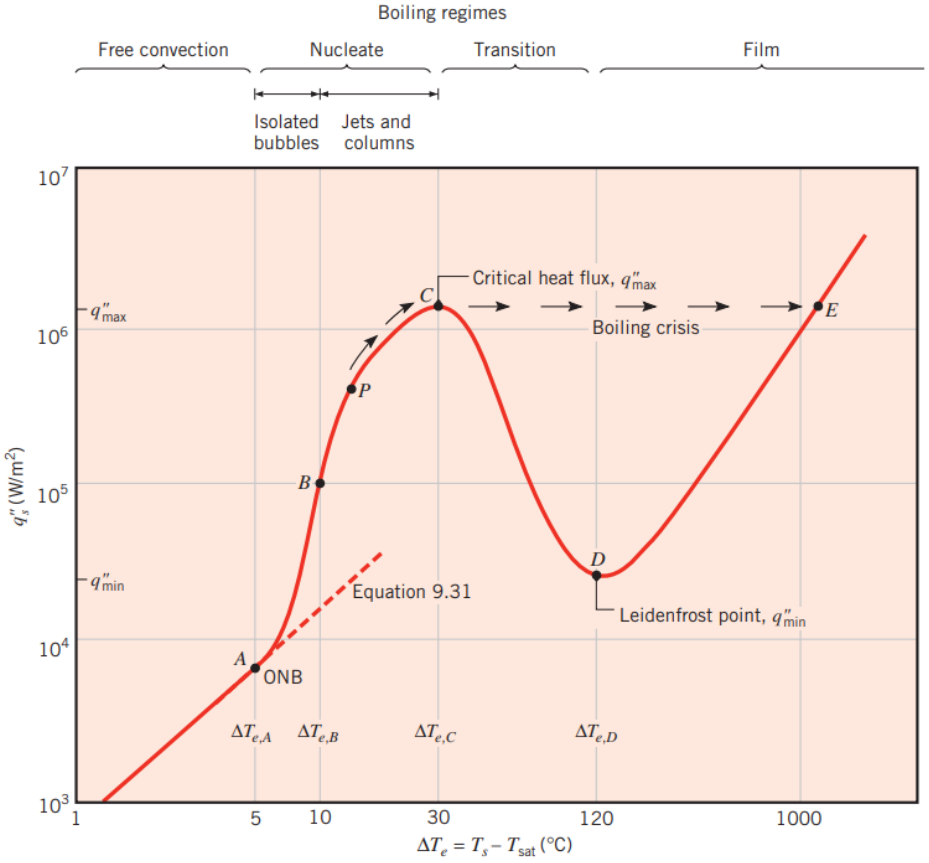

Figure 3.11: Nukiyama boiling curve and different boiling regimes [30]

Further increasing the wall superheat leads to the fully developed nucleate boiling regime, in which bubble generation becomes more intense and the heat flux increases rapidly with ΔT_e. Beyond this region, a maximum heat flux, commonly referred to as the critical heat flux, is reached. At wall superheats higher than this threshold, the boiling process enters the transition boiling regime, followed by film boiling, where a stable vapour layer forms between the surface and the liquid, significantly reducing the heat transfer coefficient.

In practical heat exchanger applications, operation is restricted to the nucleate boiling regime, which offers high and stable heat transfer coefficients while avoiding the unstable and potentially critical conditions associated with transition and film boiling. In the present work, the evaporation process is assumed to take place entirely within the nucleate pool boiling regime, as schematically indicated in the Nukiyama curve reported in Figure 3.11. Accordingly, the Rohsenow correlation is adopted to model the shell side heat transfer during evaporation [30]. The Rohsenow correlation expresses the heat flux exchanged at the wall as:

$$q'' = \mu_\ell h_{fg} \left[\frac{g(\rho_\ell - \rho_v)}{\sigma}\right]^{1/2} \left(\frac{c_{p,\ell}\,\Delta T_e}{C_{sf}\,h_{fg}\,\mathrm{Pr}_\ell^{\,n}}\right)^3, \tag{3.52}$$

where:

- C_{sf} and n are empirical constants that depend on the combination of working fluid and heating surface material, selected from the reference table reported in Figure 3.12;
- μ_ℓ is the dynamic viscosity of the refrigerant in the liquid phase;
- h_{fg} is the latent heat of vaporisation evaluated as $h_{fg} = h_{1,\mathrm{sat}} - h_9$;
- g is the gravitational acceleration;
- ρ_ℓ and ρ_v are the liquid and vapour densities, respectively;
- σ is the surface tension of the refrigerant;
- $c_{p,\ell}$ is the specific heat capacity of the liquid refrigerant;
- Tw is the tube wall temperature calculate as the average value of the water side temperature across the evaporator;
- ΔT_e is the wall superheat, defined as the difference between the tube wall temperature, Tw and the saturation temperature of the refrigerant $Tsat$;
- Tw is the tube wall temperature calculate as the average value of the water-side temperature across the evaporator;
- k is the thermal conductivity;
- Pr_ℓ is the Prandtl number evaluated for the liquid phase as $\mathrm{Pr}_\ell = \mu_\ell c_{p,\ell}/k$.

All the thermophysical properties appearing in the Rohsenow correlation are evaluated using the *REFPROP* database at saturation conditions corresponding to P_{evap}.

Surface–Fluid Combination	$C_{s,f}$	n
Water–copper		
Scored	0.0068	1.0
Polished	0.0128	1.0
Water–stainless steel		
Chemically etched	0.0133	1.0
Mechanically polished	0.0132	1.0
Ground and polished	0.0080	1.0
Water–brass	0.0060	1.0
Water–nickel	0.006	1.0
Water–platinum	0.0130	1.0
n-Pentane–copper		
Polished	0.0154	1.7
Lapped	0.0049	1.7
Benzene–chromium	0.0101	1.7
Ethyl alcohol–chromium	0.0027	1.7

Figure 3.12: Values of C_{sf} and n for various surface–fluid combinations [30].

Once the wall heat flux q_s'' is evaluated, the external heat transfer coefficient is obtained as:

$$h_{\text{ext}} = \frac{q_s''}{\Delta T_e}. \tag{3.53}$$

Water Side: in all heat exchangers considered in this work, water flows inside the tubes and undergoes a forced internal convection heat transfer process. Throughout all the part of the evaporator, but also in the condenser and subcooler, the water remains in single phase liquid conditions and is progressively cooled, without experiencing any phase change.

The internal convective heat transfer coefficient is evaluated using the correlation proposed by Gnielinski [30], which is widely adopted for turbulent flow in circular tubes. The Nusselt number is expressed as:

$$\text{Nu}_D = \frac{f}{8}\left(\text{Re}_D - 1000\right)\text{Pr}\left[1 + 12.7\left(\frac{f}{8}\right)^{1/2}\left(\text{Pr}^{2/3} - 1\right)\right]^{-1}, \tag{3.54}$$

where the friction factor f is computed as:

$$f = \left(1.58\ln\text{Re}_D - 3.28\right)^{-2}. \tag{3.55}$$

The Reynolds number is evaluated assuming a fully developed internal flow and is computed using the internal tube diameter as equivalent diameter ($D_e = D_\mathrm{i}$), while a velocity profile factor equal to unity is assumed ($u = 1$). The Reynolds and Prandtl numbers are defined as:

$$\mathrm{Re}_D = \frac{\rho\, u\, D_\mathrm{i}}{\mu}, \tag{3.56}$$

$$\mathrm{Pr} = \frac{\mu\, c_{p,\ell}}{k}. \tag{3.57}$$

The thermophysical properties of liquid water, namely dynamic viscosity μ, specific heat capacity $c_{p,\ell}$ and thermal conductivity k, are evaluated using the *REFPROP* database at the local mean water temperature and operating pressure. The Gnielinski correlation is applied within its recommended validity ranges:

$$3000 \leq \mathrm{Re}_D \leq 5 \times 10^6, \tag{3.58}$$

$$0.5 \leq \mathrm{Pr} \leq 2000. \tag{3.59}$$

Finally, the internal convective heat transfer coefficient is obtained as:

$$h_\mathrm{int} = \frac{\mathrm{Nu}_D\, k}{D_\mathrm{i}}. \tag{3.60}$$

The same correlation is adopted for the water side in all the heat exchangers of the system: evaporator, condenser and superheater. For this reason, the water side heat transfer modelling is not described again in the following sections. Although the operating conditions and the thermophysical properties of the water vary from one heat exchanger to another, the adopted correlation and the calculation procedure remain unchanged.

3.4.3. Condenser

Design

The condenser is modelled as a TEMA G-type shell and tube heat exchanger, according to the TEMA standards. This shell configuration, commonly referred to as

a split flow shell, is mainly selected because it is associated with lower shell side pressure drops when compared to other shell types, while still ensuring an effective heat transfer performance.

As showed in Figure 3.13, the G-type shell is characterised by the presence of a longitudinal baffle that divides the shell side flow into two symmetric streams. The refrigerant enters the shell through an inlet nozzle located above the longitudinal baffle and is then distributed along the heat exchanger. Additional longitudinal baffles are arranged to promote cross flow over the tube bundle and to enhance the overall heat transfer process.

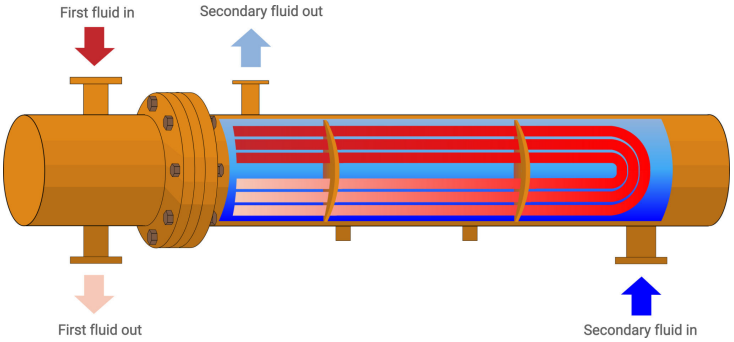

Figure 3.13: TEMA G-split flow shell heat exchanger [26].

Within this component, both desuperheating and condensation processes take place, as the superheated vapor is first cooled down to saturation conditions and subsequently condensed along the shell side flow path. The condenser is designed so that the coldest region of the shell side flow is located in the lower part of the heat exchanger, while the hottest region is positioned in the upper part. This arrangement allows a more favourable temperature distribution along the component and contributes to limiting thermal gradients and pressure losses within the shell side [26], [32].

Correlation

The condenser also involves heat transfer between two different working fluids. On the shell side, the refrigerant R1234ze flows outside the tubes and undergoes a phase change process. In particular, the refrigerant is first desuperheated and subsequently condensed within the same heat exchanger. As a result, two different heat transfer regimes are identified on the shell side and different methods are adopted to evaluate the external heat transfer coefficient in the desuperheating and condensation sections.

Inside the tubes, water from the district heating circuit flows in single phase liquid conditions and is progressively heated along the condenser. Since the thermodynamic state of the water remains liquid throughout the component, the same heat transfer correlation is applied for the tube side flow in both the desuperheating and condensation sections.

This modelling approach allows the condenser to be treated as a single component while accounting for the different heat transfer mechanisms occurring on the shell side and ensures a consistent evaluation of the heat transfer coefficients for both fluids.

Desuperheating Section: is where the refrigerant enters in superheated vapour conditions and is cooled down to the saturation temperature at the condensing pressure. On the shell side, the refrigerant flows outside the tubes and the heat transfer process is governed by forced convection, promoted by the compressor action, which drives the vapour through the heat exchanger.

As in the superheating section of the evaporator, the tube bundle is arranged in a triangular 30° staggered configuration and the flow develops across successive tube rows under turbulent conditions. Therefore, the external convective heat transfer coefficient in the desuperheating region is evaluated using the Zukauskas correlation for cross flow over tube banks, consistently with the approach adopted for the superheating section [30].

The Nusselt number is evaluated as Equation 3.48, which is applied within the validity ranges of Equation 3.50 and 3.49.

The coefficients C and m are selected as a function of the Reynolds number from the same reference table reported in Figure 3.10.

The Reynolds and Prandtl numbers are evaluated according to Equation 3.46 and 3.47, with G_s and the equivalent diameter, D_e, related to the selected tube layout.

Finally, the external heat transfer coefficient in the desuperheating section is obtained from the evaluated Nusselt number as Equation 3.51.

Condensing Section: the condensation process occurring in the condenser is modelled as film condensation on the external surface of horizontal tubes. In this regime, a continuous liquid film forms on the tube wall as the superheated vapour is cooled below the saturation temperature and condenses. The condensate film flows downward under the action of gravity and heat transfer takes place mainly by

conduction through the liquid film. A schematic representation of film condensation on a single horizontal tube is reported in Figure 3.14.

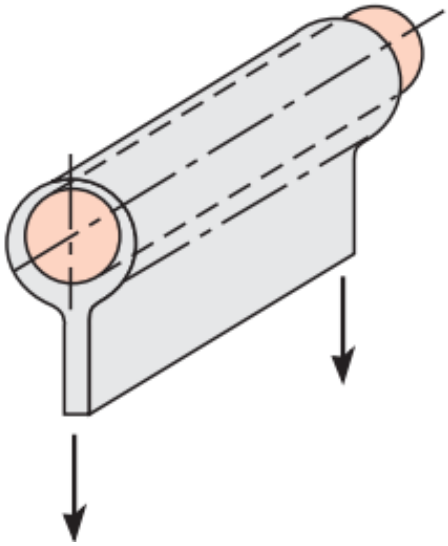

Figure 3.14: Film condensing on a single horizontal tube [30].

The modelling of film condensation is based on the classical theory developed by Nusselt, which provides an analytical description of laminar film condensation on cooled surfaces. The Nusselt theory is derived under the following main assumptions:

- the condensate film flow is laminar;
- the thermophysical properties of the liquid film are constant;
- inertia and shear stresses at the vapour liquid interface are negligible;
- heat transfer occurs only through the liquid film;
- condensation is driven by gravity.

These assumptions are consistent with the operating conditions of the condenser considered in this work, where condensation occurs on the shell side of a shell and tube heat exchanger at moderate heat fluxes and in the absence of strong vapour shear effects. For this reason, the Nusselt theory represents an appropriate and widely adopted approach for the evaluation of the external heat transfer coefficient [30].

For condensation on a horizontal cylindrical surface, the average external heat trans-

fer coefficient is expressed as:

$$h_{\text{ext}} = C \left[\frac{g\, \rho_\ell (\rho_\ell - \rho_v)\, h'_{fg}\, k_\ell^3}{\mu_\ell\, (T_{\text{sat}} - T_w)\, D_{\text{o}}} \right]^{1/4}, \tag{3.61}$$

where D_{o} is the external tube diameter and C is equal to 0.729 for horizontal tubes. In the case of a tube bundle, rappresented in Figure 3.15 the effect of multiple tube rows is taken into account by introducing the correction factor N, leading to:

$$h_{\text{ext},N} = C \left[\frac{g\, \rho_\ell (\rho_\ell - \rho_v)\, h'_{fg}\, k_\ell^3}{N\, \mu_\ell\, (T_{\text{sat}} - T_w)\, D_{\text{o}}} \right]^{1/4}, \tag{3.62}$$

where:

- g is the gravitational acceleration;
- ρ_ℓ and ρ_v are the liquid and vapour densities, respectively;
- μ_ℓ is the dynamic viscosity of the liquid refrigerant;
- k_ℓ is the thermal conductivity of the liquid refrigerant;
- h_{fg} is the latent heat of condensation at the condensing pressure, calculate as $h_{fg} = h_{5,\ell s} - h_{5,vs}$;
- $c_{p,\ell}$ is the specific heat capacity of the liquid refrigerant;
- T_{sat} is the saturation temperature at the condensing pressure;
- T_w is the tube wall temperature calculate as as the average value of the water-side temperature across the condenser;
- D_{o} is the external tube diameter;
- N is the number of tube rows crossed by the shell-side flow.

All thermophysical properties are evaluated using the *REFPROP* database. Liquid properties are computed at the film temperature, while vapour density and latent heat are evaluated at saturation conditions [30].

Water Side: on the water side, the flow inside the tubes remains in the liquid phase throughout the entire heat transfer process. As discussed previously, the procedure used to calculate the heat transfer coefficient remains the same for all the heat exchangers and follows the methodology described in Paragraph 3.4.2. The

only quantities that change are the operating conditions, which are used to evaluate the thermophysical properties.

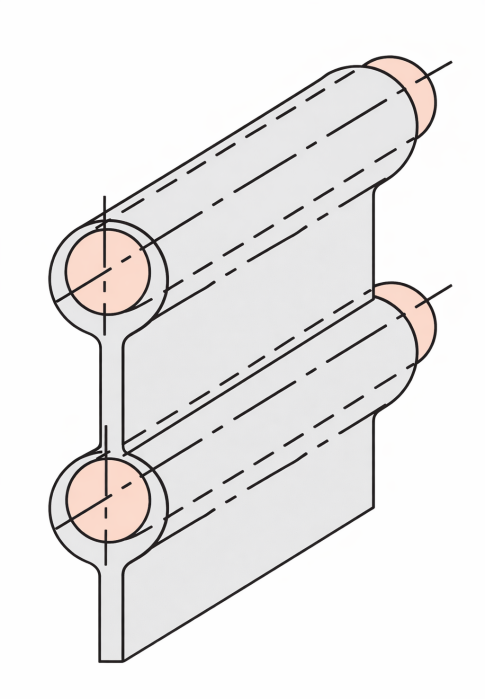

Figure 3.15: Film condensing on a a vertical tier of horizontal tubes with a continuous condensate sheet [30].

3.4.4. Subcooler

In the present system configuration, the condenser is designed to accomplish only the desuperheating and condensation processes, whereas the refrigerant subcooling is performed in a separate component to provide better control of the refrigerant outlet state and improve the stability of the expansion process.

Within the subcooler, the refrigerant flows on the shell side in single phase liquid conditions and is undercooled, while water flows inside the tubes and is progressively heated. The adoption of the same TEMA layout as the condenser is therefore justified by geometrical consistency and favourable hydraulic behaviour, whereas the heat transfer correlations are selected specifically to reflect the single phase liquid regime occurring on the refrigerant side.

Design

The subcooler is modelled as a dedicated shell and tube heat exchanger installed downstream of the condenser in order to further cool the refrigerant below its condensation temperature.

The subcooler adopts the same TEMA G-type, split flow shell configuration, selected for the condenser and showed in Figure 3.13. This choice ensures consistency in the component modelling framework and allows the same tube bundle assumptions to be retained across the heat exchangers, while benefiting from the relatively low shell side pressure drops associated with split-flow shells. The longitudinal baffle divides the shell side flow into two symmetric streams, promoting an effective distribution of the refrigerant over the tube bundle.

Correlation

In the subcooler, the refrigerant enters the heat exchanger in saturated liquid conditions and exits in subcooled liquid conditions. On the shell side, the refrigerant flows outside the tubes and the heat transfer process occurs entirely under single phase liquid conditions. As in the desuperheating section of the condenser, the shell side heat transfer is governed by forced convection.

Also in this case the tube bundle is arranged in a triangular 30° staggered configuration and the external convective heat transfer coefficient is evaluated using the Zukauskas correlation for cross flow over tube banks, consistently with the modelling approach adopted for the desuperheating and superheating regions [30].

The Nusselt number is evaluated as Equation 3.48, which is applied within the following validity ranges express in Equations 3.50 and 3.49.

The coefficients C and m are selected as a function of the Reynolds number from the same reference table reported in Figure 3.10.

The Reynolds and Prandtl numbers are evaluated according to the Equation 3.46 and 3.47, using the shell side mass velocity, G_s, and the equivalent diameter, D_e, related to the selected tube layout.

Finally, the external heat transfer coefficient in the subcooling section is obtained from the evaluated Nusselt number as expressed by Equation 3.51.

3.4.5. Logarithmic mean temperature difference correction factor F

In practice, the heat exchangers considered in this work deviate from the ideal counterflow configuration; therefore, the logarithmic mean temperature difference (ΔT_{lm}) used to evaluate the overall heat transfer rate in a heat exchanger, must be corrected by introducing a correction factor F. It accounts for the effects of the exchanger geometry, the heat capacity rate ratio and the temperature effectiveness of the device.

The corrected temperature difference is therefore expressed as $F\,\Delta T_{\text{lm}}$, as commonly adopted in shell and tube and multipass heat exchangers.

The correction factor F depends on two dimensionless parameters, namely the heat capacity rate ratio R and the temperature effectiveness parameter P, defined as:

$$R = \frac{T_{h,2} - T_{h,1}}{T_{c,2} - T_{c,1}}, \tag{3.63}$$

$$P = \frac{T_{c,2} - T_{c,1}}{T_{h,2} - T_{h,1}}, \tag{3.64}$$

where the subscripts h and c denote the hot and cold sides, respectively, and the indices 1 and 2 refer to inlet and outlet conditions. For a given heat exchanger configuration, the value of F is obtained from standard charts reported in the literature as a function of R and P [30] and rappresented in Figure 3.16.

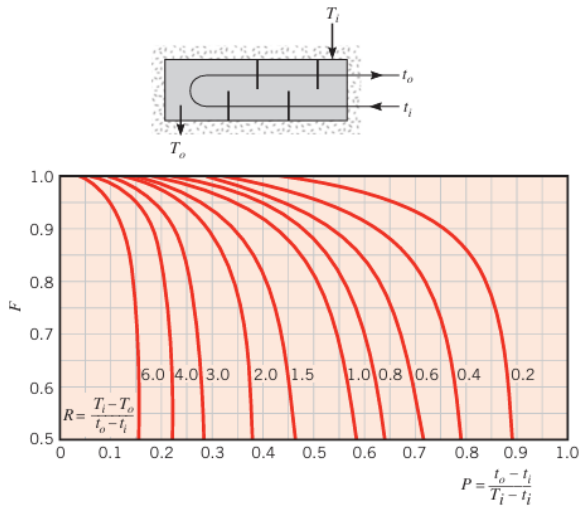

Figure 3.16: Correction factor for a shell and tube heat exchanger with one shell and any multiple of two tube passes [30].

In the present work, the correction factor F is applied to the superheating, desuperheating and subcooling sections, while is neglected for the evaporation and condensation processes, which are characterised by quasi isothermal phase change phenomena and for this the parameter P tends to zero and R tends to infinity.

3.4.6. Wastewater heat exchanger

The wastewater heat exchanger, located between the intermediate water loop and the sewer flow, is implemented as an in sewer heat exchanger, with a module installed directly within a sewer conduit as showed in Figure 3.17. Such systems are characterised by non standard geometries, typically based on modular heat exchange surfaces in contact with wastewater flowing inside the pipe. Owing to the highly variable hydraulic conditions and to the presence of solids deposition and fouling phenomena, a detailed heat transfer characterisation based on conventional correlations is non trivial, since both the flow regime and the effective heat transfer area may vary with operating conditions and wastewater quality [33], [14].

Figure 3.17: Sewer pipe element with integrated heat exchanger for wastewater heat recovery [14].

For modelling purposes, the component is therefore represented through an overall heat transfer conductance $UA_{\mathrm{EHX\_1}}$ identified from on design conditions. Specifically, using the heat balance on EHX_1 expressed by Equations 3.1 and 3.2, the value of $UA_{\mathrm{EHX\_1}}$ is computed and then kept constant in the subsequent off design simulations

$$UA_{\mathrm{EHX\_1}} = \frac{\dot{Q}_{\mathrm{EXH\_1}}}{\Delta T_{\mathrm{pp,EHX\_1}}}. \tag{3.65}$$

3.4.7. Compressor

The heat pump system analysed in this work employs two centrifugal compressors arranged in a double vapour compression configuration, namely as: low pressure compressor and high pressure compressor.

The two compression stages operate respectively between the evaporation pressure P_{evap} and the intermediate pressure P_{int} and between the intermediate pressure P_{int} and the condensation pressure P_{cond}. The detailed numerical implementation of the compressor model within the overall cycle simulation framework is presented in Chapter 4. In this section, the modelling assumptions and the performance representation of the compressors are introduced.

Centrifugal compressors exhibit a strong dependence of their performance on operating conditions, particularly in terms of mass flow rate, pressure ratio and rotational speed. For this reason, the behaviour is commonly described through characteristic compressor maps, which provide a comprehensive representation of the admissible operating domain and of the efficiency variations.

In the present work the compressor performance is represented through characteristic maps reconstructed from manufacturer technical documentation [34]. The reconstructed map, shown in Figure 3.18, is expressed in non dimensional form and is defined by the normalized volumetric flow rate, $\dot{V}/\dot{V}_{\text{nom}}$, on the horizontal axis and the normalized isentropic enthalpy difference, $\Delta h_{\text{is}}/\Delta h_{\text{is,nom}}$, on the vertical axis. Within this operating domain, the maps include:

- a surge line, which defines the lower flow stability limit of the compressor and bounds the admissible operating region;
- multiple iso efficiency islands, describing the variation of the isentropic efficiency as a function of flow rate and pressure ratio, with efficiency values ranging approximately from 0.75 to 0.96;
- distinct operating curves corresponding to different inlet guide vanes (IGVs) openings, spanning from near closed positions of 80° to fully open conditions at 20°, which allow regulation of the mass flow rate and extend the compressor operating flexibility under partial load conditions.

The presence of inlet guide vanes enables the compressors to adapt to variations in system demand, while maintaining acceptable efficiency levels and avoiding unstable operation. This aspect is particularly relevant for heat pump applications, where

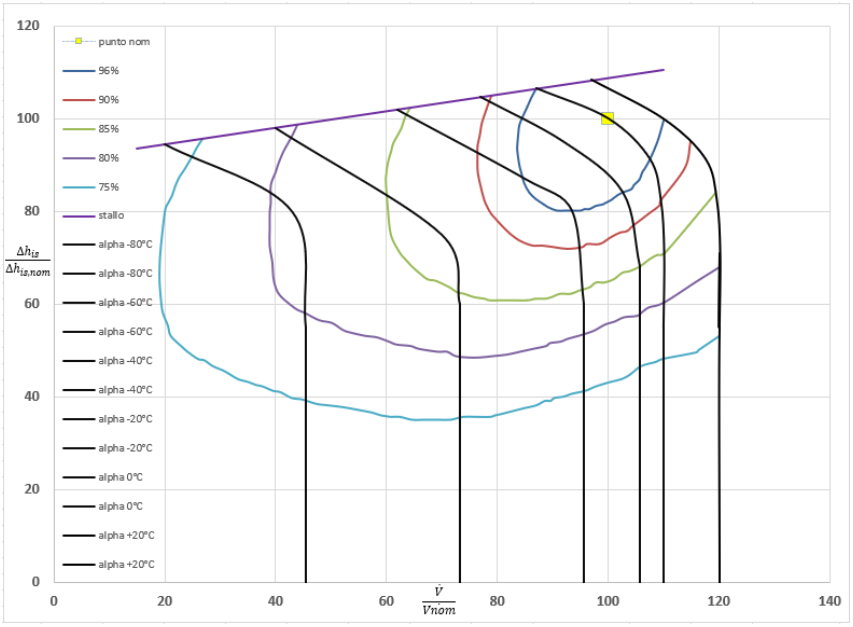

Figure 3.18: Non dimensional characteristic map of the centrifugal compressor.

off-design operation frequently occurs due to variable heat source and heat sink conditions. In the present analysis, the compressor operating points are always constrained to remain within the admissible operating domain of the characteristic map, to ensure reliable and physically consistent results.

For each compressor, a nominal operating point is defined and assumed to coincide with the on design operating conditions of the heat pump cycle. The nominal values of volumetric flow rate $\dot{V}_{\text{nom}}$ and isentropic enthalpy rise $\Delta h_{\text{is,nom}}$ are therefore set equal to the corresponding on design quantities.

Accordingly, the compressor maps are normalised with respect to this nominal point and expressed in terms of the dimensionless ratios $\dot{V}/\dot{V}_{\text{nom}}$ and $\Delta h_{\text{is}}/\Delta h_{\text{is,nom}}$. By definition, at the nominal operating point both ratios are equal to unit. This condition corresponds to the reference operating point highlighted in the compressor map with yellow marker, around which the efficiency variation is evaluated under off design conditions.

In the subsequent cycle analysis, the normalised isentropic efficiency obtained from the compressor map is scaled by the nominal isentropic efficiency assumed for the compressors, in order to obtain realistic absolute efficiency values.

The electrical power required by the compressors is evaluated through steady state energy balances. For the low pressure and high pressure compressors, the compres-

sion power is computed as:

$$\dot{W}_{\mathrm{C,LP}} = \dot{m}_{\mathrm{ref,evap}} \left(h_2 - h_1 \right), \tag{3.66}$$

$$\dot{W}_{\mathrm{C,HP}} = \dot{m}_{\mathrm{ref,cond}} \left(h_4 - h_3 \right). \tag{3.67}$$

In both cases, the inlet mass flow rate and the inlet specific enthalpy are known from the thermodynamic state of the cycle, while the outlet enthalpy is evaluated using the definition of isentropic efficiency. The isentropic efficiency of each compressor is defined as:

$$\eta_{\mathrm{is,LP}} = \frac{h_{2,\mathrm{is}}(P_{\mathrm{int}}, s_1) - h_1}{h_2 - h_1}, \tag{3.68}$$

$$\eta_{\mathrm{is,HP}} = \frac{h_{4,\mathrm{is}}(P_{\mathrm{cond}}, s_3) - h_3}{h_4 - h_3}. \tag{3.69}$$

The isentropic outlet enthalpies are evaluated at the compressor discharge pressure using the inlet entropy, while the isentropic efficiencies are obtained from the compressor maps as a function of the operating conditions. In particular, the efficiency variation is expressed as:

$$\eta_{\mathrm{is}} = f\left(\frac{\Delta h_{\mathrm{is}}}{\Delta h_{\mathrm{is,nom}}}, \frac{\dot{V}}{\dot{V}_{\mathrm{nom}}} \right). \tag{3.70}$$

This map based formulation allows the compressor performance to be evaluated consistently under both on design and off design conditions. The numerical procedure adopted to integrate the compressor maps within the heat pump cycle model is described in detail in Chapter 4.

3.4.8. Flash Chamber

The operating principle and the role of the flash chamber within the double vapour compression cycle have been described in Chapter 2. In brief, it separates the liquid and vapour phases after the first expansion valve and before the second one, allowing only the vapour fraction to be directed toward the high-pressure compressor. In this way, it contributes to a reduction in the compression work and to a more stable and efficient operation of the overall cycle.

From a modelling point of view, the flash chamber is not subject to a geometrical sizing procedure and does not require the definition of a specific internal structure.

For cycle analysis it is modelled as an ideal adiabatic separator operating at the intermediate pressure P_{int}. Phase separation is assumed to occur at thermodynamic equilibrium, with vapour withdrawn from the top and liquid collected at the bottom, while heat transfer and pressure losses are neglected.

The behaviour of the flash chamber is therefore entirely governed by the intermediate pressure level, which uniquely determines the vapour quality at the inlet and, consequently the mass flow rates of the separated streams. The mass balance across the flash chamber can be expressed as:

$$\dot{m} = x_v \dot{m} + (1 - x_v)\dot{m} = \dot{m}_{\ell,\text{evap}} + \dot{m}_{v,\text{flash}}, \tag{3.71}$$

where the vapour quality $x_v = x_6$ depends on the thermodynamic state of the refrigerant after the first expansion and is directly determined by the intermediate pressure P_{int}.

3.4.9. Mixer

The mixer combines the vapour streams exiting the flash chamber and the low-pressure compressor before the second compression stage. As mixing occurs at the same pressure level and without phase change, no geometrical sizing is required.

From a modelling standpoint, the mixer is treated as an ideal adiabatic control volume, with no work interactions or pressure losses. Its behaviour is fully described by mass and energy balance equations:

$$\dot{m}_{\text{out,mix}} = \dot{m}_{\text{out,LP}} + \dot{m}_{\text{vap,flash}}, \tag{3.72}$$

$$\dot{m}_{\text{out,mix}}\, h_{\text{out,mix}} = \dot{m}_{\text{out,LP}}\, h_{\text{out,LP}} + \dot{m}_{\text{vap,flash}}\, h_{\text{vap,flash}}. \tag{3.73}$$

The thermodynamic state of the mixed vapour stream is obtained from these balances and is used as the inlet condition for the high pressure compressor.

3.4.10. Throttling Valves

The system employs two throttling valves, as described in Chapter 2, which induce two successive expansions from the subcooler outlet to the intermediate pressure and from the intermediate to the evaporation pressure. These pressure drops determine the refrigerant thermodynamic states and thus strongly affect the cycle performance.

They are modelled as ideal adiabatic devices performing isenthalpic pressure reductions of the refrigerant streams exiting the subcooler and the flash chamber, respectively. As their behaviour is fully defined by the imposed pressure levels and the isenthalpic assumption, no geometrical sizing is performed. The throttling process, which corrispond to an isenthalpic lamination, is irreversible and entails entropy generation due to frictional dissipation. Neglecting work interactions, heat transfer, and kinetic and potential energy variations, the energy balance reduces to:

$$h_{\text{in}} = h_{\text{out}}. \tag{3.74}$$

4 | On Design Detailed Calculation Procedure

This chapter describes the numerical procedure adopted to determine the on design operating point of the heat pump system analysed in this work. While the Chapter 3 focused on the thermodynamic formulation of the cycle and on the physical models adopted for the individual components, the present one is devoted to the solution strategy and to the algorithmic implementation used to solve the resulting system of equations.

The calculation procedure is implemented in a modular numerical framework and combines the thermodynamic cycle model, the iterative determination of the condensation temperature T_{cond}, the integration of compressor performance maps, and the preliminary sizing of the main heat exchangers. The overall structure of the algorithm is designed to ensure numerical robustness, thermodynamic consistency, and extensibility toward off design analyses.

4.1. Overview of the calculation strategy

This section provides a high level description of the on design calculation strategy adopted in this work. The objective of the algorithm is to determine a thermodynamically consistent operating point of the heat pump system, that satisfies the imposed boundary conditions, thermal constraints and modelling assumptions introduced in the previous chapters.

Starting from a set of prescribed input data and design hypotheses described in Sections 3.1 and 3.2, the algorithm computes all thermodynamic state points of the refrigerant cycle including: pressures, temperatures and specific properties at each location. The solution is obtained through an iterative procedure that converges on the condensation temperature T_{cond}, which represents the key coupling variable between the refrigerant cycle and the heating water side.

At each iteration the refrigerant flow rate is determined from the imposed evaporator thermal power and the energy balances of the individual components and of the overall system are continuously verified to ensure thermodynamic consistency. The calculation framework integrates the physical models of all main components of the heat pump, including the two-stage compression system, for which the compressor efficiencies are evaluated using performance maps.

Once convergence is achieved, the algorithm provides a complete on design description of the heat pump operation, including: heat duties, compressor power consumptions and performance indicators. Based on the converged operating conditions, the heat exchangers are subsequently sized according to the adopted heat transfer correlations and geometric constraints.

4.2. Modular structure of the numerical routine

The on design calculation framework has been developed following a fully modular structure in order to clearly separate the physical modelling of the system from the numerical solution strategy and from the post processing routines. The overall algorithm is organised into six main functional modules, each responsible for a specific task within the calculation workflow.

A schematic overview of the modular structure is provided in Figure 4.1.

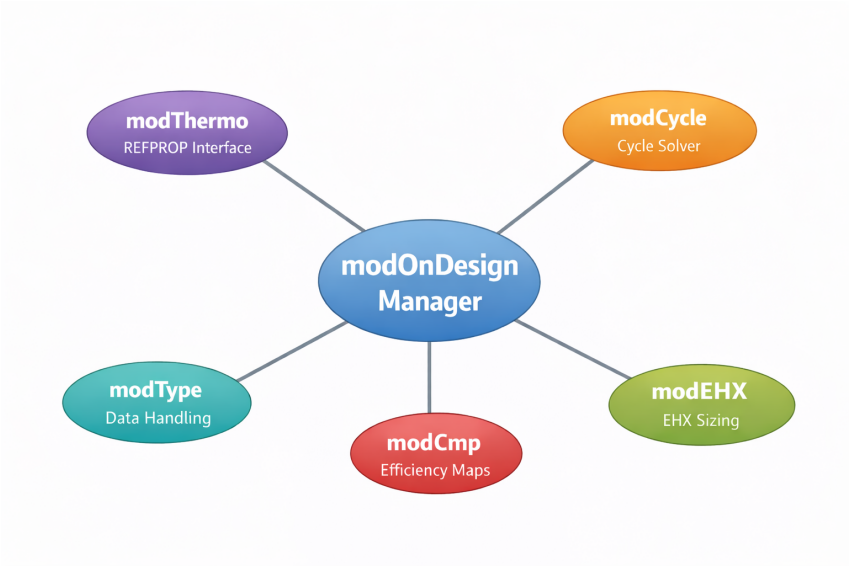

Figure 4.1: Modular structure of the on design numerical algoritm.

The numerical routine is composed as follows:

– `modOnDesignManager:` top level manager of the on design simulation work-

flow, from input acquisition to final output generation. The main routine, `RunOnDesign`, reads boundary conditions and modelling parameters from the input worksheet and iteratively converges on the condensation temperature T_{cond} using a relaxation based scheme. At each iteration, the thermodynamic cycle is evaluated, refrigerant and water side mass flow rates are updated, outlet water temperature T_x is computed and heat duties and power consumptions are determined, with convergence monitored via the condenser approach residual.

After convergence, a final cycle evaluation is performed, compressor efficiencies are updated through performance map interpolation, and the head duty, compressor works, electrical consumptions, performance indicators and energy balances are computed. The routine finally implemented the heat exchanger sizing procedures.

- `modCycle:` this module performs the deterministic calculation of all thermodynamic state points of the double stage vapour compression cycle throught the routine `RunCycle` . Given the evaporation and condensation temperatures, the intermediate pressure definition and the isentropic efficiencies of the compressors, it evaluates the thermodynamic properties at each point of the cycle by enforcing the component level physical relations described in Chapter 3.
- `modCmp:` this module provides a physics based representation of compressor performance using manufacturer efficiency maps, thereby avoiding the assumption of fixed isentropic efficiencies. Compressor performance is evaluated as a function of the actual operating conditions of the cycle. The module includes three main routines:
  - `Interp2D_Scatter` which performs two dimensional interpolation of scattered map data, using volumetric flow rate and isentropic enthalpy rise as independent variables, enabling efficiency evaluation for off grid operating points.
  - `CmpEff_Iterative` which interfaces the thermodynamic cycle solver with the compressor maps by computing volumetric flow rates from the current cycle solution, normalising the operating point with respect to nominal conditions and returning the updated isentropic efficiencies for each compression stage.
  - `Compressorefficiency_on` which applies the interpolated efficiencies within

the overall calculation framework, including correction factors for mechanical and electrical losses and is called iteratively in the on design algorithm to ensure consistent convergence between compressor performance and cycle thermodynamics.

– `modEHX:` this module performs the thermal modelling and geometrical sizing of all heat exchangers in the heat pump system, translating the thermal duties obtained from the converged cycle into physically consistent geometries based on prescribed heat transfer coefficients, temperature differences and constructive constraints.

  An area based design approach is adopted, whereby the required heat transfer surface is computed from the heat duty, the overall heat transfer coefficient and the logarithmic mean temperature difference. The global heat transfer coefficient is evaluated through a resistance in series formulation accounting for internal and external convection, wall conduction and fouling effects, while robust formulations of the ΔT_{ml} are implemented to ensure numerical stability.

  These calculations are implemented through dedicated functions, including `U_global_outer`, ΔT_{ml}`_CounterCurrent`, `AreaExt`, `AreaRequired` and `VolumeShell`, whose formulation is detailed in the sections devoted to heat exchanger sizing.

  The actual sizing is performed through three design routines:

  * `Evaporator_Design_V1` which sizes the evaporator and superheater by allocating the total exchanger length between the two thermal zones.
  * `Condenser_Design_V1`, which sizes the desuperheater and condenser by distributing the total heat transfer surface between vapour cooling and condensation within the same shell and tube geometry.
  * `Subcooler_Design_V1`, which independently sizes the subcooler based on the required subcooling duty and the associated temperature driving forces.

  For each heat exchanger, the design routines explore a predefined geometrical design space (number of tubes and total length) and select the configuration that meets the required heat transfer area while minimising the exchanger volume. The resulting geometrical parameters are returned to the on design algorithm and included in the final output.

– `modThermo:` this module provides the thermodynamic backbone of the nu-

merical framework by implementing a clean and consistent interface to the *REFPROP* database together with a set of auxiliary thermodynamic utilities. Its main role is to ensure unit consistency, numerical robustness and modular access to fluid properties throughout the entire calculation. Different functions are involved:

  * `RP_Enthalpy_TP`, `RP_Temperature_PH`, `RP_Density_TP`, `RP_Pressure` are dedicated wrapper functions which provide the access to the thermodynamic properties in the *MOLAR SI* formulation, shielding the rest of the code from direct calls to the *REFPROP* library.

  * The routines `EvalPoint_TP` and `EvalPoint_PQ` are used to construct and store thermodynamic state points in a structured form. Given a pair of independent variables like T, P or P, Q, these routines evaluate all remaining thermodynamic properties by internally calling the *REFPROP* wrapper functions, ensuring a consistent and reusable definition of temperature, pressure, enthalpy, entropy, and vapour quality at each point of the cycle.

- `modType:` this module defines the data structures and output handling routines used to store, organise and export the results of the on design calculations, thus decoupling data management from numerical logic and improving code modularity and maintainability. The main functions considered are:

  * `CyclePoint`, `CycleResult`, `PrintData` are structured data types introduced to represent thermodynamic state points, cycle level quantities and global performance indicators. In particular, `CyclePoint` stores the complete set of thermodynamic variables (T, P, h, s, x), `CycleResult` collects the full thermodynamic solution of the cycle (including state points and main quantities such as refrigerant mass flow rate, evaporator and condenser heat duties, and compressor power consumptions), while `PrintData` gathers the global on design results and performance indicators required for post processing.

  * The routine `PrintResultsClean` manages the structured export of the converged thermodynamic state points, cycle performance indicators and heat exchanger sizing outputs to a dedicated results worksheet, facilitating post-processing and analysis.

4.3. Recall of input and modelling assumptions

As discussed in detail in Section 3.1, the on design simulation is based on a set of boundary conditions and modelling assumptions that define the operating context of the heat pump system. In this section, the main inputs are briefly recalled as follows:

- **Wastewater side:** reported in Table, 3.4
- **distict line circuit:** reported in Table 3.5:
- **heat exchanger characteristic temperature differences:** reported in Table 3.6;
- **initial condensation temperature:** T_{cond} is assumed as a starting point for the calculation. This value is subsequently updated within the on design algorithm through an iterative convergence procedure, which is described in the following section;
- **Compressor reference efficiency:** the nominal isentropic efficiency of both compressor stages is prescribed and set equal to $\eta_{\text{is,nom}} = 0.8$. This value defines the reference efficiency level at the on design operating point and is used to scale the map based dimensionless efficiencies.

4.4. On Design Routine

This section provides a detailed description of the numerical algorithm adopted for the on design simulation of the heat pump system, reported in Figure 4.2.

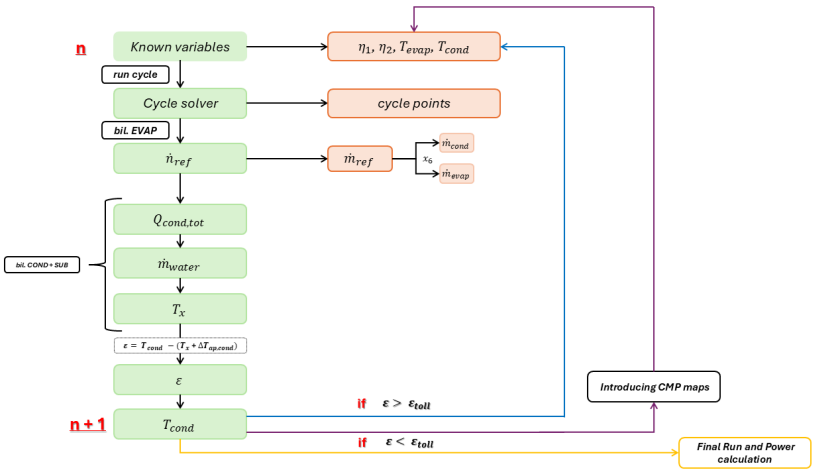

Figure 4.2: Iterative on design solution scheme.

4.4.1. Thermodynamic cycle solver and Refrigerant flow rate determination

At a generic iteration n of the on-design calculation procedure, the evaporation temperature T_{evap}, the current estimate of the condensation temperature $T_{\text{cond}}^{(n)}$ and the compressor isentropic efficiencies η_1 and η_2 are treated as known quantities.

For this set of inputs, the thermodynamic cycle is solved by calling the routine `RunCycle`, which performs a deterministic evaluation of all thermodynamic state points of the double stage vapour compression cycle according to the modelling framework introduced in Chapter 3 at Subsection 3.3.1. In particular, the following steps are carried out at each iteration:

- the saturation pressures, $P_{\text{cond}}^{(n)}$ and P_{evap}, corresponding to T_{evap} and $T_{\text{cond}}^{(n)}$ are evaluated and the intermediate pressure level is defined according to the selected criterion;
- all thermodynamic state points of the cycle are computed, including the compressor inlet and outlet states, the flash tank conditions and the saturated and subcooled liquid states at the condenser outlet;
- the complete set of molar enthalpies, entropies, temperatures and vapour qualities is stored in a structured form for subsequent calculations.

Once the thermodynamic state of all cycle points are available at iteration n, the refrigerant molar flow rate is determined by enforcing the energy balance at the evaporator. The required evaporator heat duty $\dot{Q}_{\text{evap,req}}$ is imposed as a constraint, yielding:

$$\dot{n}_{\text{ref}}^{(n)} = \frac{(\dot{Q}_{\text{evap,req}} \times 10^3)}{\left(h_1^{(n)} - h_9^{(n)}\right)\left(1 - x_6^{(n)}\right)}, \tag{4.1}$$

where $h_1^{(n)}$ and $h_9^{(n)}$ denote, respectively, the molar enthalpies at the evaporator outlet and inlet and $x_6^{(n)}$ is the vapour quality at the flash tank outlet feeding the evaporator branch.

The corresponding refrigerant mass flow rate, expressed in kg/s, is then obtained as:

$$\dot{m}_{\text{ref}}^{(n)} = \dot{n}_{\text{ref}}^{(n)} \frac{M_{\text{mol}}}{1000}. \tag{4.2}$$

Due to the presence of the flash tank, the mass flow rates through the condenser

and the evaporator are given by

$$\dot{m}_{\text{cond}}^{(n)} = \dot{m}_{\text{ref}}^{(n)}, \qquad \dot{m}_{\text{evap}}^{(n)} = \dot{m}_{\text{ref}}^{(n)} \left(1 - x_6^{(n)}\right). \tag{4.3}$$

This procedure is repeated at every iteration n of the on design algorithm. For each updated estimate of $T_{\text{cond}}^{(n)}$, a complete and thermodynamically consistent solution of the cycle and the associated refrigerant flow rates is obtained. The resulting cycle solution is then used to evaluate the condenser heat duty and the water side outlet temperature, which drive the condensation temperature convergence procedure described in the following section.

4.4.2. Condensation temperature convergence procedure

The condensation temperature T_{cond} is determined iteratively to ensure consistency between the refrigerant cycle and the condenser side heat transfer. At each iteration n, a trial value $T_{\text{cond}}^{(n)}$ is assumed and the thermodynamic cycle is fully solved.

Based on the cycle solution obtained at iteration n, the condenser side heat transfer, expressed in kW, is evaluated in order to update the hot water outlet temperature. The total heat rejected by the refrigerant at the condenser and subcooler is computed from the enthalpy drop between the compressor outlet and the subcooled liquid state as:

$$\dot{Q}_{\text{cond,tot}}^{(n)} = \frac{\dot{n}_{\text{ref}}^{(n)} \left(h_4^{(n)} - h_{5,\text{sub}}^{(n)}\right)}{1000}. \tag{4.4}$$

The water mass flow rate on the hot side of the condenser is then updated according to the imposed fraction of thermal coverage by the heat pump f_{HP}, presented in Sub section 3.3.4, as:

$$\dot{m}_{\text{water}}^{(n)} = \frac{\dot{Q}_{\text{cond,tot}}^{(n)}}{f_{\text{HP}}\, c_{p,\text{w}} \left(T_{\text{water,out}} - T_{\text{water,in}}\right)}. \tag{4.5}$$

Using the updated water mass flow rate, the outlet temperature of the water stream at the exit of the desuperheater section, denoted as $T_x^{(n)}$, is computed from the condenser side energy balance as:

$$T_x^{(n)} = T_{\text{water,in}} + \frac{\dot{Q}_{\text{cond,tot}}^{(n)}}{\dot{m}_{\text{water}}^{(n)}\, c_{p,\text{w}}}. \tag{4.6}$$

The convergence condition is defined by enforcing a prescribed approach tempera-

ture difference between the condensation temperature and the water temperature at the desuperheater outlet. This condition is written as:

$$\varepsilon^{(n)} = T_{\text{cond}}^{(n)} - \left(T_x^{(n)} + \Delta T_{\text{ap,cond}}\right), \tag{4.7}$$

where $\Delta T_{\text{ap,cond}}$ is the imposed condenser approach temperature showed in Figure 3.3. This temperature difference is referred to as an approach point, since the actual pinch point occurs between the condensing refrigerant and the water stream at the condenser outlet, rather than at the desuperheater exit.

The residual $\varepsilon^{(n)}$ is used to update the condensation temperature through a relaxation-based scheme:

$$T_{\text{cond}}^{(n+1)} = T_{\text{cond}}^{(n)} - k\,\varepsilon^{(n)}, \tag{4.8}$$

where k is a relaxation factor introduced to improve numerical stability.

The iterative procedure is repeated until the convergence criterion $|\varepsilon^{(n)}| < \varepsilon_{\text{tol}}$ is satisfied. Once convergence is achieved, a final solution of the thermodynamic cycle is performed using the converged value of T_{cond}, yielding the on design values of all state points, heat duties, power consumptions and performance indicators. Global energy balances are finally verified to ensure the thermodynamic consistency of the converged solution.

4.4.3. Compressor performance map integration

After the convergence of the condensation temperature described in the previous section, the thermodynamic cycle is available at a consistent on design operating point. At this stage, all thermodynamic state variables have been evaluated for the converged value of T_{cond}, while the compressor isentropic efficiencies η_1 and η_2 still correspond to the values assumed during the convergence loop.

The effective compressor efficiencies are then evaluated through a dedicated matching procedure implemented in the routine `CmpEff_Iterative`. This routine performs the coupling between the converged thermodynamic cycle and the compressor performance map and is executed only after the convergence on T_{cond}, in order to avoid introducing additional nonlinear dependencies within the main iterative algorithm.

The operating point of each compression stage is first identified in terms of inlet volumetric flow rate and isentropic enthalpy rise. For the low pressure and high

pressure stages, the inlet volumetric flow rates are evaluated as:

$$\dot{V}_1 = \frac{\dot{m}_{\text{evap}}}{\rho_1}, \qquad \dot{V}_2 = \frac{\dot{m}_{\text{cond}}}{\rho_3}, \tag{4.9}$$

where $\dot{m}_{\text{evap}}$ and $\dot{m}_{\text{cond}}$ are respectively the refrigerant mass flow rates through the evaporator and condenser branches and ρ_1 and ρ_3 denote the refrigerant densities at the corresponding compressor inlet states. The stage loading is represented by the isentropic enthalpy rise, computed from the isentropic reference outlet states already available from the cycle solver:

$$\Delta h_{1,\text{s}} = h_{2\text{s}} - h_1, \qquad \Delta h_{2,\text{s}} = h_{4\text{s}} - h_3. \tag{4.10}$$

In order to extract data from the compressor performance map, the operating variables are expressed in dimensionless form by normalization with respect to nominal reference values:

$$\dot{V}_{i,n} = \frac{\dot{V}_i}{\dot{V}_{i,\text{nom}}}, \qquad \Delta h_{i,\text{s},n} = \frac{\Delta h_{i,\text{s}}}{\Delta h_{i,\text{s,nom}}}, \qquad i = 1, 2. \tag{4.11}$$

The selection of the nominal reference values is a key aspect of the implementation. In the present on design routine, the nominal volumetric flow rates $\dot{V}_{i,\text{nom}}$ and nominal isentropic enthalpy rises $\Delta h_{i,\text{s,nom}}$ are directly extracted from the converged on design cycle solution. With this choice, the normalization yields, by construction,

$$(\dot{V}_{i,n}, \Delta h_{i,\text{s},n}) = (1, 1), \qquad i = 1, 2, \tag{4.12}$$

for the on design operating condition. When expressed in the percentage based representation adopted in the compressor performance map, this corresponds to the point $(100, 100)$ on the two map axes.

As shown by the red points reported in Figure 4.3, the compressor map is defined such that the nominal point $(100, 100)$ corresponds to a unitary efficiency value, $\eta_{i,\text{map}} = 1$. This convention ensures that the on design operating condition is always located at the reference point of the map, while the map itself is used to capture the relative variation of compressor efficiency with respect to changes in volumetric flow rate and stage loading around the on design point.

Once the normalized operating point is identified, the corresponding isentropic efficiencies are evaluated by two dimensional interpolation of the manufacturer data.

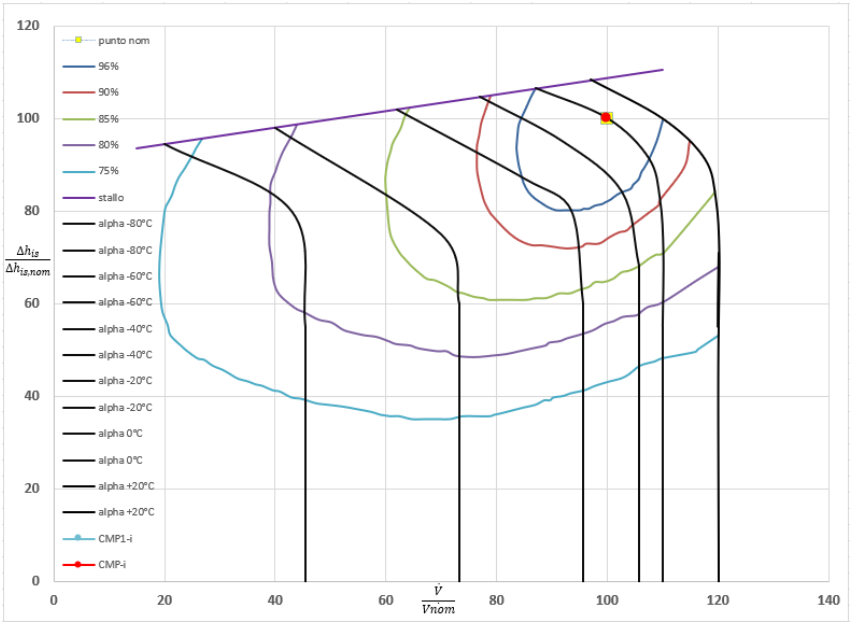

Figure 4.3: Operating points of the compressors on the performance map.

This operation is carried out by the routine `Interp2D_Scatter`, which operates on a set of scattered data points in the $(\dot{V}_{i,n}, \Delta h_{i,\mathrm{s},n})$ plane and returns the map based efficiencies $\eta_{1,\mathrm{map}}$ and $\eta_{2,\mathrm{map}}$.

Since the nominal reference point is defined to coincide with the on design operating condition, the normalized operating point is mapped to unitary coordinates. As a consequence, the efficiencies returned by the compressor performance map at this point are equal to unity by construction.

Within this framework, the map based efficiencies represent relative variations with respect to the on design condition and are therefore combined with the isentropic efficiency assumed at the on design operating point according to:

$$\eta_1 = \eta_{\mathrm{is,nom}}\,\eta_{1,\mathrm{map}}, \qquad \eta_2 = \eta_{\mathrm{is,nom}}\,\eta_{2,\mathrm{map}}, \tag{4.13}$$

with $\eta_{\mathrm{is,nom}} = 0.8$.

In this formulation, the compressor performance map accounts for the efficiency variation associated with the mass flow rates and isentropic enthalpy rises of the thermodynamic cycle, while the absolute efficiency level is fixed by the on design reference value.

4.4.4. Final powers and performance indicators evaluation

Finally, the thermodynamic cycle is solved again using the updated compressor efficiencies and the converged condensation temperature. This final run provides the on design values of all thermodynamic state points, heat duties, power consumptions and performance indicators. The thermal, mechanical and electrical power levels involved in the system, calculate with the equations reported below, are all divided by factor 10^3, in order to obtain result in [kW].

The heat duty of the evaporator, condenser and subcooler are calculate accordingly to equations express before. For completeness, they are reported in Table 4.1.

Heat duty	Reference equation
$\dot{Q}_{\text{evap}}$	Eq. (3.18)
$\dot{Q}_{\text{sh}}$	Eq. (3.19)
$\dot{Q}_{\text{cond}}$	Eq. (3.25)
$\dot{Q}_{\text{desh}}$	Eq. (3.24)
$\dot{Q}_{\text{sub}}$	Eq. (3.26)

Table 4.1: Reference of the heat duty equations used in the thermodynamic cycle.

The water side mass flow rate is then evaluated from Equation 4.5 and the corresponding water temperature at the exit of the desuperheater section, T_x, is computed as Equation 4.6.

The residual heat contribution and the total heat supplied to the heating network are evaluated as Equations 3.35 and 3.34, where $\dot{Q}_{\text{tot}}$ could be also evaluated as:

$$\dot{Q}_{\text{tot}} = Q_{\text{cond,tot}} + Q_{\text{res}}. \tag{4.14}$$

The mechanical power absorbed by the compressors is computed using Equations 3.20 and 3.21.

The corresponding electrical power consumption of the compressors and the pump of the intermediate circuit are obtained using Equations 3.29 and 3.30.

Finally, the coefficient of performance of the heat pump cycle and of the system are evaluated with Equations 3.31 and 3.36.

When $f_{\text{HP}} = 1$, as assumed in the present on design analysis, the entire heat demand

is covered by the heat pump, leading to $\dot{Q}_{\text{res}} = 0$, $T_x = T_{\text{water,out}}$ and $\dot{Q}\text{tot} = \dot{Q}_{\text{cond,tot}}$. Under this condition, the system and cycle coefficients of performance coincide, so $\text{COP}_{\text{sys}} = \text{COP}_{\text{cycle}}$.

All thermal and mechanical power terms are evaluated using the converged thermodynamic state points. At each iteration of the on design routine, energy balances are verified through two dedicated discrepancy formulations.

The first balance refers to the heat pump cycle alone and is defined as:

$$\text{Discrepancy} = \dot{Q}_{\text{cond,tot}} - \dot{Q}_{\text{eva}} - \dot{W}_{\text{cmp}} - \dot{Q}_{\text{sh}}, \tag{4.15}$$

which represents the closure of the internal energy balance of the vapour compression cycle.

A second balance is formulated at system level as:

$$\text{Bil}_{\text{glob}} = \dot{Q}_{\text{cond,tot}} - \dot{W}_{\text{cmp}} - \dot{W}_{\text{pump}} - \dot{Q}_{\text{wastewater}}, \tag{4.16}$$

accounting for the complete heat pump system, including auxiliary electrical consumptions and the thermal input from the wastewater source.

Both discrepancy terms are monitored at each iteration in order to ensure the thermodynamic consistency and numerical closure of the on design solution.

4.4.5. Heat exchanger sizing

Before performing the geometric sizing, the on design routine evaluates the integral heat transfer coefficients and the logarithmic mean temperature differences for each heat exchanger section as follows. The geometric parameters of the heat exchangers are assumed as known inputs based on the design choices introduced in Chapter 3.

In particular, the thermal conductivity of the heat exchanger wall, the fouling resistances on the external and internal side are assumed equal to:

$$k = 390 \text{ W/m K}, \qquad R_{\text{f,o}} = 0 \text{ m}^2\text{K/W}, \qquad R_{\text{f,i}} = 0.002 \text{ m}^2\text{K/W}, \tag{4.17}$$

consistent with copper based materials [35] and typical values reported in the literature [26].

Evaluation of heat transfer coefficients

Based on the heat transfer correlations introduced in Chapter 3, the local heat transfer coefficients required for the heat exchanger sizing are evaluated numerically. In order to account for the variation of thermophysical properties along the heat exchangers, the heat transfer process is resolved by discretising the thermodynamic path of the working fluids and computing local heat transfer coefficients over a finite number of sub intervals, which are subsequently integrated to obtain representative mean values. This procedure is applid only to single phase heat transfer conditions. In case of boiling and condensation, Rohsenow and Nusselt correlations described in Chapter 6 are adopted instead and no spatial integration along the exchanger length is needed.

Two distinct numerical procedures are adopted for the refrigerant side and for the water side:

- **External heat transfer coefficient for refrigerant side:** on the refrigerant side, the working fluid is R1234ze operating in single phase conditions within the superheating, desuperheating and subcooling sections. The local heat transfer coefficient is evaluated using the Zukauskas correlation reported in Equation 3.48. The integration is performed along the enthalpy coordinate between the inlet and outlet states of each heat exchanger section. The total enthalpy variation $\Delta h = h_{\text{out}} - h_{\text{in}}$ is divided into $n = 20$ equal sub intervals and the local enthalpy at each step is defined as:

$$h_i = h_{\text{in}} + i\,\frac{\Delta h}{n}, \qquad i = 0, \ldots, n. \tag{4.18}$$

  At each enthalpy level, thermophysical properties are evaluated and the corresponding local heat transfer coefficient is computed. The integral mean external heat transfer coefficient is then obtained by averaging the local values over the entire enthalpy range.

- **Internal heat transfer coefficient for water side:** on the internal side the secondary fluid is water, which remains in the liquid phase over the entire operating range considered. The local heat transfer coefficient is evaluated using the Gnielinski correlation for internal turbulent flow, reported in Equation 3.54. The integration is performed by discretising the temperature interval between the inlet and outlet water temperatures into $n = 20$ equal sub intervals.

The local temperature at each step is expressed as:

$$T_i = T_{\text{in}} + i\,\Delta T, \qquad i = 0, \ldots, n, \tag{4.19}$$

where $\Delta T = (T_{\text{out}} - T_{\text{in}})/n$. At each temperature level, thermophysical properties are evaluated and the corresponding local heat transfer coefficient is computed. The mean internal heat transfer coefficient is finally obtained by averaging the local values over the entire temperature range.

This numerical integration approach ensures that the evaluated heat transfer coefficients consistently reflect the spatial variation of fluid properties along the heat exchangers, providing a robust coupling between the thermodynamic cycle solution and the subsequent heat exchanger sizing procedure.

Evaluation of the overall heat transfer coefficient

For each heat exchanger section, once the internal and external convective heat transfer coefficients have been evaluated and the wall and fouling properties are known, the overall heat transfer coefficient is computed using the classical thermal resistance method. In the present work, the overall heat transfer coefficient is consistently referred to the external heat transfer surface.

Accordingly, the overall heat transfer coefficient is expressed as:

$$U = \left(R_{\text{conv,i}} + R_{\text{f,i}} + R_{\text{wall}} + R_{\text{f,o}} + R_{\text{conv,o}}\right)^{-1}, \tag{4.20}$$

where all thermal resistances are referred to the external surface area by multiplication with the diameter ratio $D_{\text{o}}/D_{\text{i}}$.

The individual resistance terms are defined as follows:

- **Internal convective resistance:**

$$R_{\text{conv,i}} = \frac{D_{\text{o}}}{D_{\text{i}}\,h_{\text{i}}}, \tag{4.21}$$

- **External convective resistance:**

$$R_{\text{conv,o}} = \frac{1}{h_{\text{o}}}, \tag{4.22}$$

– **Cylindrical wall conduction resistance:**

$$R_{\text{wall}} = \frac{D_{\text{o}}}{2\,k_{\text{wall}}} \ln\left(\frac{D_{\text{o}}}{D_{\text{i}}}\right), \tag{4.23}$$

– **Fouling resistances:**

$$R_{\text{f,i}}, \qquad R_{\text{f,o}}. \tag{4.24}$$

This formulation is applied consistently to all heat exchanger sections within the sizing procedure.

Evaluation of logarithmic mean temperature differences

For the purpose of heat exchanger sizing, the logarithmic mean temperature difference (ΔT_{ml}) is evaluated for each heat exchanger section using the thermodynamic state points obtained from the converged on-design cycle solution. The logarithmic mean temperature difference is computed according to the classical definition:

$$\begin{aligned} \Delta T_{\text{ml}} &= \frac{\Delta T_1 - \Delta T_2}{\ln\left(\dfrac{\Delta T_1}{\Delta T_2}\right)}, \\ \Delta T_1 &= T_{\text{h,in}} - T_{\text{c,out}}, \\ \Delta T_2 &= T_{\text{h,out}} - T_{\text{c,in}}, \end{aligned} \tag{4.25}$$

where ΔT_1 and ΔT_2 denote the temperature differences between the hot and cold streams at the two ends of the heat exchanger. All heat exchangers are modelled assuming a counter current configuration. Inlet and outlet temperatures adopted for the evaluation of ΔT_{ml}, which are specific to each heat exchanger, are summarised in Table 4.2.

Heat exchanger	$\mathbf{T}_{\text{h,in}}$	$\mathbf{T}_{\text{h,out}}$	$\mathbf{T}_{\text{c,in}}$	$\mathbf{T}_{\text{c,out}}$
Desuperheater	T_4	T_{cond}	T_{z}	$T_{\text{water,out}} = T_{\text{x}}$
Condenser	T_{cond}	T_{cond}	T_{y}	T_{z}
Subcooler	T_{cond}	$T_{5,\text{sub}}$	$T_{\text{water,in}}$	T_{y}
Superheater	T_{c}	T_{k}	T_{evap}	T_1
Evaporator	T_{k}	T_{d}	T_{evap}	T_{evap}

Table 4.2: Temperatures adopted for the evaluation of the (ΔT_{ml}).

Sizing Procedure

The sizing procedure is formulated as an iterative search over a bounded geometric design space, aimed at determining the number of tubes, the total heat exchanger length, the effective heat transfer area and the overall volume. The geometric bounds and the discretisation steps adopted for the number of tubes and the total length are reported in Table 4.3, allowing the sizing problem to be solved through a controlled exhaustive search of the admissible design space.

Parameter	Value
Minimum number of tubes, $N_{\min}$	500
Maximum number of tubes, $N_{\max}$	10 000
Minimum heat exchanger length, $L_{\min}$	1 m
Maximum heat exchanger length, $L_{\max}$	10 m
Length discretisation step, ΔL	0.1 m
Tube number discretisation step, ΔN	50

Table 4.3: Geometric bounds and discretisation steps adopted for the iterative heat exchanger sizing procedure.

The same sizing algorithm is applied to all heat exchangers considered in the system and is implemented through three dedicated numerical routines:

- `Evaporator_Design_V1` used for the evaporator and superheater sections;
- `Condenser_Design_V1` used for the condenser and desuperheater sections;
- `Subcooler_Design_V1` used for the subcooler.

The heat duty of a generical heat exchanger can be calculate as the enthalpy variation of the working fluid between the inlet and outlet thermodynamic states, as showed in Equation 3.25, or could be based on the overall heat transfer relation:

$$\dot{Q}_i = U_i \, A_i \, \Delta T_{\mathrm{lm},i}. \tag{4.26}$$

According to this, for a given heat exchanger i, the required heat transfer area is first evaluated from the imposed thermal duty as:

$$A_{\mathrm{req},i} = \frac{\dot{Q}_{\mathrm{req},i}}{U_i \, \Delta T_{\mathrm{ml},i} \, F_i} \tag{4.27}$$

where $Q_{\text{req},i}$ is the heat duty calculate from the thermodynamic points, U_i is the overall heat transfer coefficient, $\Delta T_{\text{ml},i}$ is the logarithmic mean temperature difference of the corresponding section and F_i is the logarithmic mean temperature difference reported in Subsection 3.4.5.

In Table 4.4 are reported the i heat exchangers involved in the present work and the corresponding adopted F_i values.

Section i	$\mathbf{A_{req,i}}$	$\mathbf{\dot{Q}_{req,i}}$	$\mathbf{F_i}$
Evaporator	$A_{\text{req,evap}}$	$\dot{Q}_{\text{req,evap}}$	1
Superheater	$A_{\text{req,sh}}$	$\dot{Q}_{\text{req,sh}}$	Subsec. 3.4.5
Desuperheater	$A_{\text{req,desh}}$	$\dot{Q}_{\text{req,desh}}$	Subsec. 3.4.5
Condenser	$A_{\text{req,cond}}$	$\dot{Q}_{\text{req,cond}}$	1
Subcooler	$A_{\text{req,sub}}$	$\dot{Q}_{\text{req,sub}}$	Subsec. 3.4.5

Table 4.4: Heat exchangers i considered.

The geometric design space is then explored by iterating over the number of tubes N_i and the total heat exchanger length $L_{\text{tot},i}$ within the prescribed bounds. For each geometric configuration, the available external heat transfer area is evaluated as:

$$A_i = N_i \, \pi D_{\text{o}} \, L_i, \tag{4.28}$$

and the corresponding shell volume is computed as:

$$V_i = \frac{\pi D_{\text{s}}^2}{4} \, L_{\text{tot},i}, \tag{4.29}$$

where D_{o} is the tube outer diameter and D_{s} is the shell diameter.

For heat exchangers composed of multiple thermal sections, the total length $L_{\text{tot},i}$ is further partitioned between the sections through a fractional parameter $f \in (0, 1)$:

$$L_{1,i} = f \, L_{\text{tot},i}, \qquad L_{2,i} = (1 - f) \, L_{\text{tot},i}, \tag{4.30}$$

where $L_{1,i}$ and $L_{2,i}$ denote the lengths of the two sections (i.e. evaporator and superheater, or desuperheater and condenser). The corresponding heat transfer areas

are evaluated independently as:

$$A_{1,i} = N_i \, \pi D_\mathrm{o} \, L_{1,i}, \qquad A_{2,i} = N_i \, \pi D_\mathrm{o} \, L_{2,i}. \tag{4.31}$$

A geometric configuration is considered feasible only if the area constraints are satisfied simultaneously for all sections:

$$A_{1,i} \geq A_{1,\mathrm{req},i}, \qquad A_{2,i} \geq A_{2,\mathrm{req},i}. \tag{4.32}$$

Among all feasible configurations, the sizing algorithm selects the solution that minimises the total heat exchanger volume. The resulting geometry therefore satisfies the imposed thermal requirements while yielding a compact design, consistent with the on design operating conditions of the heat pump system.

The adopted sizing procedure results in heat transfer areas A_i that are slightly larger than the minimum required values $A_{\mathrm{req},i}$, with the corresponding overdimensioning reported in the tables below. As a consequence, the designed heat exchangers are able to provide a heat duty marginally higher than the required one, leading to a conservative overestimation of the thermal performance.

Accordingly, by denoting as $A_{\mathrm{eff},i}$ the actual heat transfer area A_i obtained from the sizing procedure, the effective heat transfer rate provided by the i-th heat exchanger section is evaluated as:

$$\dot{Q}_{\mathrm{eff},i} = A_{\mathrm{eff},i} \, U_i \, \Delta T_{\mathrm{ml},i} \, F_i \tag{4.33}$$

where the correction factor F_i is applied only to the superheating, desuperheating and subcooling sections.

4.5. On design simulation results

The main results of the on design simulation are reported in this section and represent the nominal operating point of the heat pump cycle. The thermodynamic state points shown in the following tables correspond to the solution obtained by iterating on the condensation temperature T_{cond}, which ensures consistency between the cycle energy balances and the required heat transfer areas of the heat exchangers. The iterative procedure converges to a value temperature of $T_{\mathrm{cond}} = 358.152$ K.

It is worth noting that the effective heat transfer areas adopted in the final design

are slightly larger than the strictly required values. Consequently, the heat duties delivered by the real heat exchangers are marginally higher than those imposed during the on design sizing procedure. For thermofluid-dynamic consistency, the cycle can be recalculated by fixing the effective heat transfer areas and solving again for the thermodynamic state points using the off design modelling framework presented in the following chapter. This procedure will be explicitly performed; as shown in Chapter 5, the recalculated state points coincide with the on design results. This agreement is justified by the fact that the deviations in heat transfer areas are below 5%, leading to negligible variations in the cycle operating conditions.

4.5.1. Cycle Results

Table 4.5 reports the thermodynamic state points of the on design heat pump cycle, as obtained from the converged cycle simulation.

Point	T [K]	P [MPa]	h [kJ/kg]	s [kJ/(kg K)]	x [-]	Zone
P1	278.150	0.216	388.752	1.691	–	Evaporator outlet / Compressor inlet
P2s	318.448	0.819	414.3555	1.691	–	Isentropic compression (stage 1)
P2	324.505	0.819	420.756	1.711	–	Real compression (stage 1)
P3	322.279	0.819	418.409	1.704	–	Flash tank outlet
P4s	364.403	2.266	437.455	1.704	–	Isentropic compression (stage 2)
P4	367.604	2.266	442.217	1.717	–	Compressor 2 outlet
P5sub	341.150	2.232	296.930	1.310	–	Subcooled liquid
P5ls	358.149	2.232	326.065	1.393	–	Saturated liquid after flash
P5vs	358.149	2.232	428.409	1.679	–	Saturated vapour after flash
P6	315.650	0.819	296.930	1.319	0.250	Flash inlet
P7	315.650	0.819	258.715	1.198	–	Flash liquid
P8	315.650	0.819	411.380	1.681	–	Flash vapour
P9	273.689	0.221	258.715	1.215	0.315	Evaporator inlet

Table 4.5: Thermodynamic state points of the on design heat pump cycle.

Table 4.6 reported the results of the district heating water side temperatures at the condenser, desuperheater and sub cooler, while Table 4.7 reports the results of the intermediate loop water side temperatures at the evaporator, the superheater and EHX_1.

Additionally Figures 4.4, 4.5 and 4.6 illustrate the T–Q diagrams in quantitative terms for the complete condenser, evaporator and subcooler, respectively.

Point	T [°C]	T [K]
W,in	60	333.15
Y	64.013	337.16
Z	78.109	351.26
X	80	353.15

Table 4.6: Water side temperatures of the district heating line.

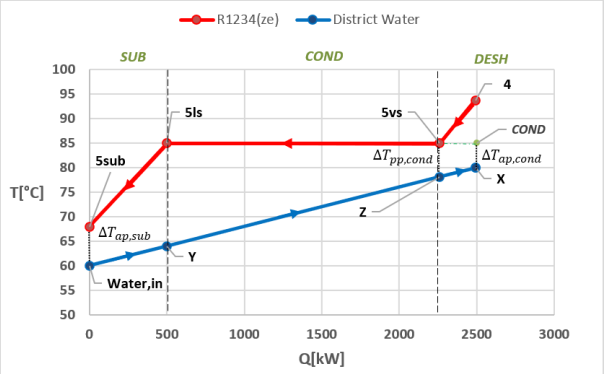

Figure 4.4: Quantitative T–Q diagram of the complete condenser.

Point	T [°C]	T [K]
A	5	278.15
B	9	282.15
C	9.012	282.16
K	8.863	282.01
D	5	278.15

Table 4.7: Water side temperatures of the intermediate loop.

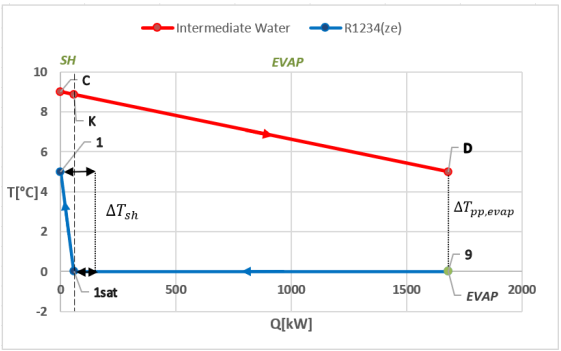

Figure 4.5: Quantitative T–Q diagram of the complete evaporator.

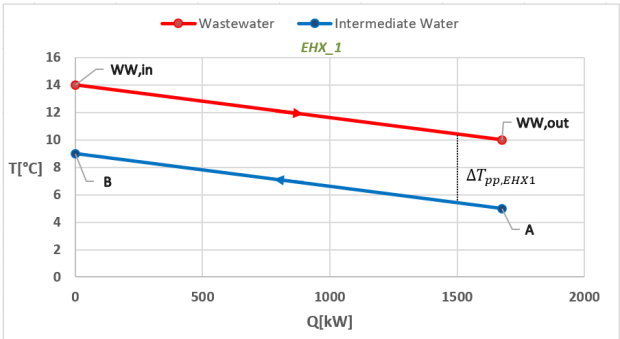

Figure 4.6: Quantitative T–Q diagram of EHX_1.

Table 4.8 presents the main results in terms of refrigerant mass flow rate, intermediate water mass flow rate, and district heating water mass flow rate.

Quantity	Value
Evaporator mass flow rate, $\dot{m}_{\text{eva}}$ [kg/s]	12.927
Condenser mass flow rate, $\dot{m}_{\text{cond}}$ [kg/s]	17.244
Intermediate water mass flow rate, $\dot{m}_{\text{in}}$ [kg/s]	99.75
Water mass flow rate, $\dot{m}_{\text{water}}$ [kg/s]	29.820

Table 4.8: On-design mass flow rates of the heat pump system.

Table 4.9 summarises the main results obtained from the on design simulation of the heat pump system, including heat duties, mechanical and electrical power consumption. Note that $Q_{\text{cond,tot}} = Q_{\text{nom}}$.

Quantity	Value
Total condenser heat duty, $\dot{Q}_{\text{cond,nom,tot}}$ [kW]	2505.269
Total evaporator heat duty, $\dot{Q}_{\text{evap,nom,tot}}$ [kW]	1681.012
Total wastewater heat duty, $\dot{Q}_{\text{ww,tot}}$ [kW]	1676.024
Compressor 1 mechanical power, $\dot{W}_{\text{cmp,1}}$ [kW]	413.731
Compressor 2 mechanical power, $\dot{W}_{\text{cmp,2}}$ [kW]	410.525
Total compressor mechanical power, $\dot{W}_{\text{cmp,mecch}}$ [kW]	824.257
Pump mechanical power, $\dot{W}_{\text{pump,mecch}}$ [kW]	4.987
Total compressor electrical power, $\dot{W}_{\text{cmp,ele}}$ [kW]	867.639
Pump electrical power, $\dot{W}_{\text{pump,ele}}$ [kW]	7.125

Table 4.9: Main on design performance results of the heat pump system.

Table 4.10 reported the coefficients of performance of the heat pump system.

Quantity	Value
Cycle coefficient of performance, $\text{COP}_{\text{cycle}}$ [-]	2.864
System coefficient of performance, $\text{COP}_{\text{system}}$ [-]	2.864

Table 4.10: On design coefficients of performance of the heat pump system.

4.5.2. Heat Exchanger Sizing Result

The main sizing results of the heat exchangers are reported in the following. Both the required heat transfer area, $A_{i,req}$, and the effective heat transfer area, $A_{i,eff}$, are provided; both quantities are referred to the external tube diameter, as showed in equations 4.20 and 4.28. In Tables 4.11, 4.13 and 4.15, the reported heat transfer area, $A_{i,ht}$, corresponds to the effective heat transfer area, $A_{i,eff}$, of each heat exchanger.

Evaporator and Superheater

The on design sizing results of the evaporator and superheater sections are reported in Table 4.11 and 4.12.

Quantity	Evaporator section	Superheater section
Number of tubes, N [-]	9600	
Section length, L [m]	1.78	0.102
Heat transfer area, A_{ht} [m^2]	1022.671	58.602
Total heat exchanger volume, V [m^3]	2.968	

Table 4.11: Results for the evaporator and superheater sections.

Section	A_{req} [m^2]	A_{eff} [m^2]	$\dot{Q}_{req}$ [kW]	$\dot{Q}_{eff}$ [kW]	Δ [%]
Evaporator	1021.437	1022.671	1623.724	1625.687	0.121
Superheater	58.214	58.602	57.289	57.671	0.663

Table 4.12: Required and effective heat transfer areas and heat duties for the evaporator and superheater sections, including the relative overdimensioning.

Condenser and Desuperheater

The on design sizing results of the condenser and desuperheater sections are reported in Table 4.13 and 4.14.

Quantity	Desuperheater section	Condenser section
Number of tubes, N [-]	8920	
Section length, L [m]	0.21	0.79
Heat transfer area, A_{ht} [m^2]	112.106	421.732
Total heat exchanger volume, V [m^3]	1.577	

Table 4.13: Results for the desuperheater and condenser sections.

Section	$\mathbf{A}_{\text{req}}[\text{m}^2]$	$\mathbf{A}_{\text{eff}}[\text{m}^2]$	$\dot{\mathbf{Q}}_{\text{req}}[\text{kW}]$	$\dot{\mathbf{Q}}_{\text{eff}}[\text{kW}]$	$\boldsymbol{\Delta}[\%]$
Desuperheater	106.902	112.106	238.104	249.694	4.642
Condenser	421.723	421.732	1764.784	1764.823	0.002

Table 4.14: Required and effective heat transfer areas and corresponding heat duties for the desuperheater and condenser sections, including the relative overdimensioning.

Subcooler

The on design sizing results of the subcooler section are reported in Table 4.15 and 4.16.

Quantity	Subcooler section
Number of tubes, N [-]	2690
Section length, L [m]	1
Heat transfer area, A_{ht} [m^2]	160.989
Total heat exchanger volume, V [m^3]	1.577

Table 4.15: Results for the subcooler section.

Section	$\mathbf{A}_{\text{req}}[\text{m}^2]$	$\mathbf{A}_{\text{eff}}[\text{m}^2]$	$\dot{\mathbf{Q}}_{\text{req}}[\text{kW}]$	$\dot{\mathbf{Q}}_{\text{eff}}[\text{kW}]$	$\boldsymbol{\Delta}[\%]$
Subcooler	160.956	160.989	502.382	502.485	0.0205

Table 4.16: Required and effective heat transfer areas and corresponding heat duties for the subcooler section, including the relative overdimensioning.

Intermediate Result

Table 4.17 summarises the main secondary thermal quantities used for heat exchanger sizing, including the integral mean convective heat transfer coefficients on both sides, the overall heat transfer coefficient from the thermal resistance network and the associated logarithmic mean temperature difference.

Section	h_{int} [$\text{W/m}^2\text{K}$]	h_{ext} [$\text{W/m}^2\text{K}$]	U [$\text{W/m}^2\text{K}$]	ΔT_{ml} [K]
Evaporator	3659.125	518.766	235.56	6.748
Superheater	3797.953	304.492	178.88	6.113
Desuperheater	7265.382	508.538	242.24	9.883
Condenser	6993.823	1164.468	330.41	12.632
Subcooler	6657.529	585.854	257.53	13.463

Table 4.17: Intermediate thermal quantities used for the sizing of the heat exchanger sections.

5 | Off Design Simulation Methodology

5.1. Off Design operating context and Modelling assumptions

The on design analysis presented in the Chapters 3 and 4 defines a nominal operating point of the heat pump system, obtained under a specific and fixed set of boundary conditions on both the heat source and heat sink sides. This operating point represents a reference condition used for component sizing and performance evaluation.

In real operation, however, the heat pump is subject to significant deviations from the nominal design conditions. In particular, the thermal demand of the district heating network and the thermal availability on the wastewater side exhibit temporal variability, leading to operating conditions that differ from those assumed in the on design analysis.

Off design operation therefore refers to the ability of the heat pump system to adapt its thermodynamic cycle to these varying boundary conditions by adjusting the internal operating variables, while remaining within the physical and operational limits of the compressors, heat exchangers and control devices. A proper off design modelling approach is essential to realistically assess the system performance, flexibility and efficiency over a wide range of operating scenarios.

5.1.1. Boundary Conditions Variability

In the off design analysis, the variability of the operating conditions is introduced through time dependent boundary conditions on both the heat source and the heat sink sides of the heat pump system. In particular, the following sources of variability are considered:

- **Wastewater side:** the inlet temperature $T_{\mathrm{ww,in}}$ and the mass flow rate $\dot{m}_{\mathrm{ww}}$ are treated as variable input parameters, representative of the temporal fluctuations of the wastewater network. The outlet temperature of the wastewater stream $T_{\mathrm{ww,out}}$ is not imposed a priori, but is computed by the model as a result of the heat extraction process at the evaporator.
- **District heating side:** the thermal demand $\dot{Q}_{\mathrm{demand}}$ represents the heat required by the district heating network and it vary over time. The supply and return temperatures of the heating water circuit are kept constant at $T_{\mathrm{water,in}} = 60\,^{\circ}\mathrm{C}$ and $T_{\mathrm{water,out}} = 80\,^{\circ}\mathrm{C}$, consistently with the network operating requirements and with the on-design analysis. For each operating condition, the corresponding water mass flow rate required to meet the thermal demand is therefore determined as:

$$\dot{m}_{\mathrm{water}} = \frac{\dot{Q}_{\mathrm{demand}}}{c_{p,\mathrm{w}} \left(T_{\mathrm{water,out}} - T_{\mathrm{water,in}}\right)}. \tag{5.1}$$

The procedure adopted to define, process and organise the time varying boundary conditions on both the wastewater and district heating sides is described in detail in Chapter 6.

5.1.2. Regulation Strategy and Cycle Adaptation

Under off design operating conditions, the heat pump adapts its thermodynamic cycle to the time varying boundary conditions described in the previous section by regulating internal operating variables, while keeping the component geometry fixed. In particular, the heat exchanger surfaces determined during the on design analysis are retained unchanged throughout the off design simulations.

The off design behaviour of the heat pump system is governed by the following regulation principles:

- **Fixed heat exchanger geometry:** the heat transfer areas of the evaporator, condenser, superheater, desuperheater and subcooler are fixed to the values obtained from the on design sizing procedure. Accordingly, for each heat exchanger section i, the heat transfer area is assumed constant under off design conditions, i.e. $A_{i,\mathrm{OFF}} = A_{i,\mathrm{ON}}$. No re sizing of the heat exchangers is performed during off design operation.
- **Fixed intermediate water mass flow rate:** the mass flow rate of the in-

termediate water loop, $\dot{m}_{\text{int}}$, is kept constant and equal to its on design value. As a consequence, the hydraulic power consumption of the circulation pump, W_{pump}, and the associated temperature rise across the pump, ΔT_{pump}, are assumed constant throughout the off design simulations.

- **Constant overall conductance in EHX_1:** for the wastewater heat exchanger EHX_1, the overall conductance $UA_{\text{EHX\_1}}$ is assumed constant and equal to its on design value. This assumption reflects the high uncertainty and variability of the wastewater side heat transfer conditions and avoids the re evaluation of U at each off design iteration. Heat transfer in EHX_1 is therefore computed using a fixed $UA_{\text{EHX\_1}}$ and the corresponding equivalent logarithmic mean temperature difference.
- **Variable heat capacity rates in EHX_1:** while the intermediate water mass flow rate remains constant, the wastewater mass flow rate $\dot{m}_{\text{ww}}$ varies under off design conditions. As a result, the heat capacity rates of the two streams in the wastewater heat exchanger EHX_1:

$$C_{\text{int}} = \dot{m}_{\text{int}} c_{p,\text{int}}, \qquad C_{\text{ww}} = \dot{m}_{\text{ww}} c_{p,\text{ww}}, \tag{5.2}$$

  are generally not equal. This leads to non-parallel profiles in T-Q diagram and this implies that the temperature difference is not constant along the heat exchanger length. Consequently, heat transfer in EHX_1 is characterised using the corresponding equivalent logarithmic mean temperature difference.
- **Refrigerant mass flow rate control:** variations in the available heat source and in the thermal demand are accommodated by regulating the refrigerant mass flow rate through the two centrifugal compressors.
- **Compressor modulation via IGVs:** the refrigerant mass flow rate is controlled by means of inlet guide vanes, whose opening angle is allowed to vary from near closed position $-80°$ up to fully open operation $+20°$, enabling continuous capacity modulation within the limits imposed by the compressor performance maps.
- **Cycle adaptation:** changes in the refrigerant mass flow rate cause variations of the thermodynamic cycle, including evaporation and condensation pressures and the characteristic temperature differences across the heat exchangers.
- **Re-evaluation of heat transfer performance:** since the heat transfer areas are fixed, off design operation requires the re-calculation of thermophysical

properties, local convective heat transfer coefficients and overall heat transfer coefficients to ensure consistency between the cycle solution and heat exchanger performance.

– **Hybrid system operation:** the heat pump operates within a hybrid configuration including an auxiliary electric boiler. When the thermal demand of the district heating network exceeds the maximum heat output achievable by the heat pump under the given off design conditions, the heat pump is operated at its allowable limit and the remaining thermal demand is supplied by the auxiliary system.

The specific numerical procedure adopted to determine the off design operating point of the heat pump cycle, including the iterative solution of the variables and the enforcement of component constraints, is described in detail in Section 5.3.

5.2. Non Linear Off Design Solver Formulation

5.2.1. Mathematical Formulation of the Problem

The off design operating point of the heat pump system is determined by solving a non linear algebraic problem that enforces thermodynamic cycle balances, heat exchanger constraints and compressor operating limits. During off design, the boundary conditions at the heat source and sink differ from the design case, while component geometries remain fixed; consequently, the internal cycle variables adjust to ensure consistency with the imposed external conditions and component behaviour.

The off design problem can therefore be expressed in compact form as a system of non linear equations:

$$\mathbf{F}(\mathbf{x}) = \mathbf{0}, \tag{5.3}$$

where $\mathbf{x}$ denotes the vector of independent unknown operating variables and $\mathbf{F} : \mathbb{R}^n \to \mathbb{R}^n$ is a non linear vector function represents the set of governing equations describing the system and the thermal closure conditions of the cycle.

In the present work, the vector of unknown variables is defined as:

$$\mathbf{x} = \begin{bmatrix} P_{\text{evap}} & P_{\text{cond}} & \Delta T_{\text{sub}} \end{bmatrix}^{\text{T}}, \tag{5.4}$$

where P_{evap} and P_{cond} denote respectively the evaporation and condensation pres-

sures of the refrigerant and ΔT_{sub} is the degree of subcooling at the condenser outlet.

The vector $\mathbf{x}$ is determined by solving three non linear equations $F_i(x)$, which enforce the thermal closure in the different heat exchanger sections, obtained by equating the heat transfer rate from the heat exchanger model to the corresponding refrigerant enthalpy change as follows:

$$F_i(\mathbf{x}) = Q_{\text{hex}}(\mathbf{x}) - Q_{\text{ref}}(\mathbf{x}) \equiv UA\,\Delta T_{\text{lm}} - \dot{m}\Delta h. \tag{5.5}$$

The heat exchangers are modelled by separating the different thermodynamic regions, with the heat transfer coefficients and the driving temperature differences being iteratively updated according to the current operating point, while the heat transfer surfaces remain fixed to the on design values.

5.2.2. Numerical Solution Method

The solution of the system described in Equation 5.3 is obtained using a Newton type iterative method. At each iteration k, the system is locally linearised around the current estimate $\mathbf{x}^{(k)}$, leading to the linear system:

$$\mathbf{J}(\mathbf{x}^{(k)})\,\Delta\mathbf{x}^{(k)} = -\mathbf{F}(\mathbf{x}^{(k)}), \tag{5.6}$$

where $\mathbf{J}(\mathbf{x}^{(k)})$ is the Jacobian matrix of the system and $\Delta\mathbf{x}^{(k)}$ is the Newton correction. The solution is then updated according to:

$$\mathbf{x}^{(k+1)} = \mathbf{x}^{(k)} + \lambda^{(k)}\,\Delta\mathbf{x}^{(k)}, \tag{5.7}$$

where $\lambda^{(k)} \in (0, 1]$ is a damping parameter introduced to control the magnitude of the update and improve numerical stability.

To further enhance robustness under highly off design operating conditions, a continuation strategy is employed. The original non linear system is replaced by a family of modified systems:

$$\mathbf{F}_\theta(\mathbf{x}) = \mathbf{F}(\mathbf{x}) - \theta\,\mathbf{F}(\mathbf{x}^{(0)}), \tag{5.8}$$

where $\theta \in [0, 1]$ is a continuation parameter gradually reduced from an initial value to zero, allowing the solver to approach the final solution progressively and avoiding abrupt transitions in the solution space.

When the Jacobian matrix becomes numerically unstable or the Newton correction fails to provide a suitable descent direction for the residual norm, a Levenberg Marquardt regularisation is applied. In this case, the Newton system is replaced by:

$$\left(\mathbf{J}^{\mathrm{T}}\mathbf{J} + \mu\mathbf{I}\right)\Delta\mathbf{x} = -\mathbf{J}^{\mathrm{T}}\mathbf{F}, \tag{5.9}$$

where μ is a regularisation parameter and $\mathbf{I}$ is the identity matrix. This formulation improves numerical conditioning and ensures stable progress toward convergence.

The combination of Newton linearisation, adaptive damping, continuation and Levenberg Marquardt regularisation, results in a robust and efficient solver for the resolution of the coupled non linear off design problem [36].

5.3. General Framework of the Routine

The off design simulation is organised as a multilevel algorithm composed of three embedded levels, each characterised by a well defined role and by a clear separation between numerical operations and physical calculations. The structure is presented in Figure 5.1 and explained in Section 5.4. It allows the numerical solution of the off design problem to be decoupled from the thermodynamic modelling of the heat pump cycle, improving both robustness and modularity of the simulation framework.

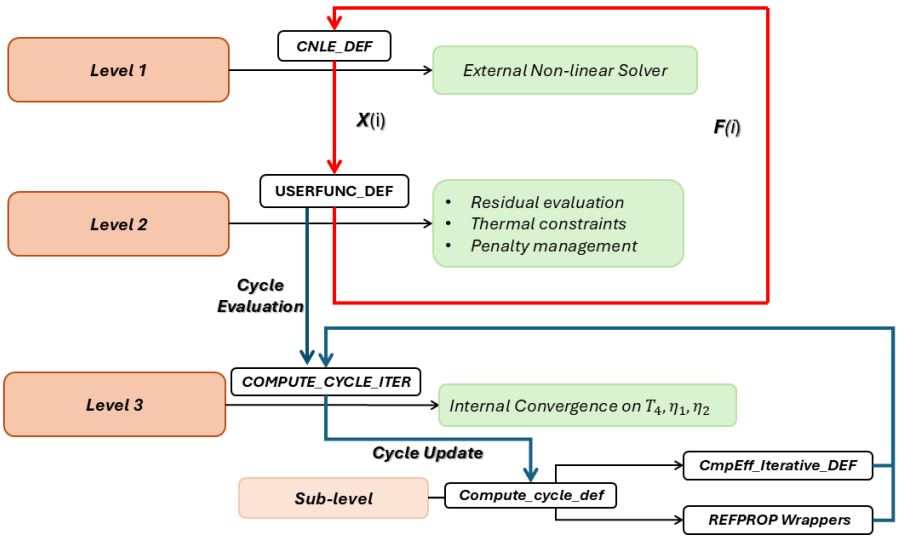

Figure 5.1: Rappresentation of the different levels composing the routine.

Level 1: explained in Subsection 5.4.1, it is the outermost level, where the off design problem is treated as a purely numerical non linear system governed by Equations 5.3 and 5.4.

This level is handled by the routine `CNLE_DEF`, which implements an external non linear iteration. At this stage, the solver does not contain any information about the physical structure of the heat pump cycle and operates exclusively at a numerical level. The interaction with the thermodynamic model is limited to repeated calls to a black box residual evaluation function, implemented in the routine `USERFUNC_DEF`.

Level 2: explained in Subsection 5.4.2, it performs the physical evaluation of the heat pump cycle for a given estimate of the unknown vector $\mathbf{x}$ and is implemented in the routine
`USERFUNC_DEF`, which interfaces the numerical solver with the thermodynamic model. At this stage, all physical calculations and operational constraints are enforced, including critical pressure limits, cycle evaluation, compressor operating checks, computation of logarithmic mean temperature differences, overall heat transfer coefficients and the construction of the residual equations F_1, F_2, F_3. As a result, `USERFUNC_DEF` represents the core of the off design simulation and plays a central role in determining the operating point.

***Level 3*:** explained in Subsection 5.4.3, it consists of an internal iterative procedure embedded within the physical cycle evaluation. This level is implemented by the routine `Compute_cycle_Iter` and is required to resolve implicit dependencies within the thermodynamic model. In particular, the internal iteration is used to achieve convergence of the outlet temperature of the second compression stage, T_4, as well as of the compressor efficiencies. This iteration is physical in nature and is performed independently of the external non linear solver until convergence of the cycle variables is achieved.

In addition to the three main algorithmic levels, the off design simulation relies on auxiliary modules. The routine `Compute_cycle_Def` evaluates a single thermodynamic cycle for given operating conditions, while `CmpEf_Iterative_DEF` computes compressor efficiencies via interpolated performance maps with smoothing. Thermophysical properties and phase consistency are handled by dedicated `Off_REFPROP` wrapper functions, including `Of_PhaseCheck_PH`. These auxiliary modules are called within the internal algorithmic levels and are not discussed further.

5.4. Off Design Solution Algorithm

5.4.1. External Non Linear Iteration

The external non linear iteration represents the outermost layer, identified as *Level 1*, of the off design solution algorithm and is responsible for the numerical determination of the unknown operating variables defining the heat pump cycle. This level is implemented through the routine `CNLE_DEF`, which acts as a general purpose solver for systems of non linear algebraic equations.

Within the overall algorithmic structure described in Subsection 5.2.1, `CNLE_DEF` operates exclusively at a numerical level. Its task is limited to updating the vector of unknowns $\mathbf{x}$ with the objective of driving the residual vector $\mathbf{F}(\mathbf{x})$ to zero. From the perspective of the solver, the routine `USERFUNC_DEF` acts as a black box residual evaluator, mapping the current estimate of $\mathbf{x}$ to the corresponding residual vector without exposing any information on the underlying thermodynamic model. No thermodynamic assumptions or component level information are embedded within the solver itself.

At each external iteration, `USERFUNC_DEF` provides the residuals for the current $\mathbf{x}$ and the solver updates the unknowns using the strategy described in Section 5.2, remaining decoupled from the physical model. Convergence is assessed based on the residual norm and the magnitude of the applied correction and non-convergent cases are flagged, while the encapsulation of the numerical solver in `CNLE_DEF` ensures modularity between numerical resolution and physical modelling.

5.4.2. Cycle Evaluation and Internal Convergence

At *Level 2*, the routine `USERFUNC_DEF` evaluates the thermodynamic and heat transfer model of the heat pump system for a given estimate of the unknown vector $\mathbf{x} = [P_{\text{evap}},\, P_{\text{cond}},\, \Delta T_{\text{sub}}]^{\text{T}}$, provided by the external non linear solver.

The purpose of this routine is twofold:

- to compute a physically consistent cycle solution under the imposed off design boundary conditions;
- to construct the residual vector $\mathbf{F}(\mathbf{x})$ enforcing thermal closure between the refrigerant side enthalpy balances and the heat exchanger capabilities with fixed on design areas.

Inputs and fixed parameters

The inputs handled by `USERFUNC_DEF` can be classified into:

- the unknown variables **x** provided by the solver, summarises in Table 5.1;
- the boundary conditions and fixed parameters associated with the current off design time step and using like inputs, summarises in Table 5.2.

Input parameter	Description
P_{evap}	Evaporation pressure
P_{cond}	Condensation pressure
ΔT_{sub}	Subcooling degree at condenser outlet

Table 5.1: Solver unknown.

Input parameter	Description
$UA_{\text{EHX\_1}}$	Overall conductance of wastewater
$T_{\text{ww,in}}$	Wastewater inlet temperature
$\dot{m}_{\text{ww}}$	Wastewater mass flow rate
$c_{p,\text{ww}}$	Wastewater specific heat capacity
$T_{\text{water,in}}$	District heating return temperature
$T_{\text{water,out}}$	District heating supply temperature
m_{int}	Intermediate mass flow rate
$c_{p,\text{int}}$	Intermediate specific heat capacity
$\dot{Q}_{\text{demand}}$	Imposed thermal demand of the district heating network
$c_{p,\text{w}}$	District heating water specific heat capacity
$\dot{W}_{\text{pump}}$	Auxiliary circulation pump power
ΔT_{pump}	Temperature increase across the auxiliary pump
$A_j^{(n)}$	On-design heat exchanger areas (fixed geometry)
$T_{4,\text{guess}}$	Initial guess for internal cycle closure

Table 5.2: Main input parameters employed by the routine `USERFUNC_DEF`.

The district heating water mass flow rate, as we see in Sub section 5.4.2, is computed internally to satisfy the imposed demand. The quantity $\dot{m}_{\text{w}}$ is therefore an output of the routine and is updated at each call, consistently with the current boundary condition $\dot{Q}_{\text{demand}}$.

Step by step procedure implemented in USERFUNC_DEF

The routine follows a deterministic workflow reflecting the physical causality of the off design problem; for clarity, the sequence of operations is reported below as implemented.

Step 1: feasibility constraints and penalty strategy.
Before executing the full thermodynamic cycle evaluation, the routine `USERFUNC_DEF` enforces a set of preliminary feasibility constraints aimed at preventing the external non linear solver from exploring non physical operating regions.

First, a subcritical operation constraint is imposed on the condensation pressure:

$$P_{\text{cond}} < P_{\text{cond,max}} = 0.99\, P_{\text{crit}}. \tag{5.10}$$

If Equation 5.10 is violated, the residual vector is artificially set to a large penalty value

$$F_i = 10^9, \qquad i = 1, 2, 3 \tag{5.11}$$

and the routine terminates immediately. This strategy preserves the structure of the original system of equations and avoids the introduction of additional explicit inequality constraints.

An analogous penalty strategy is applied whenever the compressor operating point falls outside the valid performance map domain (these point are identify by a flag called `flag_cmp_offmap`), as well as in the presence of violated thermal feasibility constraints. Large residuals are deliberately assigned to flag physically infeasible operating points, therefore steering the external solver away from such regions without introducing explicit inequality constraints.

Step 2: thermodynamic cycle evaluation.
For the estimation of the current variables, the thermodynamic cycle is solved by calling `Compute_cycle_Iter`. This routine returns the complete set of cycle states, stored in the structure `CycleResult`, and the refrigerant mass flow rates $\dot{m}_{\text{evap}}$ and $\dot{m}_{\text{cond}}$.

The internal iteration embedded in `Compute_cycle_Iter` resolves implicit dependencies (T_4 and compressor efficiencies) and is discussed in detail in Sub Section 5.4.4; here it is treated as an internal closure of the cycle evaluation.

Step 3: refrigerant side heat duties from enthalpy differences.
Once the cycle is converged, the specific heat duties associated with each section are computed from enthalpy differences, consistently with the thermodynamic model. Using molar enthalpies from *REFPROP* and the molar mass M_{mol}, the specific contributions are:

$$Q_{\mathrm{cond}} = \frac{h_{5,\mathrm{vs}} - h_{5,\mathrm{ls}}}{M_{\mathrm{mol}}}, \qquad Q_{\mathrm{desh}} = \frac{h_4 - h_{5,\mathrm{vs}}}{M_{\mathrm{mol}}}, \tag{5.12}$$

$$Q_{\mathrm{sub}} = \frac{h_{5,\mathrm{ls}} - h_{5,\mathrm{sub}}}{M_{\mathrm{mol}}}, \qquad Q_{\mathrm{evap}} = \frac{h_{1,\mathrm{sat}} - h_9}{M_{\mathrm{mol}}}, \tag{5.13}$$

$$Q_{\mathrm{sh}} = \frac{h_1 - h_{1,\mathrm{sat}}}{M_{\mathrm{mol}}}. \tag{5.14}$$

The corresponding heat rates are then:

$$\dot{Q}_j = \dot{m}_j \, Q_j, \tag{5.15}$$

with $\dot{m}_j = \dot{m}_{\mathrm{evap}}$ for evaporator and superheater and $\dot{m}_j = \dot{m}_{\mathrm{cond}}$ for condenser, desuperheater and subcooler.

Step 4: external temperature nodes for wastewater and water loops.
The converged heat duties are used to update the external temperature levels needed to evaluate driving temperature differences and logarithmic mean temperature differences (ΔT_{ml}).

The net heat extracted from wastewater is:

$$\dot{Q}_{\mathrm{ww}} = \dot{Q}_{\mathrm{evap}} + \dot{Q}_{\mathrm{sh}} - \dot{W}_{\mathrm{pump}}. \tag{5.16}$$

Given the fixed conductance $UA_{\mathrm{EHX\_1}}$, an equivalent logarithmic temperature difference is computed:

$$\Delta T_{\mathrm{log,hx1}} = \frac{\dot{Q}_{\mathrm{ww}}}{UA_{\mathrm{EHX\_1}}}, \tag{5.17}$$

and the wastewater outlet temperature follows from an energy balance:

$$T_{\mathrm{ww,out}} = T_{\mathrm{ww,in}} - \frac{UA_{\mathrm{EHX\_1}} \, \Delta T_{\mathrm{log,EHX\_1}}}{\dot{m}_{\mathrm{ww}} \, c_{p,\mathrm{ww}}}. \tag{5.18}$$

In addition, the intermediate nodes of HX1 used by the algorithm are defined as:

$$T_d = T_{\mathrm{ww,in}} - \Delta T_{\mathrm{log,EHX\_1}}, \qquad T_a = T_d + \Delta T_{\mathrm{pump}}. \tag{5.19}$$

Water temperatures across the EHX_1, T_a and T_b, which are rappresented in Figure, are obtained by numerically solving the coupled non-linear system:

$$\begin{cases} UA_{\text{EHX\_1}}\,\Delta T_{\text{lm}} = \dot{m}_{\text{int}} c_{p,\text{int}}\,(T_b - T_a)\,, \\ \Delta T_{\text{lm}} = \dfrac{(T_{\text{ww,in}} - T_b) - (T_{\text{ww,out}} - T_a)}{\ln\left(\dfrac{T_{\text{ww,in}} - T_b}{T_{\text{ww,out}} - T_a}\right)}. \end{cases} \tag{5.20}$$

Accordingly, the temperatures at the evaporator and superheater nodes indicated in Figure 4.5 are obtained by successive energy balances along the evaporator heat exchanger. In particular:

$$T_k = T_c - \frac{\dot{Q}_{\text{sh}}}{\dot{m}_{\text{int}} c_{p,\text{int}}}, \qquad T_d = T_k - \frac{\dot{Q}_{\text{evap}}}{\dot{m}_{\text{int}} c_{p,\text{int}}}, \qquad T_d \equiv T_a. \tag{5.21}$$

Finally, the water temperatures rise across condenser and subcooler side section, reported in 4.4, are computed sequentially:

$$T_y = T_{\text{w,in}} + \frac{\dot{Q}_{\text{sub}}}{\dot{m}_{\text{w}}\, c_{p,\text{w}}}, \qquad T_z = T_y + \frac{\dot{Q}_{\text{cond}}}{\dot{m}_{\text{w}}\, c_{p,\text{w}}}, \qquad T_x = T_z + \frac{\dot{Q}_{\text{desh}}}{\dot{m}_{\text{w}}\, c_{p,\text{w}}}, \tag{5.22}$$

by considering the energy balance across condenser and subcooler heat exchangers.

Step 5: thermal feasibility checks.
After updating all temperature nodes, `USERFUNC_DEF` verifies that a positive driving force is maintained in each heat exchanger section by enforcing a consistent temperature ordering. In practice, this is implemented through a set of inequalities:

$$\begin{cases} T_4 \le T_{\text{w,out}} \\ T_{5,\text{ls}} \le T_{\text{y}} \\ T_{5,\text{ls}} \le T_{\text{z}} \\ T_{5,\text{sub}} \le T_{\text{w,in}} \\ T_{\text{a}} \le T_1 \\ T_{\text{b}} \le T_9 \end{cases} \tag{5.23}$$

If any condition is violated, the evaluation is penalised by assigning a fixed residual value expressed in Equation 5.11 and the residual evaluation is terminated.

Step 6: ΔT_{ml} evaluation for each exchanger section.
Assuming counter current operation, the logarithmic mean temperature difference for each section is computed using the dedicated equation 4.25. $\Delta T_{\mathrm{lm,desh}}$, $\Delta T_{\mathrm{lm,cond}}$, $\Delta T_{\mathrm{lm,sub}}$, $\Delta T_{\mathrm{lm,evap}}$ and $\Delta T_{\mathrm{lm,sh}}$ are evaluated from the corresponding end temperatures of the water,intermediate loop nodes and the refrigerant temperatures returned by the cycle model.

Step 7: off design heat transfer coefficients and overall U.
Given the updated mass flow rates and thermophysical states, the convective heat transfer coefficients on the water side and on the refrigerant side are recomputed using the equation 4.20, thus capturing the dependency on Reynolds number, phase and heat flux.

For each section j, the overall heat transfer coefficient is assembled through a global resistance model, including wall conduction and fouling:

$$U_j = U(h_{\mathrm{i},j}, h_{\mathrm{o},j}, D_{\mathrm{i}}, D_{\mathrm{o}}, k_{\mathrm{wall}}, R_{f,i}, R_{f,o}), \qquad j \in \{\text{evap, sh, cond, desh, sub}\}. \tag{5.24}$$

Since the heat exchanger geometry is fixed, the on design areas $A_j^{(n)}$ are retained unchanged during off design operation.

Step 8: heat rates predicted by the heat exchanger model.
For each section j, the heat transfer model predicts the exchanged thermal power as Equation 4.26. We use factor 10^-3 in order to convert W into kW, consistently with the adopted unit system.

Step 9: residual construction and physical meaning.
Finally, `USERFUNC_DEF` constructs the residual vector returned to the external solver applying Equation 5.5 on the evaporator, condenser and subcooler heat exchanger and taking into account all the sections. The system of equations is reported below:

$$\begin{cases} F_1(\mathbf{x}) = \left(U_{\mathrm{evap}} A_{\mathrm{evap}} \Delta T_{\mathrm{lm,evap}} + U_{\mathrm{sh}} A_{\mathrm{sh}} \Delta T_{\mathrm{lm,sh}} F\right) - \dot{m}_{\mathrm{evap}} \left(h_{\mathrm{out,evap}} - h_{\mathrm{in,evap}}\right) = 0 \\ F_2(\mathbf{x}) = \left(U_{\mathrm{cond}} A_{\mathrm{cond}} \Delta T_{\mathrm{lm,cond}} + U_{\mathrm{desh}} A_{\mathrm{desh}} \Delta T_{\mathrm{lm,desh}} F\right) - \dot{m}_{\mathrm{cond}} \left(h_{\mathrm{in,cond}} - h_{\mathrm{out,cond}}\right) = 0 \\ F_3(\mathbf{x}) = U_{\mathrm{sub}} A_{\mathrm{sub}} \Delta T_{\mathrm{lm,sub}} F - \dot{m}_{\mathrm{cond}} \left(h_{\mathrm{in,sub}} - h_{\mathrm{out,sub}}\right) = 0 \end{cases} \tag{5.25}$$

Therefore, enforcing $\mathbf{F}(\mathbf{x}) \to \mathbf{0}$ has a direct physical meaning: the off design operating point defined by $(P_{\mathrm{evap}}, P_{\mathrm{cond}}, \Delta T_{\mathrm{sub}})$ is the one for which the refrigerant enthalpy balances are simultaneously compatible with the heat transfer capability

of each fixed area heat exchanger section under the current off design boundary conditions.

Once convergence of the non linear solver is achieved, all thermal powers ($\dot{Q}_{\text{evap}}$, $\dot{Q}_{\text{sh}}$, $\dot{Q}_{\text{cond}}$, $\dot{Q}_{\text{desh}}$, $\dot{Q}_{\text{sub}}$), compressor power consumptions ($\dot{W}_{\text{cmp,1}}$, $\dot{W}_{\text{cmp,2}}$ and $\dot{W}_{\text{el}}$), and the coefficient of performance (COP) are re evaluated using the same thermodynamic formulations adopted in the on design analysis.

5.4.3. Internal Cycle Closure and Compressor Performance Iteration

The off design solution of the heat pump cycle requires the resolution of implicit dependencies between thermodynamic state variables and component performance parameters. In particular, the outlet temperature of the high pressure compressor, T_4, and the corresponding compressor efficiencies cannot be prescribed a priori, but must be determined consistently with the cycle operating conditions. For this reason, an internal iteration is embedded within the cycle evaluation procedure.

Iteration on the high pressure compressor outlet temperature.
For assigned values of the external solver variables $[P_{\text{evap}}, P_{\text{cond}}, \Delta T_{\text{sub}}]$, the thermodynamic cycle is evaluated by the routine `Compute_cycle_Iter`. This function performs a fixed point iteration on the outlet temperature of the second compression stage, T_4.

Starting from an initial guess for T_4, the cycle is solved through the deterministic routine `Compute_cycle_Def`, which computes all thermodynamic states, the refrigerant mass flow rates and the compressor power consumption. A new value of T_4 is obtained from the high pressure compressor model based on the updated cycle conditions. The procedure is repeated until convergence of T_4 is achieved within a prescribed tolerance. This internal iteration guarantees thermodynamic consistency between the compression process and the overall cycle solution.

Compressor performance evaluation and regulation.
Within each internal cycle iteration, the performance of the two centrifugal compressors is evaluated by means of the routine `CmpEff_Iterative_DEF`. For each compressor, the volumetric flow rate $\dot{V}$ and the specific isentropic enthalpy rise Δh_{is} are obtained from the current thermodynamic state of the cycle and subsequently normalised with respect to their nominal design values, $\dot{V}_{\text{nom}}$ and $\Delta h_{\text{is,nom}}$,

according to Equation 4.11.

The compressor efficiency $\eta_{i,\mathrm{map}}$ is determined through a bi dimensional interpolation of the corresponding performance map as a function of the normalised volumetric flow rate and the normalised specific isentropic enthalpy rise, as expressed in Equation 3.70. The interpolated efficiency is then scaled by the nominal isentropic efficiency $\eta_{\mathrm{is,nom}} = 0.8$ according to Equation 4.13, providing the effective compressor efficiency η_i.

To ensure physical consistency of the solution and to prevent the numerical evaluation of the compressor model outside the domain of validity of the available performance maps, explicit upper and lower bounds are imposed on the admissible operating region. In the present implementation, the upper bound is defined as:

$$\left(\frac{\dot{V}}{\dot{V}_{\mathrm{nom}}}, \frac{\Delta h_{\mathrm{is}}}{\Delta h_{\mathrm{is,nom}}} \right) \leq (120,\, 110), \tag{5.26}$$

while the lower bound is given by:

$$\left(\frac{\dot{V}}{\dot{V}_{\mathrm{nom}}}, \frac{\Delta h_{\mathrm{is}}}{\Delta h_{\mathrm{is,nom}}} \right) \geq (20,\, 100). \tag{5.27}$$

The adopted bounds are intentionally conservative and are selected to guarantee a robust and physically meaningful evaluation of the compressor performance, avoiding extrapolation beyond the region covered by the manufacturer performance maps, where the predictive capability of the model would be highly uncertain.

If any of these limits is violated, the operating point falls outside the validated map domain and the compressor model cannot be reliably evaluated. In such cases, a dedicated flag is triggered and the cycle calculation is terminated.

The corresponding off design operating state is excluded from the solution of the external non linear system by penalising the residual defined in Equation 5.11. Whenever the compressor operating point exceeds the admissible map bounds, a penalty term is added to the residual vector, artificially increasing its norm and preventing convergence in the physically infeasible region.

The internal iteration on T_4 and compressor efficiencies is completed before the evaluation of heat exchanger performance and residual equations; it is therefore fully decoupled from the external non linear solver.

5.4.4. Convergence Criteria and Output Quantities

The primary outputs of the off design simulation are the cycle regulating variables: P_{evap}, P_{cond} and ΔT_{sub}. In addition, the solution provides the complete set of thermodynamic states of the refrigerant, the refrigerant mass flow rates in the evaporator and condenser branches: $\dot{m}_{\text{evap}}$, $\dot{m}_{\text{cond}}$, and the thermal powers exchanged in each component of the system.

The validity of a converged solution is not assessed solely through the satisfaction of the residual equations F_1, F_2 and F_3, which enforce local consistency between heat exchanger performance and refrigerant enthalpy variations, but is further verified by means of global energy balance checks.

First, the heat pump system are verified and the overall energy balances of the heat pump global cycle:

$$\dot{Q}_{\text{cond}} + \dot{Q}_{\text{desh}} + \dot{Q}_{\text{sub}} = \dot{Q}_{\text{evap}} + \dot{Q}_{\text{sh}} + \dot{W}_{\text{cmp}}, \tag{5.28}$$

$$\dot{Q}_{\text{cond}} + \dot{Q}_{\text{desh}} + \dot{Q}_{\text{sub}} = \dot{Q}_{\text{ww}} + \dot{W}_{\text{pump}} + \dot{W}_{\text{cmp}}, \tag{5.29}$$

where

$$\dot{Q}_{\text{demand}} = \dot{Q}_{\text{cond}} + \dot{Q}_{\text{desh}} + \dot{Q}_{\text{sub}}. \tag{5.30}$$

Second, consistency of the heat exchange in the wastewater-auxiliary heat exchanger EHX_1 is verified:

$$\dot{Q}_{\text{HX1}} = \dot{Q}_{\text{evap}} + \dot{Q}_{\text{sh}} - \dot{W}_{\text{pump}}. \tag{5.31}$$

Only solutions which satisfying simultaneously the residual equations and all the energy balance checks reported above are considered physically consistent and retained for the off design performance analysis.

Then, with Equations 3.31 and 3.36, coefficients of performance are evaluated.

5.5. Off Design Response to Thermal Load Variation: Case Study

The off design solver provides, for each operating condition, the converged values of the evaporation and condensation pressures of P_{evap}, P_{cond} and ΔT_{sub}, the refrigerant mass flow rates $\dot{m}_{evap}$ and $\dot{m}_{cond}$, the thermal powers $\dot{Q}_{evap}$, $\dot{Q}_{sh}$, $\dot{Q}_{cond}$, $\dot{Q}_{desh}$ and $\dot{Q}_{sub}$. In addition, the model determines the district heating water mass flow rate $\dot{m}_{w}$, the wastewater outlet temperature $T_{ww,out}$, the resulting coefficient of performance COP and the complete set of thermodynamic state points of the cycle. In order to verify the robustness and physical consistency of the proposed off design modelling framework before addressing more general operating scenarios, a simplified case study is first considered. In this analysis the wastewater side boundary conditions are kept constant, with fixed wastewater mass flow rate $\dot{m}_{ww}$ and inlet temperature $T_{ww,in}$ equal to their on design values, while the geometry of all components is maintained equal $A_{i,req}$.

The off design response of the heat pump is then analysed by varying the imposed thermal demand according to $\dot{Q}_{demand} \in \{\dot{Q}_{nom}, \dot{Q}_{low}, \dot{Q}_{high}\}$, whose values are reported in Table 5.3.

Condition	Definition	Expression	$\dot{Q}$demand [kW]
Nominal	Q_{nom}	$1.0 \cdot \dot{Q}_{nom}$	2505.269
Partial load	Q_{low}	$0.6 \cdot \dot{Q}_{nom}$	1503.162
Overload	$\dot{Q}_{high}$	$1.10 \cdot \dot{Q}_{nom}$	2755.796

Table 5.3: Thermal demand levels considered in the off design analysis.

The main results are reported and discussed in the following subsections.

5.5.1. Solver Variables Solution

Tables 5.4, 5.5 and 5.6 report the unknowns computed by the off design solver.

Variable	Value	Unit
P_{evap}	0.2533	MPa
P_{cond}	2.0014	MPa
ΔT_{sub}	16.4409	K

Table 5.4: $\dot{Q}_{low}$

Variable	Value	Unit
P_{evap}	0.2164	MPa
P_{cond}	2.2325	MPa
ΔT_{sub}	16.9932	K

Table 5.5: $\dot{Q}_{nom}$

Variable	Value	Unit
P_{evap}	0.2083	MPa
P_{cond}	2.2663	MPa
ΔT_{sub}	16.948	K

Table 5.6: $\dot{Q}_{high}$

5.5.2. Main Variables Solution

Tables 5.7, 5.8 and 5.9 report the corresponding solutions of the main operating variables.

Quantity	Value	Unit
$\dot{m}_{\text{evap}}$	7.442	kg/s
$\dot{m}_{\text{cond}}$	9.387	kg/s
Q_{evap}	961.180	kW
Q_{sh}	33.488	kW
Q_{cond}	1036.899	kW
Q_{desh}	210.804	kW
Q_{sub}	255.457	kW
$W_{\text{cmp,1}}$	260.648	kW
$W_{\text{cmp,2}}$	247.842	kW
T_4	369.641	K
$T_{\text{ww,out}}$	11.638	°C
$\dot{m}_{\text{w}}$	17.937	kg/s
COP	2.771	–

Table 5.7: $\dot{Q}_{\text{low}}$

Quantity	Value	Unit
$\dot{m}_{\text{evap}}$	12.929	kg/s
$\dot{m}_{\text{cond}}$	17.245	kg/s
Q_{evap}	1623.889	kW
Q_{sh}	57.296	kW
Q_{cond}	1764.759	kW
Q_{desh}	237.808	kW
Q_{sub}	502.634	kW
$W_{\text{cmp,1}}$	413.173	kW
$W_{\text{cmp,2}}$	410.843	kW
T_4	367.704	K
$T_{\text{ww,out}}$	10	°C
$\dot{m}_{\text{w}}$	29.895	kg/s
COP	2.865	–

Table 5.8: $\dot{Q}_{\text{nom}}$

Quantity	Value	Unit
$\dot{m}_{\text{evap}}$	13.921	kg/s
$\dot{m}_{\text{cond}}$	18.803	kg/s
Q_{evap}	1741.8866	kW
Q_{sh}	61.473	kW
Q_{cond}	1901.396	kW
Q_{desh}	304.946	kW
Q_{sub}	549.458	kW
$W_{\text{cmp,1}}$	477.328	kW
$W_{\text{cmp,2}}$	475.112	kW
T_4	369.881	K
$T_{\text{ww,out}}$	9.708	°C
$\dot{m}_{\text{w}}$	32.884	kg/s
COP	2.729	–

Table 5.9: $\dot{Q}_{\text{high}}$

5.5.3. Thermodynamic State Points of the Cycle

Tables 5.10, 5.11 and 5.12 summarise the thermodynamic state points computed for the three off design operating conditions.

Point	T [K]	P [MPa]	h [kJ/kg]	s [kJ/(kg K)]	x
P1	282.483	0.253	391.55	1.691	–
P2s	318.122	0.811	414.10	1.691	–
P2	330.106	0.811	426.73	1.729	–
P3	327.008	0.811	423.54	1.720	–
P4s	363.285	2.031	441.41	1.720	–
P4	369.642	2.031	449.86	1.743	–
P5sub	336.561	2.0014	289.74	1.289	–
P5ls	353.002	2.0014	317.00	1.368	–
P5vs	353.002	2.0014	427.40	1.681	–
P6	315.243	0.811	289.74	1.296	0.207
P7	315.243	0.811	258.05	1.196	–
P8	315.243	0.811	410.92	1.681	–
P9	278.042	0.258	258.05	1.208	0.285

Table 5.10: $\dot{Q}_{\text{low}}$

Point	T [K]	P [MPa]	h [kJ/kg]	s [kJ/(kg K)]	x
P1	278.143	0.216	388.75	1.691	–
P2s	318.448	0.819	414.36	1.691	–
P2	324.504	0.819	420.76	1.711	–
P3	322.278	0.819	418.41	1.704	–
P4s	364.411	2.266	437.46	1.704	–
P4	367.533	2.266	442.22	1.717	–
P5sub	341.153	2.232	296.93	1.310	–
P5ls	358.158	2.232	326.06	1.393	–
P5vs	358.158	2.232	428.41	1.679	–
P6	315.651	0.819	296.93	1.319	0.250
P7	315.651	0.819	258.72	1.198	–
P8	315.650	0.819	411.38	1.681	–
P9	273.681	0.221	258.72	1.215	0.3150

Table 5.11: $\dot{Q}_{\text{nom}}$

Point	T [K]	P [MPa]	h [kJ/kg]	s [kJ/(kg K)]	x
P1	277.097	0.208	387.95	1.691	–
P2s	318.292	0.816	414.17	1.691	–
P2	325.904	0.816	422.17	1.716	–
P3	323.187	0.816	419.34	1.707	–
P4s	366.003	2.30	438.80	1.707	–
P4	369.8814	2.30	444.52	1.723	–
P5sub	341.928	2.266	298.04	1.313	–
P5ls	358.876	2.266	327.28	1.397	–
P5vs	358.876	2.266	428.40	1.679	–
P6	315.487	0.816	298.04	1.323	0.259
P7	315.487	0.816	258.41	1.197	–
P8	315.487	0.816	411.02	1.681	–
P9	272.632	0.212	258.41	1.215	0.320

Table 5.12: $\dot{Q}_{\text{high}}$

5.5.4. Compressors maps and efficiency

Tables 5.13, 5.14 and 5.15 report the resulting compressor efficiencies, including both the values obtained from the performance maps and the actual operating efficiencies, while

the compressor performance maps are shown in Figures 5.2, 5.3 and 5.4. Subscript 1 refers to the low pressure compressor and subscript 2 to the high pressure compressor.

Quantity	Value	Unit
η_1	0.6401	–
η_2	0.6799	–
$\eta_{1,\text{map}}$	0.8001	–
$\eta_{2,\text{map}}$	0.8499	–

Table 5.13: $\dot{Q}_{\text{low}}$

Quantity	Value	Unit
η_1	0.8002	–
η_2	0.8002	–
$\eta_{1,\text{map}}$	1.0003	–
$\eta_{2,\text{map}}$	1.0003	–

Table 5.14: $\dot{Q}_{\text{nom}}$

Quantity	Value	Unit
η_1	0.7620	–
η_2	0.7803	–
$\eta_{1,\text{map}}$	0.9525	–
$\eta_{2,\text{map}}$	0.9753	–

Table 5.15: $\dot{Q}_{\text{high}}$

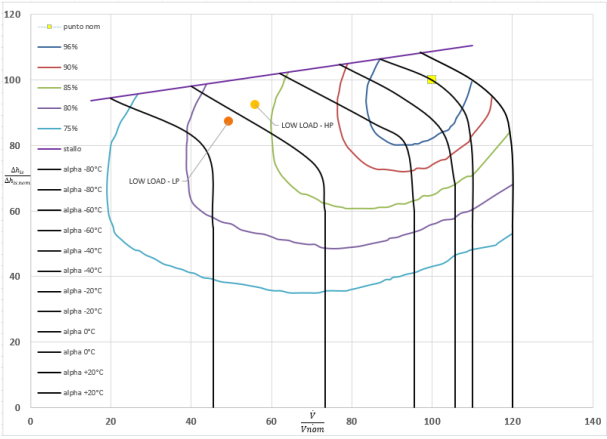

Figure 5.2: $\dot{Q}_{\text{low}}$

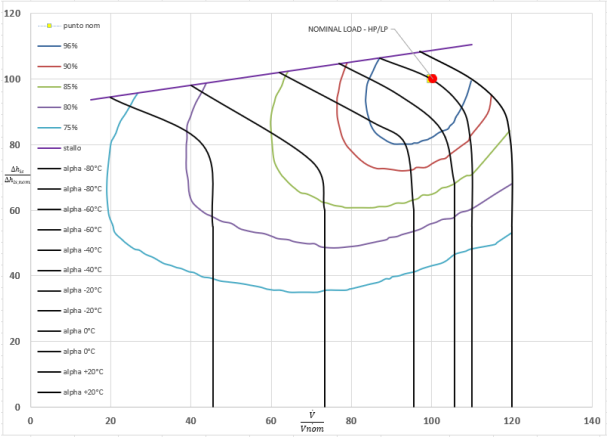

Figure 5.3: $\dot{Q}_{\text{nom}}$

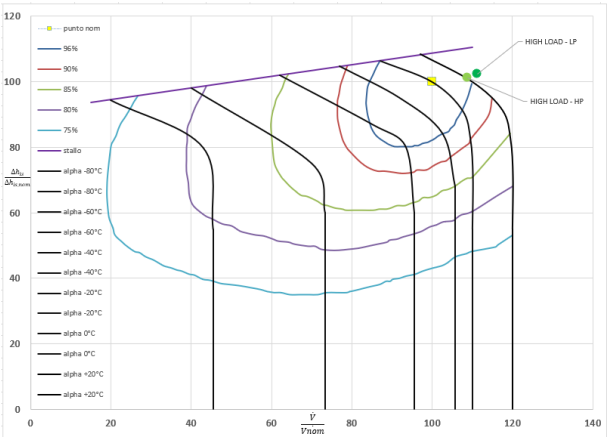

Figure 5.4: $\dot{Q}_{\text{high}}$

5.5.5. Analysis of the Off Design Behaviour

The nominal demand level $\dot{Q}_{\text{nom}}$ is first reconsidered within the off design framework and directly compared with the on design solution.

A direct comparison between Table 4.5, reporting the on design state points and Table 5.11, corresponding to the $\dot{Q}_{\text{nom}}$ off design case, shows that the thermodynamic variables coincide for all state points, confirming that the solver correctly reproduces the nominal operating condition and is numerically consistent.

The behaviour under partial load ($\dot{Q}_{\text{low}}$) and overload ($\dot{Q}_{\text{high}}$) conditions reflects the thermodynamic adaptation of the cycle. A reduction in thermal demand leads to higher P_{evap} and lower P_{cond}, whereas overload conditions result in lower P_{evap} and higher P_{cond}. In both cases, the temperature lift ($T_{\text{cond}} - T_{\text{evap}}$) increases, reducing the COP since a larger lift requires higher compressor work without a proportional increase in useful heat output. Consequently, fixing wastewater datas, the COP reaches its maximum at the nominal condition and decreases when moving away from the design point.

The compressor maps further confirm the physical coherence of the solution: the operating points remain within the admissible regions for all load levels and the efficiencies are lower than the nominal ones, consistently with the imposed map efficiency equal to unity at the design point.

Having verified the correct reproduction of the nominal condition and the physical consistency of the off design results, the model can now be confidently employed for its primary objective. In Chapter 6, the validated heat pump model will be used in daily simulations to determine the optimal heat demand profile in terms of emissions reduction and quantify the achievable CO_2 savings.

6 | Demand Variability Modelling and CO_2 Emission Assessment

Following the on design sizing of the wastewater heat pump and the development of the off design modelling framework, the overall system illustrated in Figure 2.1 is now considered. The validated off design model is therefore employed as a predictive tool for system level analysis under realistic operating conditions.

The objective of this final stage of the work is to evaluate the annual performance of the integrated heat pump boiler system and to determine the district heating demand level that maximises the achievable CO_2 emission savings, with respect to a reference scenario in which the entire thermal demand is supplied by a natural gas boiler.

Since both the wastewater source conditions and the district heating thermal demand vary over time, the corresponding datasets must be processed and organised consistently. For this purpose, the wastewater boundary conditions and the thermal demand profiles are structured according to the same aggregation logic, ensuring full compatibility between source side and demand side inputs.

The model is then executed under the combined hourly variability of wastewater conditions and district heating demand. For a given and fixed annual variability of the wastewater source, different thermal demand scenarios are analysed and the resulting annual CO_2 emissions of the heat pump–boiler system are evaluated and compared with those of the reference natural gas only configuration.

A parametric scaling of the district heating demand is subsequently applied in order to identify the demand level that maximises the annual CO_2 emission savings achievable under the imposed wastewater side availability constraints. This chapter addresses both the modelling of the temporal variability on the wastewater and demand sides and the methodology adopted for the calculation of the resulting annual CO_2 emissions.

6.1. Data Processing: Variability, Reconstruction And Aggregation

This section accounts for the temporal variability of the boundary conditions affecting the heat pump system. Both the thermal demand of the district heating network and the availability of the wastewater heat source vary over time. In order to avoid handling an excessive amount of raw data, the original datasets are processed and organised into a structured set of representative inputs suitable for systematic off design simulations.

6.1.1. Thermal Demand

Dataset Description

The analysis is based on an hourly thermal demand dataset provided for a district heating network serving a residential area consisting of 21 apartment buildings, with a total of 362 apartments. The dataset covers a continuous one year period, from 01/05/2022 to 30/04/2023 and reports the thermal power demand for each hour of the day.

The original dataset exhibits a high temporal resolution and strong day to day variability, which makes its direct use in off design simulations computationally inefficient and poorly representative of typical operating conditions. For this reason, a dedicated data processing procedure was adopted to re organise the available information and extract representative thermal load profiles suitable for steady state off design simulations.

The primary objectives of the data reorganisation are:

- to reduce the dimensionality of the original time series while preserving its main physical trends;
- to construct consistent and repeatable thermal load profiles to be used as boundary conditions for the off design model;
- to enable a systematic analysis of the heat pump response under varying operating conditions.

The adopted data processing methodology is described in detail in Subsection 6.1.1.

Aggregation Methodology

In order to reduce the dimensionality of the original hourly dataset and to derive representative thermal demand profiles suitable for off design simulations, a data aggregation

procedure based on ambient conditions was adopted.

For each day within the analysed period, the corresponding meteorological information was collected for the city of Milan from the 3B Meteo online archive [37], including the daily mean ambient temperature $\overline{T_{\text{amb}}}$, the daily minimum and maximum temperatures ($T_{\min}$, $T_{\max}$), the relative humidity and the ambient pressure P_{amb}. These variables were used exclusively for data classification purposes and not directly as inputs to the thermodynamic model.

The daily thermal demand profiles were then classified according to the value of the ambient temperature $\overline{T_{\text{amb}}}$.

The full temperature range observed over the year, spanning from 1 °C to 31 °C, was divided into discrete temperature bands of 3 °C width (except for the last band which is 4 °C range), identified as k. The ambient temperature ranges considered are:

[1–3, 4–6, 7–9, 10–12, 13–15, 16–18, 19–21, 22–24, 25–27, 28–31] °C

Each day of the dataset was assigned to the corresponding temperature class based on its mean daily ambient temperature.

Let that $\dot{Q}_d(h)$ denote the thermal power demand at hour h of day d, with $h = 1, \ldots, 24$. Each day d is assigned to a temperature class k according to the value of its daily mean ambient temperature $\overline{T_{\text{amb}}}$.

First, a *pivot table* was used to quantify the occurrence of each ambient condition over the year. Specifically, the daily mean ambient temperature $\overline{T_{\text{amb}}}$ was associated with each day of the dataset and the *pivot table* was built to compute the number of days corresponding to each value of $\overline{T_{\text{amb}}}$. The number of days belonging to each ambient temperature range, denoted as N_k, is determined by counting the days whose mean ambient temperature falls within the corresponding k-th interval. This step provides the frequency distribution of the meteorological conditions and allows the statistical representativeness of the subsequent aggregation to be assessed.

Second, another dedicated *pivot table*, coupled with a *pivot chart*, was constructed to perform the aggregation of the hourly thermal demand profiles within each temperature band k. After filtering the dataset by a selected $\overline{T_{\text{amb}}}$ range, the *pivot table* retrieves all daily demand profiles associated with that class, while the linked *pivot chart* visualises the corresponding set of hourly curves.

The representative demand profile of the selected temperature band k is then obtained by averaging the hourly thermal power values across all the days included in the filter.

Formally, for a given temperature band k, the representative hourly demand profile $\overline{\dot{Q}_k(h)}$ is computed as:

$$\overline{\dot{Q}_k(h)} = \frac{1}{N_k} \sum_{d=1}^{N_k} \dot{Q}_{d,k}(h), \qquad h = 1, \ldots, 24. \tag{6.1}$$

An example of the aggregation workflow is reported in Figure 6.1 for the ambient temperature range 1_3 °C, which occurs on a total of 24 days over the analysed year. The figure shows the set of daily hourly thermal demand profiles corresponding to all days whose mean ambient temperature falls within this interval. For clarity and readability, only the graphical representation of the demand profiles is reported, while the corresponding tabular data are omitted, as they would involve a large number of columns and offer limited additional insight.

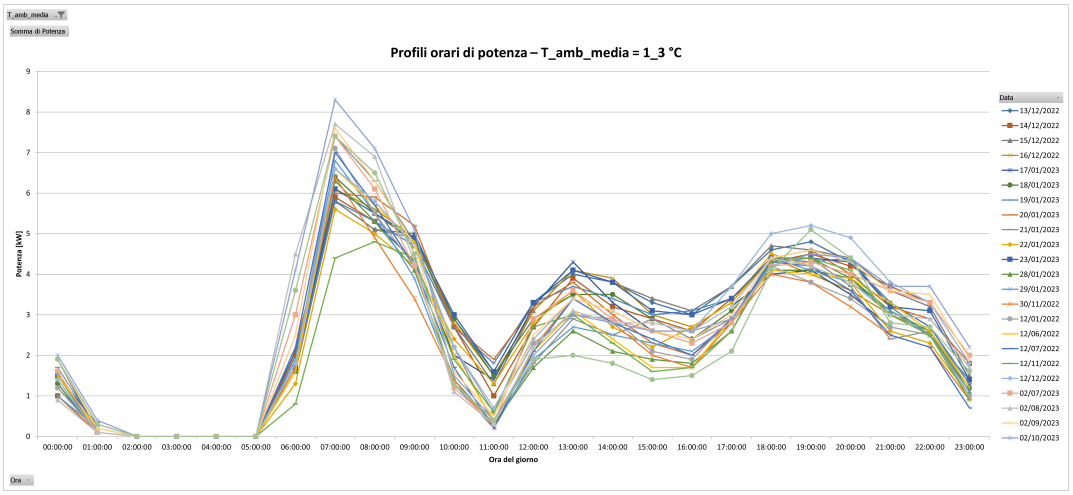

Figure 6.1: Daily hourly thermal demand profiles for all days with mean ambient temperature $\overline{T_{\text{amb}}}$ =1_3 °C.

This procedure is performed for each ambient temperature range k. The hourly thermal demand profiles of all corresponding days are averaged on an hour by hour basis, resulting in a single representative daily demand profile for that temperature class k. The resulting profiles are reported in Table 6.1 and in Figure 6.2.

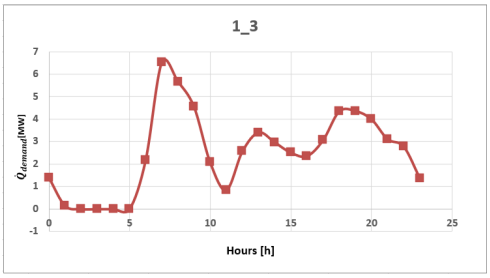

Figure 6.2: Average hourly thermal demand profiles for $\overline{T_{\text{amb}}}$ =1_3 °C.

Hour	1–3	4–6	7–9	10–12	13–15	16–18	19–21	22–24	25–27	28–31
0	1.396	1.510	1.241	1.482	1.573	1.335	0.933	1.021	0.928	0.929
1	0.150	0.370	0.248	0.518	1.055	1.100	0.425	0.945	0.884	0.868
2	0.000	0.253	0.196	0.525	0.952	1.137	0.475	0.929	0.870	0.812
3	0.000	0.253	0.257	0.685	1.148	1.188	0.617	0.919	0.867	0.838
4	0.000	0.253	0.302	0.863	1.330	1.198	0.842	0.924	0.854	0.826
5	0.000	0.253	0.324	0.940	1.445	1.184	0.942	0.940	0.826	0.832
6	2.175	1.559	1.444	2.210	2.645	1.541	1.983	0.990	0.866	0.856
7	6.512	5.670	5.235	5.205	3.670	1.864	2.117	1.110	0.932	0.935
8	5.667	5.039	4.424	4.245	3.251	1.737	1.617	1.152	1.050	1.034
9	4.537	3.922	3.004	2.782	2.273	1.257	1.150	1.183	1.036	1.076
10	2.075	2.077	1.322	1.447	1.474	0.788	1.000	1.179	1.048	1.009
11	0.846	0.876	0.639	0.815	1.009	0.718	1.092	1.195	1.048	0.994
12	2.567	2.310	1.509	1.243	1.094	0.943	1.092	1.188	1.044	1.021
13	3.404	2.979	1.633	1.295	1.261	1.016	1.233	1.202	1.080	1.015
14	2.967	2.365	1.259	1.235	1.418	1.143	1.283	1.248	1.070	1.035
15	2.508	2.025	1.076	1.290	1.452	1.231	1.267	1.200	1.046	1.009
16	2.354	2.145	1.311	1.435	1.582	1.173	1.325	1.186	1.076	1.000
17	3.058	2.893	1.765	1.715	1.615	1.190	1.217	1.155	1.049	0.971
18	4.338	4.156	3.070	2.895	1.997	1.304	1.700	1.126	1.048	0.994
19	4.358	3.942	2.937	2.762	2.197	1.273	1.442	1.160	1.080	0.976
20	3.992	3.648	2.674	2.655	2.373	1.365	1.450	1.183	1.036	1.018
21	3.108	2.785	1.867	2.132	2.330	1.351	1.142	1.181	1.046	1.026
22	2.779	2.353	1.696	1.927	2.145	1.398	1.133	1.167	1.031	0.985
23	1.375	1.193	1.028	1.605	1.952	1.412	1.175	1.131	1.018	0.968

Table 6.1: Average hourly thermal demand data for $\overline{T_{\text{amb}}}$ =1_3 °C.

6.1.2. Wastewater Side

Available Information and Data Limitations

The off design analysis of the heat pump system requires the definition of realistic hourly boundary conditions for the wastewater inlet temperature $T_{\text{ww,in}}$ and mass flow rate $\dot{m}_{\text{ww}}$ over a full reference year, in order to ensure temporal consistency with the district heating thermal demand profiles adopted for the case study. However, detailed long term measurements of wastewater temperature and flow rate for the specific sewer conduit considered in the present study, and more generally for the city of Milan, were not available.

The only site specific information accessible for the Milan case is provided by a feasibility study published by MM S.p.A. [15], which reports short term monitoring data of wastewater temperature and flow rate for a sewer section located in via Marcello Dudovich. This document is therefore used as the primary reference to define the order of magnitude of the wastewater boundary conditions in Milan, but it does not include a sufficiently extended time series to characterise the required daily and seasonal variability.

To reconstruct coherent hourly profiles over the full year, additional sources were employed to represent the temporal variability of the wastewater boundary conditions. Wastewater

temperature variability was derived from graphical representations reported in a technical study on sewer heat recovery for the district heating network of the city of Zurigo [16]. The available graphs describe both the variation of the daily mean wastewater temperature and the typical intra day temperature evolution over representative days. Since no numerical dataset or continuous annual time series is provided, these graphical trends were extracted and post processed to reconstruct consistent hourly temperature profiles.

Additionally, wastewater flow rate variability was characterised using operational data from the official dataset of the WWTP Köln–Weiden [38], which provides measured wastewater flow rates with high temporal resolution. Although the dataset refers to a different urban context, it was adopted as a physically realistic reference for sewer flow. Since the original measurements do not cover the full 24 hour period and present missing data during night time hours, the time series was further processed to reconstruct a complete and temporally consistent dataset. The original time series was then rescaled to obtain a complete hourly flow rate profile for each day of the reference year, aligned with the real sewer pipeline adopted in this study. The details of the processing, reconstruction and scaling procedures are discussed in the Subsections 6.1.2.

Reconstruction and Variability

Temperature

In order to generate a continuous hourly time series of the wastewater inlet temperature $T_{\mathrm{ww,in}}$ suitable for off design simulations, a synthetic reconstruction procedure was adopted, follows standard modelling practices for energy system simulations [39]. It is noted that, although Figure 6.4 reports both influent and effluent wastewater temperatures, only the influent temperature is considered in the present analysis, as the outlet temperature is explicitly computed. In particular, reference was made to the data reported in the ENEA research report on wastewater heat recovery for the Zurich wastewater treatment plant (EAWAG), which publish both annual and daily variations of the influent wastewater temperature, reported in Figures 6.3 and 6.4 [16].

The wastewater temperature was reconstructed by means of an analytical formulation combining a annual and a daily contribution, both represented through sinusoidal functions. The resulting hourly temperature profile is expressed as:

$$T_{\mathrm{ww,in}}(d,h) = \overline{T}_{\mathrm{ww}} + A_{\mathrm{year}} \sin\left(\frac{2\pi}{365}\left(d - \phi_{\mathrm{year}}\right)\right) + A_{\mathrm{day}} \sin\left(\frac{2\pi}{24}\left(h - \phi_{\mathrm{day}}\right)\right),$$

where d denotes the day of the year ($d = 1, \ldots, 365$), h the hour of the day ($h = 1, \ldots, 24$),

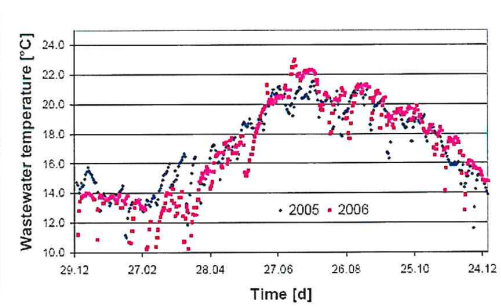

Figure 6.3: Annual evolution.

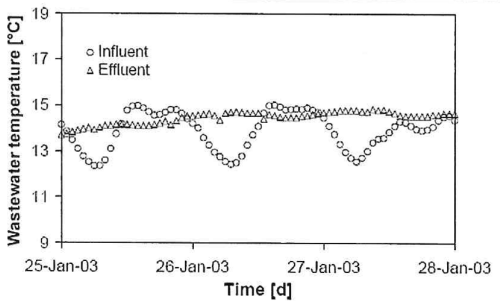

Figure 6.4: Daily variation.

$\overline{T}_{\mathrm{ww}}$ is the annual mean wastewater temperature, A_{year} and A_{day} are the amplitudes of the seasonal and diurnal temperature oscillations, respectively, and ϕ_{year} and ϕ_{day} are phase shifts.

This formulation allows decoupling the low frequency annual evolution of the wastewater temperature from the limited intra day variability, in accordance with the thermal inertia of the sewer system highlighted by the experimental data. The phase shifts were determined by aligning the extrema of the analytical reconstruction with the corresponding annual and daily extrema observed in Figures 6.3 and 6.4, ensuring consistency in both amplitude and temporal positioning of the reconstructed temperature signal.

The reconstruction was performed at hourly resolution for each day of the reference year 2006, yielding a smooth and continuous wastewater temperature profile, suitable for subsequent coupling with the heat pump off-design model.

Flow Rate

The temporal variability of the wastewater flow rate, $\dot{m}_{\mathrm{ww}}$, was derived from an external dataset providing hourly volumetric flow rate measurements over a full reference year. The selected dataset was chosen for its hourly resolution and its ability to capture both diurnal and seasonal flow rate dynamics typical of urban wastewater systems [38].

The original flow rate data is provided in volumetric units [m^3/h] and is converted into mass flow rate [kg/s], in order to be consistent with the formulation adopted in the heat pump model. Assuming a constant wastewater density ρ_{ww} equal to that of water and calculated with *REFPROP*, the conversion is performed as:

$$\dot{m}_{\mathrm{ww}}(t) = \frac{\rho_{\mathrm{ww}}}{3600}\,\dot{V}_{\mathrm{ww}}(t). \tag{6.2}$$

where $\dot{V}_{\mathrm{ww}}(t)$ is the volumetric wastewater flow rate expressed in [m^3/h], $\dot{m}_{\mathrm{ww}}(t)$ is the

corresponding mass flow rate in [kg/s] and t denotes the hourly time index.

In order to obtain a complete and continuous hourly time series, missing or irregular data points, mainly occurring during night time low flow periods, is reconstructed through linear temporal interpolation between adjacent valid measurements. For each missing hourly value at time t, the wastewater mass flow rate was estimated as:

$$\dot{m}_{\mathrm{ww}}(t) = \dot{m}_{\mathrm{ww}}(t_1) + \frac{t - t_1}{t_2 - t_1} \left[\dot{m}_{\mathrm{ww}}(t_2) - \dot{m}_{\mathrm{ww}}(t_1) \right]. \tag{6.3}$$

where t_1 and t_2 denote the nearest time instants with valid measurements before and after the missing data point, respectively. This interpolation approach preserves the continuity of the flow rate time series while maintaining the characteristic low flow behaviour observed during night time periods.

The resulting processing produce a continuous hourly wastewater mass flow rate time series $\{ \dot{m}_{\mathrm{ww}}(t) \}_{t=1}^{8760}$, representative of the diurnal and seasonal variability of wastewater flow and suitable for subsequent scaling and off-design simulations.

Aggregation with respect to $\overline{T}_{\mathrm{amb}}$.

In order to ensure full consistency between the wastewater side boundary conditions and the district heating thermal demand, the reconstructed hourly wastewater datasets were organised as a function of the daily mean ambient air temperature $\overline{T_{\mathrm{amb}}}$, following the same aggregation strategy adopted in Subsection 6.1.1.

Days characterised by the same ambient temperature range k were identified, and the corresponding hourly values of wastewater temperature and flow rate were grouped accordingly.

For each ambient temperature class, an hourly averaging procedure is applied to find the representative hourly wastewater inlet temperature profile $\overline{T_{\mathrm{ww,in},k}(h)}$ and the hourly wastewater mass flow rate profile $\overline{\dot{m}_{\mathrm{ww},k}(h)}$ as follows:

$$\overline{T_{\mathrm{ww,in},k}(h)} = \frac{1}{N_k} \sum_{d=1}^{N_k} T_{\mathrm{ww,in},d,k}(h), \qquad h = 1, \ldots, 24, \tag{6.4}$$

$$\overline{\dot{m}_{\mathrm{ww},k}(h)} = \frac{1}{N_k} \sum_{d=1}^{N_k} \dot{m}_{\mathrm{ww},d,k}(h), \qquad h = 1, \ldots, 24, \tag{6.5}$$

where h denotes the hour of the day, d indexes the days belonging to the k-th ambient temperature class, N_k is the total number of days in that class, $T_{\mathrm{ww,in},d,k}(h)$ is the wastewater inlet temperature, and $\dot{m}_{\mathrm{ww},d,k}(h)$ is the corresponding wastewater mass flow rate at hour h of day d.

This aggregation process results in a discrete set of characteristic hourly wastewater profiles, each associated with a specific ambient temperature range k. The resulting profiles constitute the wastewater side input data for the off design simulations and are directly compatible with the aggregated thermal demand profiles. The numerical results of this procedure are summarised in Tables 6.2 and 6.3.

Hour	1–3	4–6	7–9	10–12	13–15	16–18	19–21	22–24	25–27	28–31
0	13.42	13.60	13.97	14.76	16.32	17.94	17.91	19.95	21.43	22.06
1	13.19	13.35	13.69	14.44	15.98	17.67	17.61	19.73	21.22	21.76
2	12.83	13.11	13.45	14.18	15.74	17.45	17.39	19.49	20.92	21.51
3	12.66	12.89	13.26	14.00	15.53	17.16	17.24	19.19	20.68	21.27
4	12.48	12.70	12.97	13.70	15.14	16.93	17.01	18.99	20.46	21.01
5	12.20	12.37	12.73	13.50	15.04	16.76	16.77	18.70	20.31	20.70
6	12.13	12.25	12.51	13.32	14.85	16.46	16.62	18.56	20.10	20.54
7	12.13	12.14	12.58	13.17	14.74	16.40	16.36	18.46	20.04	20.49
8	11.91	12.12	12.48	13.21	14.71	16.40	16.57	18.48	19.98	20.44
9	12.03	12.12	12.53	13.20	14.84	16.53	16.50	18.50	19.96	20.51
10	12.14	12.27	12.59	13.31	14.91	16.54	16.75	18.60	20.09	20.67
11	12.33	12.40	12.82	13.56	14.99	16.68	16.72	18.75	20.26	20.82
12	12.41	12.61	12.99	13.72	15.21	16.86	16.95	18.93	20.39	20.95
13	12.65	12.84	13.20	13.94	15.40	17.11	17.10	19.30	20.68	21.24
14	12.90	13.13	13.52	14.23	15.68	17.44	17.44	19.48	21.00	21.56
15	13.24	13.36	13.70	14.46	16.02	17.68	17.74	19.74	21.13	21.76
16	13.35	13.64	13.97	14.69	16.26	17.90	18.04	19.97	21.48	21.92
17	13.68	13.80	14.21	14.94	16.46	18.20	18.30	20.15	21.64	22.24
18	13.85	13.95	14.32	15.03	16.69	18.26	18.40	20.36	21.81	22.39
19	13.86	14.06	14.45	15.21	16.72	18.30	18.47	20.46	21.98	22.40
20	14.01	14.08	14.47	15.17	16.74	18.41	18.35	20.45	21.96	22.47
21	13.89	14.04	14.42	15.15	16.69	18.42	18.27	20.46	21.96	22.47
22	13.84	14.00	14.32	15.14	16.62	18.31	18.39	20.33	21.77	22.33
23	13.67	13.79	14.19	14.88	16.39	18.17	18.17	20.14	21.70	22.09

Table 6.2: Representative hourly influent wastewater temperature profiles.

Hour	1–3	4–6	7–9	10–12	13–15	16–18	19–21	22–24	25–27	28–31
0	91.46	94.13	101.69	99.95	95.98	96.60	98.22	95.48	97.05	96.22
1	91.56	94.25	101.35	99.51	95.80	96.42	98.04	95.30	96.87	96.04
2	92.97	94.73	99.77	99.45	96.02	96.64	98.26	95.51	97.09	96.26
3	111.39	116.25	119.47	121.35	117.37	118.13	120.11	116.75	118.68	117.66
4	112.44	116.92	120.27	121.99	118.18	118.94	120.94	117.56	119.49	118.47
5	112.75	115.46	121.09	121.84	118.11	118.88	120.87	117.49	119.43	118.41
6	111.40	114.19	117.60	119.92	116.07	116.82	118.79	115.46	117.37	116.36
7	114.81	118.67	122.04	124.83	120.45	121.23	123.26	119.82	121.79	120.75
8	105.44	107.54	110.17	111.99	108.28	108.98	110.81	107.71	109.49	108.55
9	103.95	107.13	107.75	110.91	106.90	107.59	109.40	106.34	108.09	107.17
10	103.90	105.19	108.08	109.07	105.79	106.48	108.26	105.24	106.97	106.05
11	97.69	98.03	102.12	101.48	99.17	99.81	101.49	98.65	100.27	99.41
12	97.27	98.24	101.95	101.49	99.47	100.12	101.80	98.95	100.58	99.72
13	92.26	93.29	96.24	98.34	94.48	95.09	96.69	93.99	95.54	94.72
14	87.25	90.28	94.74	93.42	91.01	91.60	93.13	90.53	92.02	91.23
15	88.39	89.38	93.44	92.12	90.73	91.32	92.85	90.26	91.74	90.96
16	87.69	89.35	94.33	92.35	90.78	91.37	92.90	90.31	91.79	91.01
17	89.39	91.39	95.62	93.00	92.42	93.01	94.58	91.93	93.45	92.65
18	91.39	97.06	97.11	95.31	95.15	95.76	97.37	94.65	96.21	95.38
19	103.08	105.44	109.71	106.00	105.56	106.24	108.02	105.00	106.73	105.82
20	101.96	106.36	109.16	105.11	105.25	105.93	107.71	104.69	106.42	105.51
21	99.25	104.37	106.92	103.32	102.98	103.64	105.39	102.44	104.13	103.23
22	108.22	111.06	115.20	111.73	111.47	112.19	114.07	110.89	112.71	111.75
23	103.59	107.09	114.25	111.73	110.04	110.75	112.61	109.46	111.27	110.31

Table 6.3: Representative hourly wastewater flow rate profiles.

6.2. Overall CO_2 Emission Assessment and Demand Scaling Effects

This section evaluates the overall CO_2 emission performance of the proposed wastewater heat pump overall system by running the off design model under the combined variability of wastewater side conditions and district heating demand. Due to operational constraints of the heat pump, the auxiliary electric boiler is activated outside the feasible operating range. The resulting annual CO_2 emissions are compared with a reference natural gas boiler scenario, and a parametric scaling of the district heating demand is performed to identify the demand level that maximises emission savings.

6.2.1. Simulations under hourly demand profiles And Scaling Procedure

For each ambient temperature range, the off design model is executed for every hour of the day by simultaneously varying the district heating thermal demand $\dot{Q}_{\text{demand}}$, the wastewater mass flow rate $\dot{m}_{\text{ww}}$ and the wastewater inlet temperature $T_{\text{ww,in}}$ according to the corresponding representative hourly profiles. For each hourly simulation, the operating regime of the system is therefore determined as a function of the imposed thermal demand and of the feasibility of the resulting heat pump operating point.

Based on the operational limits of the heat pump discussed in Chapter 5, the maximum and minimum thermal demand depend on the wastewater inlet conditions adopted as model input. Consequently, the upper and lower bounds of $\dot{Q}_{\text{demand}}$ would vary from case to case.

However, in order to avoid introducing an additional iterative search procedure at each simulation step, fixed representative limits are selected according to the admissible operating region of the compressors. Accordingly, the thermal demand bounds are assumed as $\dot{Q}_{\text{demand,min}} = 950$ kW and $\dot{Q}_{\text{demand,max}} = 2950$ kW for the subsequent analysis.

According to this the following cases are identified:

- $\dot{Q}_{\text{demand}} = 0$: no thermal energy is required and both the heat pump and the auxiliary boiler remain inactive;
- $0 < \dot{Q}_{\text{demand}} < \dot{Q}_{\text{HP,min}}$: the thermal demand is below the minimum operable load of the heat pump and is therefore fully supplied by the auxiliary electric boiler;
- $\dot{Q}_{\text{HP,min}} \leq \dot{Q}_{\text{demand}} \leq \dot{Q}_{\text{HP,max}}$ and successful convergence of the off-design solver: the thermal demand is entirely covered by the heat pump;
- $\dot{Q}_{\text{demand}} > \dot{Q}_{\text{HP,max}}$: the heat pump operates at its maximum feasible thermal power, while the residual demand is supplied by the auxiliary electric boiler;

STATUS	Condition	Thermal power balance
OFF	$\dot{Q}_{\text{demand}} = 0$	$\dot{Q}_{\text{HP}} = 0, \quad \dot{Q}_{\text{boiler}} = 0$
BOILER_ONLY	$0 < \dot{Q}_{\text{demand}} < \dot{Q}_{\text{HP,min}}$	$\dot{Q}_{\text{HP}} = 0, \quad \dot{Q}_{\text{boiler}} = \dot{Q}_{\text{demand}}$
OK	$\dot{Q}_{\text{HP,min}} \leq \dot{Q}_{\text{demand}} \leq \dot{Q}_{\text{HP,max}}$ and solver convergence	$\dot{Q}_{\text{HP}} = \dot{Q}_{\text{demand}}, \quad \dot{Q}_{\text{boiler}} = 0$
HIGH_LOAD	$\dot{Q}_{\text{demand}} > \dot{Q}_{\text{HP,max}}$	$\dot{Q}_{\text{HP}} = \dot{Q}_{\text{HP,max}}, \quad \dot{Q}_{\text{boiler}} = \dot{Q}_{\text{demand}} - \dot{Q}_{\text{HP}}$

Table 6.4: Mapping between thermal demand conditions, operating regimes and status flag assigned to each hourly off design simulation.

In order to assess the sensitivity of the overall CO_2 emission savings to the district heating demand level, a demand scaling procedure was applied to the reference thermal demand profiles. Starting from the aggregated hourly demand corresponding to the reference district heating network serving 362 apartments, the entire thermal demand dataset was uniformly scaled by a multiplicative *demand scaling factor* α, defined in the range $0.8 \leq \alpha \leq 4.0$.

The scaling procedure was applied consistently to all the representative hourly demand profiles associated with each ambient temperature range $\overline{T}_{\text{amb}}$. For each value of the scal-

ing factor α, all the hourly thermal demand values reported in Table 6.1 were multiplied by the same factor, according to:

$$\dot{Q}^{(\alpha)}_{\text{demand},i} = \alpha\, \dot{Q}_{\text{demand},i}, \qquad i = 1, \ldots, N,$$

where $\dot{Q}_{\text{demand},i}$ denotes the i-th hourly value of the original district heating demand profile and N is the total number of hourly data points across all ambient temperature classes. This operation preserves both the intra day variability and the dependence of the demand on ambient temperature, while generating synthetic district heating demand scenarios corresponding to proportionally smaller or larger numbers of connected apartments.

Therefore, given a value of α, for each hourly run and for each ambient temperature range, the off design simulation yields the following set of output variables:

[Hour, Q_{demand}, $T_{\text{ww,in}}$, $T_{\text{ww,out}}$, $\dot{m}_{\text{ww}}$, INFO, Q_{HP}, W_{HP}, COP_{HP}, $T_{x,\text{HP}}$, Q_{boiler}, P_{cond}, ΔT_{sub}, P_{evap}, STATUS].

Table 6.5 and Table 6.6 reports an example of the output results corresponding to the temperature range T_{1_3} and T_{25_27} for $\alpha = 1$.

Ora	Q_{dem}	Q_{HP}	W_{HP}	**COP**	T_x	Q_{boiler}	P_{cond}	ΔT_{sub}	P_{evap}	**STATUS**
0	1395.8	1395.9	467.5	2.80	80.00	0	1.989	16.45	0.254	OK
1	150.0	0	0	0	80	150.0	0	0	0	BOILER_ONLY
2	0	–	–	–	–	–	–	–	–	OFF
3	0	–	–	–	–	–	–	–	–	OFF
4	0	–	–	–	–	–	–	–	–	OFF
5	0.07	0	0	0	80	0.07	0	0	0	BOILER_ONLY
6	2175.1	2174.7	724.0	2.83	80.00	0	2.157	16.94	0.213	OK
7	6512.5	2950.0	1113.0	2.50	69.06	3562.5	2.288	16.98	0.194	HIGH_LOAD
8	5666.6	2950.0	1118.0	2.49	70.41	2716.6	2.286	16.98	0.192	HIGH_LOAD
9	4537.4	2950.0	1115.2	2.50	73.00	1587.4	2.287	16.98	0.193	HIGH_LOAD
10	2075.0	2074.2	683.7	2.85	79.99	0	2.138	16.93	0.216	OK
11	845.9	0	0	0	80	845.9	0	0	0	BOILER_ONLY
12	2566.7	2566.8	872.5	2.77	80.00	0	2.238	16.98	0.203	OK
13	3404.2	2950.0	1101.5	2.53	77.33	454.2	2.291	16.98	0.197	HIGH_LOAD
14	2966.7	2950.0	1096.0	2.54	79.89	16.7	2.292	16.98	0.199	HIGH_LOAD
15	2508.3	2508.8	832.1	2.84	80.00	0	2.231	16.99	0.211	OK
16	2354.2	2353.2	773.5	2.86	79.99	0	2.198	16.98	0.217	OK
17	3058.4	2950.0	1078.8	2.58	79.29	108.4	2.296	16.97	0.204	HIGH_LOAD
18	4337.5	2950.0	1074.6	2.59	73.60	1387.5	2.297	16.97	0.205	HIGH_LOAD
19	4358.3	2950.0	1074.3	2.59	73.54	1408.3	2.297	16.97	0.205	HIGH_LOAD
20	3991.6	2950.0	1071.1	2.60	74.78	1041.6	2.297	16.97	0.206	HIGH_LOAD
21	3108.3	2950.0	1073.6	2.59	78.98	158.3	2.297	16.97	0.206	HIGH_LOAD
22	2779.1	2778.8	964.0	2.72	80.00	0	2.275	16.97	0.208	OK
23	1375.0	1375.5	462.0	2.79	80.01	0	1.983	16.41	0.258	OK

Table 6.5: $\alpha = 1$, T_{1_3} hourly off design simulation results.

Ora	Q_{dem}	Q_{HP}	W_{HP}	COP	T_x	Q_{boiler}	P_{cond}	ΔT_{sub}	P_{evap}	STATUS
0	928.0	0	0	0	80	928.0	0	0	0	BOILER_ONLY
1	884.0	0	0	0	80	884.0	0	0	0	BOILER_ONLY
2	870.0	0	0	0	80	870.0	0	0	0	BOILER_ONLY
3	867.0	0	0	0	80	867.0	0	0	0	BOILER_ONLY
4	854.0	0	0	0	80	854.0	0	0	0	BOILER_ONLY
5	826.0	0	0	0	80	826.0	0	0	0	BOILER_ONLY
6	866.0	0	0	0	80	866.0	0	0	0	BOILER_ONLY
7	932.0	0	0	0	80	932.0	0	0	0	BOILER_ONLY
8	1050.0	1050.2	323.3	3.02	80.00	0	1.936	16.33	0.337	OK
9	1036.0	1036.2	318.6	3.03	80.00	0	1.935	16.33	0.337	OK
10	1048.0	1048.2	322.1	3.03	80.00	0	1.936	16.33	0.338	OK
11	1048.0	1048.2	321.3	3.04	80.00	0	1.936	16.33	0.340	OK
12	1044.0	1044.2	319.3	3.04	80.00	0	1.936	16.33	0.342	OK
13	1080.0	1080.3	330.2	3.05	80.01	0	1.941	16.34	0.343	OK
14	1070.0	1070.2	325.3	3.06	80.00	0	1.940	16.34	0.347	OK
15	1046.0	1046.2	316.5	3.07	80.00	0	1.937	16.35	0.350	OK
16	1076.5	1076.7	325.1	3.08	80.00	0	1.941	16.35	0.353	OK
17	1049.0	1049.2	315.1	3.10	80.00	0	1.938	16.36	0.356	OK
18	1047.5	1047.6	313.8	3.10	80.00	0	1.938	16.36	0.358	OK
19	1080.0	1080.2	323.9	3.10	80.00	0	1.942	16.36	0.358	OK
20	1036.0	1036.1	309.3	3.11	80.00	0	1.937	16.36	0.360	OK
21	1046.0	1046.1	312.6	3.11	80.00	0	1.938	16.36	0.360	OK
22	1031.0	1031.1	308.5	3.11	80.00	0	1.936	16.36	0.359	OK
23	1018.0	1018.1	304.5	3.11	80.00	0	1.935	16.36	0.358	OK

Table 6.6: $\alpha = 1$, T_{25_27} hourly off design simulation results.

It can be observed that the coefficient of performance is not constant throughout the year but varies as a function of the wastewater side conditions. In particular, for higher ambient temperature ranges, the wastewater inlet temperature $T_{ww,in}$ is higher, as showed in Table 6.2, resulting in a higher evaporation temperature T_{evap}. Since the temperature lift of the cycle decreases, the compression ratio is reduced and the compressor work decreases accordingly. As a consequence, the COP increases.

During the annual simulations, this variability of COP directly affects the specific CO_2 emissions of the heat pump. Therefore, seasonal variations in wastewater temperature lead to a non uniform environmental performance over the year, influencing the total annual emission balance.

Using this set of results for each temperature range, the resulting annual CO_2 emissions of the combined heat pump and auxiliary boiler system were then evaluated and compared with those of a reference natural gas boiler supplying the same scaled thermal demand, according to the CO_2 emission calculation procedure described in the subsection 6.2.2.

The entire procedure is carried out for every value of α considered in the parametric

analysis, in this way the net CO_2 emission savings were finally analysed as a function of the demand scaling factor α, allowing the identification of the thermal demand level, and the corresponding number of connected apartments, for which the integration of the wastewater heat pump achieves the maximum overall emission reduction under fixed wastewater availability.

6.2.2. ΔCO_2 Emission Calculation Methodology

For a given district heating demand scenario defined by the scaling factor α, the CO_2 emission savings are evaluated by comparing the proposed system configuration, consisting of a wastewater heat pump supported by an auxiliary electric boiler, with a reference scenario in which the entire thermal demand is supplied by a natural gas fired boiler.

The emission assessment is performed separately for each ambient temperature range $\overline{T}_{\mathrm{amb}}$. For each range, the off design simulations provide the hourly thermal energy delivered by the heat pump $\dot{Q}_{\mathrm{HP},h}$ and by the auxiliary electric boiler $\dot{Q}_{\mathrm{boiler},h}$. Since an hourly resolution is adopted, thermal power and thermal energy are numerically equivalent and hourly values are directly interpreted as $\mathrm{MWh_{th}}$.

The specific CO_2 emission factors adopted in the analysis are [40]:

$$e_{\mathrm{el}} = 215.9\ \mathrm{kgCO_2/MWh_{el}}, \qquad e_{\mathrm{GN}} = 213.06\ \mathrm{kgCO_2/MWh_{fuel}}.$$

The equivalent CO_2 emission factors associated with each technology are therefore defined as:

$$e_{\mathrm{boiler}} = \frac{e_{\mathrm{el}}}{\mathrm{COP}_{\mathrm{boiler}}}, \quad e_{\mathrm{HP},h} = \frac{e_{\mathrm{el}}}{\mathrm{COP}_{\mathrm{HP},h}}, \quad e_{\mathrm{GN,ref}} = \frac{e_{\mathrm{GN}}}{\eta_{\mathrm{boiler,ref}}}, \tag{6.6}$$

where $\mathrm{COP}_{\mathrm{boiler}} = 1$ is assumed for the electric boiler, $\mathrm{COP}_{\mathrm{HP},h}$ is the hourly coefficient of performance of the heat pump obtained from the off-design simulations, and $\eta_{\mathrm{boiler,ref}} = 0.95$ is the assumed efficiency of the natural gas boiler in the reference scenario [41].

For each hour h of a representative day within a given ambient temperature range j, the hourly CO_2 emissions of the proposed system are computed as:

$$\mathrm{CO}^{\mathrm{sys}}_{2,i,h} = \dot{Q}_{\mathrm{HP},i,h}\, e_{\mathrm{HP},i,h} + \dot{Q}_{\mathrm{boiler},i,h}\, e_{\mathrm{boiler}}, \tag{6.7}$$

while the emissions of the reference natural gas boiler supplying the same thermal demand are given by:

$$\mathrm{CO}^{\mathrm{ref}}_{2,i,h} = \dot{Q}_{\mathrm{demand},i,h}\, e_{\mathrm{GN,ref}}, \tag{6.8}$$

where the subscript i denotes the demand scenario associated with the scaling factor α.

The daily CO_2 emissions associated with the j-th ambient temperature range are obtained by summing the hourly contributions over the 24 hours of the day:

$$\mathrm{CO}_{2,i,\mathrm{day}}^{(j)} = \sum_{h=1}^{24} \mathrm{CO}_{2,i,h}. \tag{6.9}$$

By multiplying the daily emissions by the number of days N_j associated with the corresponding ambient temperature range, the total CO_2 emissions for that range are obtained:

$$\mathrm{CO}_{2,i,\mathrm{range}}^{(j)} = N_j \, \mathrm{CO}_{2,i,\mathrm{day}}^{(j)}. \tag{6.10}$$

Finally, for a given demand scaling factor α, the total annual CO_2 emission savings are computed by summing the contributions of all ambient temperature ranges:

$$\Delta\mathrm{CO}_2^{(\alpha)} = \sum_{j=1}^{N_T} \left(\mathrm{CO}_{2,i,\mathrm{range}}^{(j),\mathrm{ref}} - \mathrm{CO}_{2,i,\mathrm{range}}^{(j),\mathrm{sys}} \right), \tag{6.11}$$

where N_T denotes the total number of ambient temperature ranges considered. The resulting value represents the annual CO_2 emission reduction associated with the integration of the wastewater heat pump for the thermal demand level corresponding to the scaling factor α, and is directly linked to the total annual thermal energy supplied to the district heating network.

In addition to the CO_2 emission assessment, the total thermal energy supplied to the district heating network is evaluated for each demand scaling factor α. For each ambient temperature range j, the daily thermal energy delivered is obtained by summing the hourly thermal demand over the 24 hours of the representative day:

$$E_{i,\mathrm{day}}^{(j)} = \sum_{h=1}^{24} \dot{Q}_{\mathrm{demand},i,h} \tag{6.12}$$

and by multiplying it by the number of days N_j associated with the corresponding ambient temperature range, the total annual thermal energy is computed as:

$$E_{i,\mathrm{range}}^{(j)} = N_j \, E_{i,\mathrm{day}}^{(j)}. \tag{6.13}$$

The total annual thermal energy supplied for the demand scenario i is then obtained by

summing the contributions of all ambient temperature ranges:

$$E_i^{\text{tot}} = \sum_{j=1}^{N_T} E_{i,\text{range}}^{(j)}. \tag{6.14}$$

As a result, for each value of the demand scaling factor α in the range $0.8 \leq \alpha \leq 4.0$, a corresponding pair $\left[E_{\text{th,ann}}(\alpha), \Delta\text{CO}_2(\alpha)\right]$ is obtained, where $E_{\text{th,ann}}$ represents the total annual thermal energy supplied to the district heating network. This relationship allows identifying the thermal demand level, the associated annual heat supply, and the corresponding number of connected apartments for which the integration of the wastewater heat pump achieves the maximum CO_2 emission savings under fixed wastewater-side conditions.

6.3. Final Result

The procedure described establishes a direct relationship between the total annual thermal energy supplied to the district heating network and the corresponding net CO_2 emission savings for different values of the demand scaling factor α.

For $0.8 \leq \alpha \leq 4.0$, the annual thermal energy $MWh_{\text{th,tot}}$, the associated CO_2 emission reduction ΔCO_2, and the peak-to-heat-pump power ratio $P_{\text{peak}}/P_{\text{HP}}$ are reported in Table 6.7 and graphically represented in Figure 6.5.

As expected, the annual thermal energy supplied to the district heating network increases almost proportionally with α, ranging from approximately 10.6 GWh_{th}/year to more than 53 GWh_{th}/year over the investigated interval. In contrast, the behaviour of ΔCO_2 is clearly non-monotonic.

As the heat pump covers a progressively larger share of the annual thermal demand, the emission savings initially increase, reaching a maximum value of 1747.5 tCO_2/year for $\alpha = 2$, corresponding to an annual heat supply of about 26.6 GWh_{th}/year. The interpolation of the discrete simulation points confirms the presence of this optimum within the analysed range.

For values of α above 2, the net CO_2 savings decrease despite the higher total heat delivered. This behaviour is explained by the increasing contribution of the auxiliary electric boiler under peak-load conditions, as highlighted by the monotonic growth of the $P_{\text{peak}}/P_{\text{HP}}$ ratio. As the mismatch between the installed heat pump capacity and the peak thermal demand widens, a larger fraction of the additional load is supplied by the boiler,

thereby reducing the marginal emission benefit.

The results therefore demonstrate the existence of an optimal district heating demand level for which the integration of the wastewater heat pump maximises annual CO_2 emission reduction under fixed wastewater side availability. This optimum corresponds to a specific annual thermal supply and, consequently, to a well defined equivalent number of connected apartments.

α	MWh_{th}	ΔCO_2 [t/y]	$P_{\text{peak}}/P_{\text{HP}}$
0.8	10645.120	467.168	1.766
1.0	13307.159	1100.827	2.208
1.2	15968.527	1438.534	2.649
1.4	18628.470	1549.575	3.091
1.6	21289.680	1648.177	3.532
1.8	22462.519	1707.332	3.974
2.0	26612.100	1747.445	4.415
2.2	29273.309	1744.175	4.857
2.4	31934.519	1718.944	5.298
2.6	34595.729	1650.771	5.740
2.8	37264.629	1593.853	6.181
3.0	39918.149	1454.059	6.623
3.2	42579.359	1290.625	7.064
3.4	45240.569	1111.773	7.506
3.6	47901.779	921.199	7.947
3.8	50562.989	755.934	8.389
4.0	53224.199	570.312	8.830

Table 6.7: Annual thermal energy, CO_2 emission savings and peak to heat pump power ratio as a function of the demand scaling factor α.

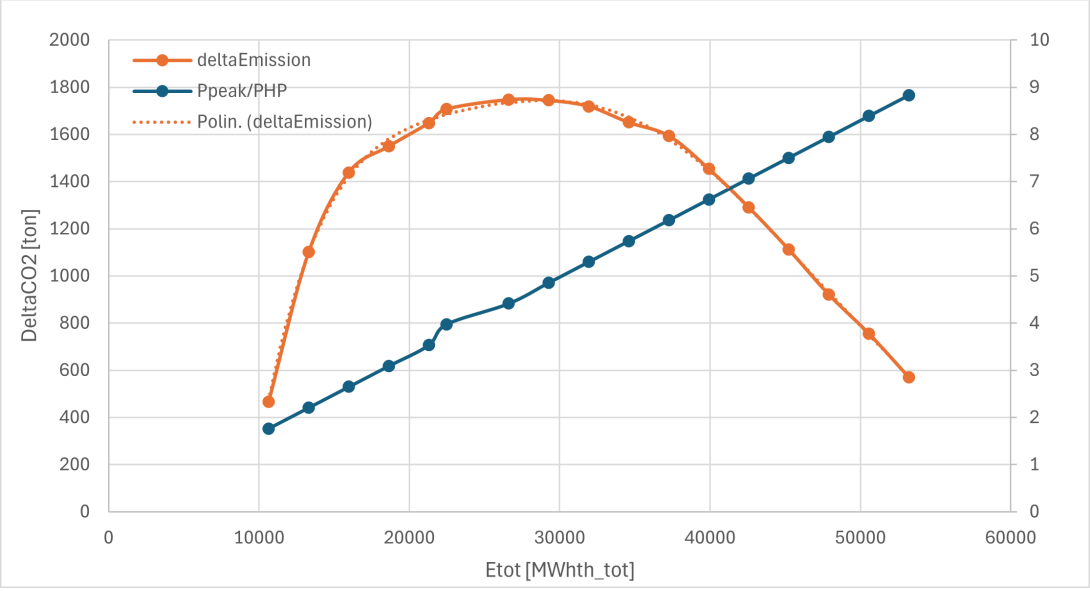

Figure 6.5: Graphical representation of ΔCO_2 and $P_{\text{peak}}/P_{\text{HP}}$ as a function of the demand scaling factor α.

7 | Conclusion and Future Development

The aim of this thesis is to develop and apply a comprehensive modelling framework for the assessment of a wastewater source heat pump integrated into a district heating system. The adoption of wastewater as a heat source is justified by its continuous availability and relatively stable temperature in urban environments, which make it particularly suitable for district heating integration and long operating hours.

The analysed configuration consists of a two stage vapour compression heat pump supplying a district heating network and supported by an auxiliary electric boiler to ensure full load coverage. The performance of the integrated system is compared with a reference scenario in which the same thermal demand is entirely met by a natural gas boiler.

First, a detailed on design thermodynamic model of the heat pump is formulated to determine all cycle state points and to size the main components under nominal operating conditions.

Second, an off design model is developed to describe the adaptive behaviour of the heat pump under variable wastewater temperatures, mass flow rates and thermal demand. This solver is then used as the core predictive tool for system level simulations.

Finally, the validated off design model is embedded within an annual simulation framework with hourly resolution. Wastewater boundary conditions and district heating demand are consistently processed to reproduce realistic seasonal variability. A parametric scaling of the demand through a factor α is introduced to identify the demand level that maximises annual CO_2 emission savings with respect to the natural gas reference scenario.

7.1. Methodological Contribution

The principal contribution of this thesisis the development of an integrated thermodynamic and environmental assessment framework for wastewater source heat pump systems

coupled to district heating networks.

A first methodological contribution consists in the implementation of a dedicated on-design computational model of a two stage vapour compression heat pump. A structured code was developed to determine the complete set of thermodynamic state points from prescribed boundary conditions, including wastewater temperature and mass flow rate, district heating supply temperature and design thermal load. The solver resolves mass and energy balances for all components and automatically computes refrigerant mass flow rate, compressor work, heat duties of the all heat exchanger and the resulting coefficient of performance. On this basis, the main components are dimensioned at nominal conditions, ensuring accurate sizing of compressors and heat exchangers. This guarantees thermodynamic closure and numerical consistency of the reference configuration, which serves as the foundation for subsequent analyses.

The second methodological contribution is the formulation and validation of an off design modelling framework capable of capturing the adaptive response of the heat pump under variable boundary conditions. The solver iteratively determines evaporating and condensing pressures, subcooling degree, refrigerant mass flow rate and performance indicators while respecting compressor maps and operational constraints. The agreement between on design and nominal off design solutions confirms both numerical robustness and physical reliability.

A further methodological advancement is the construction of an annual simulation environment with hourly resolution. Rather than directly employing high dimensional raw datasets, wastewater boundary conditions and district heating demand are processed through a structured aggregation procedure based on ambient temperature ranges. This approach preserves seasonal variability, reduces computational complexity and ensures consistency between source side and demand side inputs.

The thesis also introduces a systematic and generalisable procedure for annual CO_2 emission assessment. Emissions are calculated hour by hour for both the proposed heat pump boiler configuration and a reference natural-gas boiler scenario, using consistent emission factors and efficiency assumptions. The annual emission balance is obtained by integrating hourly contributions across all temperature ranges, thereby maintaining coherence between operational variability and environmental impact.

Although applied to a wastewater source heat pump, the modelling architecture is inherently modular and not restricted to the specific case study. The on design and off design codes are formulated within a general thermodynamic structure and can be adapted to alternative configurations, refrigerants or heat sources. Likewise, the annual emission as-

sessment methodology can be extended to other electrically driven heat pump systems or hybrid architectures.

Finally, the introduction of a parametric demand scaling factor α, enables the identification of the district heating demand level that maximises annual CO_2 savings under fixed source side availability. Through this parametric formulation, the framework evolves from a cycle level performance simulator into a quantitative design instrument capable of supporting capacity matching and emission oriented integration strategies.

Overall, the thesis delivers a physically grounded, computationally robust and transferable methodology for the thermodynamic design and environmental evaluation of large scale heat pump applications in urban energy systems.

7.2. Main Scientific Findings

The main scientific outcomes of this thesis emerge from the consistent integration of thermodynamic modelling, off design validation and annual environmental assessment.

The on design analysis presented in Chapter 4 establishes the nominal operating condition of the wastewater heat pump through a complete thermodynamic resolution of the cycle. All state points, thermal duties and the nominal coefficient of performance are determined throught mass and energy balances and the evaporator, condenser, subcooler and compressors are dimensioned accordingly. This defines a physically consistent reference configuration in terms of pressures, temperatures, heat transfer rates and design COP.

The off design framework developed in Chapter 5 is validated by fixing the wastewater inlet temperature and mass flow rate at their nominal values while varying the imposed thermal demand. Under these conditions, the off design solver correctly reproduces the on design operating point, confirming numerical consistency. When the thermal load deviates from nominal, the model predicts a systematic reduction in COP due to the lower compressor efficiency under off design conditions and to the fact that the heat exchangers are dimensioned for the nominal on design operating point, thus reflecting the expected performance degradation outside the design condition.

The system level simulations described in Chapter 6 lead to the central result of this thesis: the annual CO_2 emission savings exhibit a clear maximum at a demand scaling factor $\alpha = 2$, corresponding to approximately 1747 tCO_2/year. The relationship between emission savings and α is therefore non monotonic.

For values of α lower than the optimum, the thermal demand is insufficient to fully

exploit the installed heat pump capacity over the year, limiting the achievable emission reduction. Conversely, for values of α higher than 2, the growing mismatch between heat pump capacity and peak thermal demand results in an increasing contribution of the auxiliary electric boiler. As a consequence, a larger fraction of the additional load is supplied under less favourable emission conditions, reducing the marginal environmental benefit. The decrease in emission savings beyond the optimal point is thus directly linked to excessive reliance on the auxiliary boiler under high demand scenarios.

The annual simulations further highlight the influence of wastewater temperature on thermodynamic performance. Lower wastewater temperatures, typically associated with lower ambient temperatures, lead to reduced evaporation temperatures and consequently to lower COP values. This seasonal variability directly affects the hourly emission intensity of the heat pump and contributes to the overall annual emission balance.

The main scientific outcome is therefore that maximum decarbonisation is not achieved through a simple increase in connected thermal demand, but through an optimal balance between wastewater availability, heat pump capacity and demand level.

7.3. Future Developments

Although the proposed framework provides a coherent thermodynamic and environmental analysis, several aspects could be further refined. A first improvement concerns seasonal modelling. The present study adopts reconstructed and aggregated datasets; future analyses could rely on long term measured wastewater temperature and flow data specific to the Milan sewer network, allowing a more accurate representation of extreme winter conditions and inter-annual variability. A dedicated seasonal sensitivity analysis could also assess whether the optimal demand scaling factor α varies throughout the year, since both COP and thermal demand are intrinsically season dependent.

A second extension is the integration of a GIS based spatial assessment. Mapping sewer infrastructure, district heating networks and urban heat demand density would help identify the most suitable areas for wastewater heat recovery and enhance the practical applicability of the methodology.

Further developments may include a techno economic evaluation and the extension of the framework to hybrid multi-source configurations, improving economic robustness and seasonal performance stability.

These perspectives would further consolidate the role of wastewater heat recovery as a strategic option for urban decarbonisation.

Bibliography

[1] International Energy Agency. Heat – tracking clean energy progress. `https://www.iea.org/reports/renewables-2023/heat`, 2023.

[2] International Energy Agency. Buildings – heating. `https://www.iea.org/energy-system/buildings/heating`, 2023.

[3] Diana Ürge Vorsatz, Luisa F. Cabeza, Susana Serrano, Camila Barreneche, and Ksenia Petrichenko. Heating and cooling energy trends and drivers in buildings. *Renewable and Sustainable Energy Reviews*, 2015.

[4] Intergovernmental Panel on Climate Change (IPCC). Climate change 2022: Mitigation of climate change. contribution of working group iii to the sixth assessment report, 2022.

[5] Hannah Ritchie and Max Roser. Co2 and greenhouse gas emissions. `https://ourworldindata.org/co2-and-greenhouse-gas-emissions`, 2020. Our World in Data.

[6] United Nations Environment Programme and Global Alliance for Buildings and Construction. Global status report for buildings and construction 2024, 2024.

[7] Monica Crippa, Greet Janssens-Maenhout, Diego Guizzardi, and Frank Dentener. Contribution of residential combustion to pm2.5 and black carbon in europe. *Atmospheric Chemistry and Physics*, 2016.

[8] Ville-Veikko Paunu, Jukka Karjalainen, Timo Lehtinen, and Risto P. Hämäläinen. Impacts of heat pumps on the decarbonisation of space heating in buildings. *Energy and Buildings*, 2019.

[9] Anil Markandya, Jon Sampedro, Steven J. Smith, Rita Van Dingenen, Cristina Pizarro-Irizar, Iñaki Arto, and Mikel González-Eguino. Health co-benefits from air pollution and mitigation costs of the paris agreement: a modelling study. *The Lancet Planetary Health*, 2018.

[10] International Energy Agency. The future of heat pumps, 2022.

[11] Kurt E. Herold, Reinhard Radermacher, and Sanford A. Klein. *Absorption Chillers and Heat Pumps*. 2016.

[12] Naoyuki Funamizu, Shigeki Iwai, and Yoshitaka Sato. Reuse of heat energy in wastewater: implementation examples in japan. *Water Science and Technology*, 2001.

[13] Stefano S. Cipolla and Marco Maglionico. Heat recovery from urban wastewater: analysis of the potential and applications. *Energy and Buildings*, 2014.

[14] Author Name. Recupero di calore dalle acque reflue urbane mediante pompe di calore. Master's thesis, Politecnico di Milano, 2018.

[15] MM S.p.A. Studio di fattibilità per il recupero di energia termica da reflui fognari mediante pompe di calore in edifici erp. Technical report, Metropolitana Milanese S.p.A., Milano, Italy, 2019.

[16] ENEA. Recupero di energia termica dalle acque reflue urbane. Technical report, Agenzia nazionale per le nuove tecnologie, l'energia e lo sviluppo economico sostenibile, 2019.

[17] S. Ferrari. A gis-based procedure for estimating the energy demand profiles in an urban context. *Energies*, 2021.

[18] Angelo Sileo. Recupero del calore dalle acque reflue della città di milano. Master's thesis, Politecnico di Milano, 2024.

[19] MM S.p.A. Progetto sperimentale per un impianto pilota di cogenerazione asservito alla centrale ap salemi – relazione generale. Progetto esecutivo, Metropolitana Milanese S.p.A., Milano, Italy, 2017.

[20] MM S.p.A. Relazione specialistica assetto car e bilanci di produzione di energia. Progetto esecutivo, Metropolitana Milanese S.p.A., Milano, Italy, 2017.

[21] MM S.p.A. Capitolato generale tecnico. Progetto esecutivo, Metropolitana Milanese S.p.A., Milano, Italy, 2017.

[22] R. Ben Jemaa, R. Mansouri, and A. Bellagi. Energy and exergy investigation of r1234ze as r134a replacement in vapor compression chillers. *International Journal of Hydrogen Energy*, 2017.

[23] Arif Hepbasli and Yildiz Kalinci. A review of heat pump water heating systems. *Renewable and Sustainable Energy Reviews*, 2009.

[24] T. Zakula, P. R. Armstrong, and L. K. Norford. Variable-speed heat pump model for a wide range of cooling conditions and loads. *HVAC Research*, 2011.

[25] Tatyana Babak, Neven Dui, Gennadiy Khavin, Stanislav Boldyryev, and Goran Kraja. Possibility of heat pump use in hot water supply systems. *Journal of Sustainable Development of Energy, Water and Environment Systems*, 2016.

[26] Tubular Exchanger Manufacturers Association Inc. *Standards of the Tubular Exchanger Manufacturers Association*. 2007.

[27] United Nations Environment Programme and United for Efficiency. Energy efficiency requirements for electric motors, 2025.

[28] A. Marchi, A. R. Simpson, and N. Ertugrul. Assessing variable speed pump efficiency in water distribution systems. *Drinking Water Engineering and Science*, 2012.

[29] M. Mohammadi and F. Shahraki. Numerical investigation of shell-side flow in shell-and-tube heat exchangers with different baffle configurations. *Applied Thermal Engineering*, 2009.

[30] T. L. Bergman, A. S. Lavine, F. P. Incropera, and D. P. DeWitt. *Fundamentals of Heat and Mass Transfer*. 2011.

[31] B. Jacimovic, S. Genic, N. Budimir, and M. Jaric. Criteria for the vapor space design in kettle reboilers. *Scientific Bulletin of the "Politehnica" University of Timisoara, Transactions on Mechanics*, 2008.

[32] Krishna P. Singh and Michael J. Holtz. Generalization of the split-flow heat exchanger geometry for enhanced heat transfer. In *AIChE Symposium Series (Heat Transfer—San Diego 1979)*, 1979.

[33] H. Jouhara, N. Khordehgah, S. Almahmoud, B. Delpech, A. Chauhan, and S. A. Tassou. Waste heat recovery technologies and applications. *Thermal Science and Engineering Progress*, 2018.

[34] Atlas Copco. Centrifugal compressor performance maps and technical specifications. Technical report, Atlas Copco, 2020.

[35] G. F. Hewitt, G. L. Shires, and T. R. Bott. *Process Heat Transfer*. 1994.

[36] John E. Dennis and Robert B. Schnabel. *Numerical Methods for Unconstrained Optimization and Nonlinear Equations*. 1996.

[37] 3B Meteo. Historical weather data for milan. `https://www.3bmeteo.com/meteo/milano`, 2024. Accessed: 2024.

[38] Stadtentwässerungsbetriebe Köln. Operational wastewater flow rate data from wwtp köln–weiden, 2020.

[39] J. Blanco and M. Santarelli. Modelling of solar thermal systems using periodic functions for boundary conditions reconstruction. *Energy Conversion and Management*, 2010.

[40] ISPRA. Le emissioni di co_2 nel settore elettrico nazionale e regionale, 2025.

[41] European Commission. Commission regulation no 813/2013 of 2 august 2013 implementing directive 2009/125/ec with regard to ecodesign requirements for space heaters and combination heaters. `https://eur-lex.europa.eu/legal-content/EN/TXT/?uri=CELEX:32013R0813`, 2013.

List of Figures

List of Tables